5-2018

Engineering the Structure of the Human Acidic Fibroblast Growth Factor to Enhance its Stability and Cell Proliferation Activity

Julie Davis Eberle
University of Arkansas, Fayetteville

Engineering the Structure of the Human Acidic Fibroblast Growth Factor to Enhance its Stability and Cell Proliferation Activity

A dissertation submitted in partial fulfillment
of the requirements for the degree of
Doctor of Philosophy in Chemistry

by

Julie Davis
University of Central Arkansas
Bachelor of Science in Biochemistry, 2014

May 2018
University of Arkansas

This dissertation is approved for recommendation to the Graduate Council.

_____
Suresh Thallapuranam, Ph.D.
Dissertation Director

_____   _____
Roger Koeppe, Ph.D.   Frank Millett, Ph.D.
Committee Member   Committee Member

_____   _____
Paul Adams, Ph.D.   Wei Shi, Ph.D.
Committee Member   Committee Member

Abstract

Human acidic fibroblast growth factor (hFGF1) is a protein well known for its role in cell growth and differentiation. To elicit these cell-signaling processes, hFGF1 non-selectively binds to any one of the seven cell surface hFGF receptor isoforms. Due to its significant involvement in tissue repair activity, hFGF1 is a prime candidate for novel wound healing therapeutics. However, one drawback toward its use as a novel wound healing therapeutic is the poor inherent thermal stability of hFGF1, as it has been found to unfold near physiological temperature. The cause of this instability is strong electrostatic repulsion created by a dense cluster of positively charged amino acids near the c-terminus. This instability leads to proteolytic degradation of the unfolded protein, which severely limits the bioavailability of hFGF1. To counteract this instability, hFGF1 binds with high affinity to the heavily sulfated glycosaminoglycan, heparin, which eliminates the charge-charge repulsion via electrostatic interactions with the positively charged residues near the c-terminus in the region known as the heparin-binding pocket. However, recently several disadvantages have been acknowledged with the use of heparin in hFGF1 wound-healing therapeutics. Thus, to address these issues, we have genetically engineered several rationally designed point mutations within and near by the heparin-binding region of hFGF1 to modulate the heparin-binding affinity and to increase the thermal stability and cell proliferation activity of the protein. Study of each mutation is performed with biophysical experiments as well as molecular dynamics simulations (which are found as supplementary files).

Acknowledgements

I would like to thank my Lord and Savior Jesus Christ for the hope and purpose I have in life through His salvation. I would like to thank my husband, Richard Eberle, and my family for the constant support and encouragement throughout my graduate career. I would like to thank Dr. Kumar and my committee for the professional guidance they have given me in my research projects and in the publication process. I would like to thank my colleagues in the Kumar lab, and the friends I have made through the chemistry department for their friendship and for always inspiring me with their own hard work.

Table of Contents

Abbreviations

human acidic fibroblast growth factor-1 (hFGF1); wildtype hFGF1 (wt-hFGF1); site directed mutagenesis (SDM); circular dichroism (CD); heteronuclear single quantum coherence (HSQC); American Type Culture Collection (ATCC); Visual Molecular Dynamics (VMD); isothermal titration calorimetry (ITC)

List of Published Papers

1. Chapter 1: Eberle Davis, J., et al., Probing the role of Proline -135 on the structure, stability, and cell proliferation activity of Human Acidic Fibroblast Growth Factor. Archives of Biochemistry and Biophysics, 2018. (In Review)

2. Chapter 2: Eberle Davis, J., et al., Effect of Extension of the Heparin Binding Pocket on the Structure, Stability, and Cell Proliferation Activity of the Human Acidic Fibroblast Growth Factor. Biochemistry and Biophysics Reports, 2018. 13: p. 45-57. (Published)

Introduction

FGF Gene evolution

The fibroblast growth factor (FGF) gene family has greatly expanded through the process of evolution from primal multicellular organisms such as *Caenorhabditis elegans*, in which only two FGF genes and one FGF receptor (FGFR) gene is identified, to complex vertebrates such as mice and humans, in which 22 FGF genes and four FGFR genes are identified [1]. The evolutionary FGF gene expansion has occurred in two stages. The first stage involved duplication from two or three to six FGF genes during primitive metazoan evolution. The second stage involved two large FGF genome duplications, as well as alternative splicing of FGFR genes during primitive vertebrate evolution [1]. Gene expansion has greatly enriched the signaling diversity of the FGF and FGFR families, which has led to the vast involvement of these proteins in developmental, metabolic, tissue regeneration, and physiological processes.

The chromosomal locations of most human FGF (hFGF) genes have been determined. hFGF genes are spread throughout the genome, which advocates evolution not only through gene duplication but also gene translocation [1]. However, some hFGF genes are clustered together. For example hFGF3, hFGF4, and hFGF19 are separated by 40kb and 10kb respectively, while FGF6 and FGF23 are separated by only 55kb [1]. Such gene clustering indicates an order of evolutionary expansion in which local gene duplication occurred first and subsequent genome duplication occurred second.

Human FGF family

hFGFs play critical roles during embryonic morphogenesis by regulating the differentiation of cells during lung, liver, heart, brain, pancreas, kidney and ear development [2].

In adults, hFGFs regulate tissue regeneration and injury response, and they also play a role in metabolic and mineral homeostasis. Specifically, hFGFs consist of approximately 150-300 amino acids, and range in molecular weight from 17-34kDa [3]. Of the entire amino acid sequence, roughly 120 residues make up the protein core, among which there is 30-60% amino acid sequence conservation [1]. The hFGF family is categorized into seven subfamilies, and the members within a subfamily share an even higher level of amino acid sequence identity.

Functions of FGFs - by subfamily

FGFs in the same subfamily share common receptor-binding and expression properties. All FGFs in subfamilies 1, 4, 7, 8, and 9 are classified as paracrine FGFs, which are exported to the extracellular matrix and initiate biological responses upon binding to cell surface FGFRs [4, 5]. These paracrine FGFs are also characterized by their high affinity for glycosaminoglycans such as heparin, and binding with these ligands not only stabilizes FGFs, but also retains the proteins in reservoirs around the cell surface. FGFs in subfamily 19 are endocrine signaling molecules that exhibit a reduced affinity for glycosaminoglycans, and thereby mediate cell signaling through distant target cells via binding to cell surface FGFRs [4].
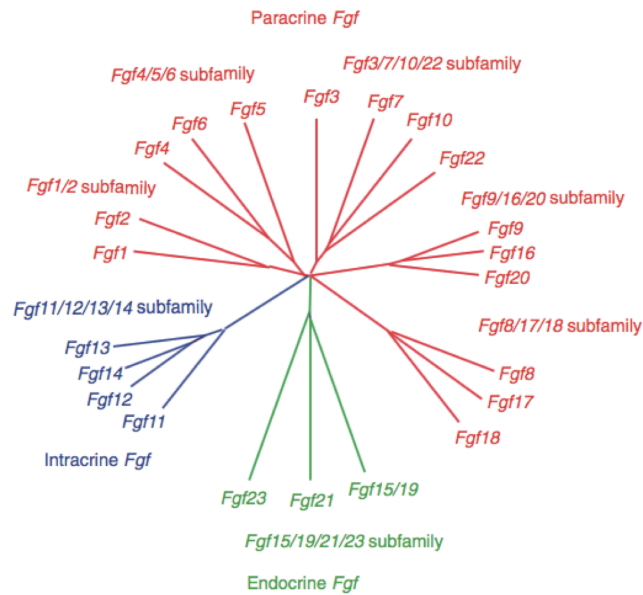
Figure 1. Classification of FGFs by subfamily and type of signaling.

The FGF1 Subfamily

The FGF1 subfamily consists of FGF1 and FGF2, proteins that are both well known for their cell proliferating activity and expression in both developmental and adult stages. The FGF1 subfamily is unique from all other FGF subfamilies in that it is the only subfamily that binds with high affinity to all FGFR isoforms [6]. FGF1 consists of 154 amino acids and is expressed in microvascular endothelial cells. FGF1 is highly involved in cell differentiation, specifically adipogenesis, cell growth and survival, embryonic development, and tissue repair [7]. FGF1 was the first growth factor isolated in the FGF family and is also called acidic FGF as its isoelectric point (approximately 6.5) is relatively acidic compared to basic FGF (FGF2) whose isoelectric point is 9.6 [6]. Additionally, FGF1 plays a role in brain development as it has been found in several types of brain cells including sensory and motor neurons as well as several other types of subcortical neuronal cells [6]. FGF1 is also found in endothelial cells, fibroblasts, and

3

keratinocytes (along with FGF2 and FGF7) where it participates in wound healing. Lastly, FGF1 may be transported to the nucleus via a nuclear localization sequence where it participates in DNA synthesis [8].

FGF2 contains 155 amino acids and has a molecular weight of 18-24KDa. Four additional, heavier versions of FGF2 are also reported, which contain amino terminal sequences that signal for their location to the nucleus where their activity is not well understood [3]. FGF2 is highly expressed in the lateral ventricles of the brain where it is involved in neurogenesis and lesion repair, and is involved in development and maintenance of cardiovascular physiology [9, 10]. FGF2 also has mitogenic activity towards 3T3 fibroblasts [8].

The FGF4 Subfamily

The FGF4 subfamily includes FGF4, FGF5, and FGF6. FGF4 is a 206 amino acid protein expressed only during embryonic stages that contains both an amino signaling sequence for classical secretion as well as an *N*-glycosylation site [3, 8]. From genomic-based studies, FGF4 is thought to be a gene duplication of FGF3 [8]. FGF4 is dominantly involved with differentiation of presomatic mesoderm during vertebrate embryo development as well as trophoblast stem cell proliferation [11, 12]. FGF4 is also known to transform fibroblast cells and drive angiogenesis; however, removal of the amino terminal signal sequence severely inhibits the former activity. With deletion of the N-glycosylation site, the activity of FGF4 was improved compared to the non-deleted form, indicating that this site is not important for protein function but rather hinders activity [8].

FGF5 is a 267 amino acid protein which contains a secretion signal sequence and is mostly expressed at embryonic stages of development, but is also found (much less abundantly)

in adult tissues [3, 13]. The FGF5 gene was identified as an oncogene and can transform cells when transfected in mammals [13]. Specifically, FGF5 is responsible for determining hair length in mammals. Studies from 2007 report that proline to histidine mutations in the FGF5 gene result in cats with longhair phenotypes [14].

FGF6 is a 25kDa protein found in varying lengtheparin (208, 198, or 175 amino acids). FGF6 has a 27 amino acid signal sequence at its N-terminus and is secreted into the extracellular matrix. FGF6 is expressed at both embryonic and adult stages of development and interacts with high affinity to several FGFRs including FGFR1 (IIIc) FGFR2 (IIIc) and FGFR4 [3]. Mouse studies involving FGF6 indicate that this protein plays a key role in muscle regeneration. High doses of FGF6 in FGF6 knockout mice directly induced stem cell proliferation for regeneration of calf muscles while low doses were more active toward muscle cell differentiation [15].

The FGF7 Subfamily

The FGF7 subfamily includes FGF3, FGF7, FGF10, and FGF22. Human FGF3 is a 239 amino acid protein expressed only during embryonic stages and is secreted via the classical secretion pathway due to an amino terminal signal sequence [3, 8]. FGF3 also contains a carboxy terminal sequence that localizes the protein to the nucleus. The destination of FGF3 is a result of competition between these two sequences. Activity of normal FGF3 in the nucleus is not well understood; however, mutated FGF3 lacking the amino secretion signal sequence yet containing the carboxy nuclear localization sequence, causes a buildup of FGF3 in the nucleus that inhibits DNA synthesis as well as cell proliferation [8].

FGF7 is a 28kDa protein with 194 amino acids and a 31 amino acid N-terminus sequence that signals for its secretion. FGF7 dominantly signals through the receptor, FGFR2b, and is well

known as the keratinocyte growth factor due to its mitogenic activity on skin keratinocytes [16]. FGF7 is also reported to be the most significant gene up regulated with the advancement of upper tract and bladder urothelial carcinoma [17]. Furthermore this growth factor is expressed with FGFR2b in hepatocytes, and both *in vivo* and *in vitro* studies show that FGF7 and its corresponding receptor promote proliferation of hepatocytes following liver damage, disease, and partial hepatectomy [18].

FGF10 is a 209 amino acid protein with a relatively hydrophobic 35 amino acid signal sequence at its N-terminus. This protein is expressed in many cell types including fibroblasts, adult pre-adipocytes, lung mesenchyme, and posterior limb mesoderm and mesenchyme. FGF10 is expressed at both embryonic and adult stages and is reported to mediate limb, lung, and brain development. FGF10 knockout mice died at birth due to impartial lung development [3, 19]. FGF10 also plays a role in liver development by maintaining survival of hepatoblasts [18].

FGF22 is a 209 amino acid protein with a molecular weight of 23kDa. This FGF member has a 22 amino acid signal sequence and is expressed in cerebellar granule cells [20]. *In vivo* studies reveal that FGF22 is a presynaptic organizing molecule and neutralization of FGF22 inhibits differentiation of mossy fibers involved in signal transmission at sites of contact with granule cells. FGF22 has also been found in the inner root sheath of hair follicles, which indicates a role in hair development [21]. Furthermore, this FGF member has more recently been reported to have a potential pro-oncogenic role in the development skin cancer, as FGF22 knockout mice were found to develop fewer papillomas than control mice in a carcinogenesis challenge study [21].

The FGF8 subfamily is comprised of FGF8, FGF17, and FGF18, which are all paracrine signaling molecules. Human FGF8 and FGF17 are unique in that these members are found to have multiple human isoforms (with additional isoforms in mice) [22]. The variation is derived from alternative splicing within the first exon, which causes the N-terminus sequence to vary in length from 62 to 156 amino acids [23]. Such splicing variation has been demonstrated to regulate the biological activity of these FGFs in midbrain and hindbrain patterning and development [22]. In addition, crystal structure comparison of the FGF8-FGFR2c and FGF17-FGFR2c complexes reveals that the N-terminus sequence discrepancy modulates receptor binding such that FGF17 binds the receptor with stronger affinity than FGF8 [24]. Both FGF8 and FGF17 are only expressed during embryonic development and they specifically regulate neuroepithelial proliferation in the brain at a junction in the mid-hind region [3, 25]. FGF8 is also essential for embryonic limb development as well as development of the central nervous system, and FGF8 gene knockout mice died within 10 days of embryonic maturation [3].

FGF18 is a 207 amino acid protein with an N-terminus 26 amino acid secretion signal sequence [25]. During embryonic development, FGF18 expression has been reported in lung, midbrain, pancreas, muscles, and the intestinal tract where it plays a role in morphogenesis. Beyond this, FGF18 is reported to play a dominant role in skeletal development regarding both cartilage formation and osteogenesis [25]. FGF18 knockout mice died within 30 days after birth due to poor circulation of oxygen in the blood and were also found to have incomplete and deformed skeletal systems [25].

The FGF9 subfamily includes FGF9, FGF16, and FGF20, all of which are secreted outside of the cell and are paracrine signaling. FGF9 is a 30kDa protein with 208 amino acids, and while it has no distinct N-terminus signal sequence, it does contain an unusual hydrophobic sequence that is a compulsory part of its secretion [3]. FGF9 is expressed in kidney, lung, and prostatic stromal cells, and in multiple cells types in the central nervous system. FGF9 is largely known for its role in male sex determination as FGF9 knockout mice undergo male to female sex reversal [26]. This growth factor also plays an important role in the proliferation of lung mesenchyme, which in turn produces other FGFs including FGF3, FGF7, FGF10, and FGF22. Thus, FGF9 regulates the production of these additional FGFs and the overall development of lung tissue [26].

FGF16 is a 26kDa protein with 207 amino acids and is not classically secreted, as it does not contain an amino terminal signal sequence. FGF16 is expressed in cardiac myocytes and in brown adipose tissue during embryonic development. Expression of this growth factor is reduced in adult stages and FGF16 knockout mice are found to have severe cardiac abnormalities [26, 27].

FGF20 is a 23kDa protein with 211 amino acids and no signal sequence. FGF20 is expressed in a region of the midbrain known as the substantia nigra pars compacta where it preserves dopaminergic neurons, which helps prevents onset of Parkinson's disease. FGF20 interaction with FGFR1c on proximal cells in this region of the midbrain stimulates the MAPK pathway, which ultimately sustains the dopaminergic neurons and helps prevent Parkinson's disease [28].

The FGF11 Subfamily

The FGF11 subfamily consists of FGF11-FGF14. These FGFs are known as homologous factors and exhibit high levels of sequence homology. Specifically, these homologous factors share between 58-71% sequence identity with each other and only up to 30% sequence identity with other members of the FGF family [29]. FGF11-14 are not secreted from cells and thus are intracrine signaling proteins that function independently of cell surface FGFRs [4]. Specifically, FGFs in this subfamily interact with voltage-gated sodium and calcium channels where they facilitate transmission of synaptic signaling as well as heart contractions [4, 5].

The FGF19 Subfamily

As mentioned, FGFs in subfamily 19 (FGF19, FGF21, and FGF23) are endocrine signaling. Studies on FGF15, the mouse ortholog of FGF19, reveal that FGF19 is involved in regulation of bile acid homeostasis in the liver via interaction with FGFR4 expressed on hepatocytes [30]. FGF19 contains 216 amino acids and has a 22 amino acid N-terminal signal sequence. Studies of FGF19 transgenic mice reported an increase in fatty acid oxidation, a reduction of liver triglycerides and glucose levels, and increased sensitivity to insulin [26]. Application of FGF19 is being further investigated for treatment of diabetes via reduction of brown adipose tissue [26]. FGF19 signals dominantly through binding with FGFR4 in the liver, but can also interact with other FGFRs when in the presence of the single-pass transmembrane protein, β-Klotho [4, 26].

FGF21 is a 171 amino acid protein with a molecular weight of approximately 19kDa. FGF21 is expressed in liver, pancreas, and white adipose tissue, and although it can activate most all FGFR isoforms, it preferentially binds to FGFR1c. FGF21 binding with FGFRs is also

accompanied by β-Klotho [4, 26]. FGF21 is well known for its metabolic role in enhancing insulin sensitivity and glucose uptake, stimulating fatty acid oxidation, and inducing the adaptive starvation response [31].

FGF23 is composed of 251 amino acids with a 24 amino acid N-terminus signal sequence, and has a molecular weight of approximately 28kDa. FGF23 is expressed in bone cells but dominantly interacts with FGFR1c (complexed with the transmembrane protein α-Klotho) in the kidney to regulate serum phosphate levels as well as vitamin D levels by preventing reabsorption in both the proximal tubule as well as in the intestine [32]. FGF23 is also reported to interact with the parathyroid gland to inhibit secretion of the parathyroid hormone, which regulates uptake of phosphate from bone [26].

hFGF1 structure

The structure of hFGF1 is of the β-trefoil family. The β-trefoil is one of 10 fundamental protein superfolds, which is composed of three connected trefoil units [33, 34]. In epidermal growth factors this β-trefoil structure has been found as a monomeric unit, while in certain protease inhibitors as well as in fibroblast growth factors, the β-trefoil is found in dimeric and trimeric units respectively [34]. Thus the evolution of this structure is thought to be derived from sequential gene duplication(s)/fusion(s) [33, 34]. The β-trefoil structure is common among several types of proteins including fibroblast growth factors, interleukin-1α and -1β, Kunitz soybean trypsin inhibitors, plant cytotoxins and bacterial toxins such as the ricin-like toxins, as well as some carbohydrate-binding proteins including xylanase [33, 35, 36].

The β-trefoil is composed of twelve β-strands that are folded into six β-hairpins. The overall structure of the β-trefoil within FGFs is divided into two parts, top and bottom, with the top half (consisting of three β-hairpins) forming a barrel composed of strands 1, 4, 5, 8, 9, and 12, and the bottom half forming a β-hairpin triplet composed of the remaining strands. The β-trefoil structure is unique in that it is the only superfold with an axis of 3-fold symmetry through the center of the structural barrel that separates the barrel into three trefoil subdomains [33]. These β-hairpins are held together by hydrogen bonds and are characteristically angled approximately 56° to the barrel axis [37]. The total barrel cavity has a diameter of 16 A°[37].
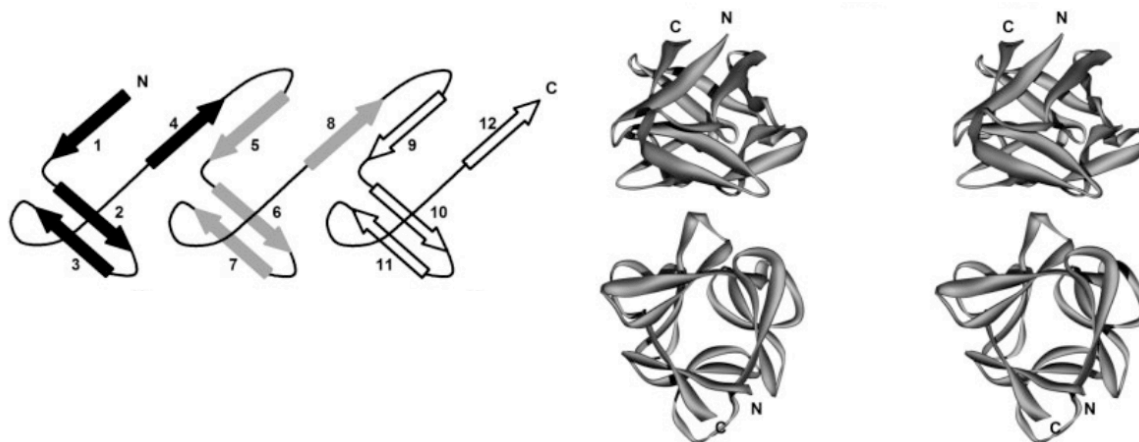

Figure 2. Left: diagram of hFGF1's twelve β-strands folded into β-hairpins. Right: Top is the side view of the tertiary fold, and bottom is the view down the axis of symmetry through the barrel [33].

Different portions of the hFGF1 structure are responsible for heparin binding and receptor binding. β-strands 1-5 are involved in receptor binding and are more flexible than β-strands 6-12, which are involved in heparin binding and are collectively more rigid [33].

Heparin

Chemistry and structure of heparin

Heparin is a member of a group of molecules, which are classified as glycosaminoglycans (GAGs). These molecules are composed of repeating disaccharide units that most commonly include D-glucosamine and L-iduronic acid, but may also less frequently include D-glucuronic acid, *N*-acetylglucosamine, as well as unsubstituted glucosamine units [38, 39]. These sugar units are linked via α-(1→4) glycosidic linkages and are heavily sulfated. Sulfate groups are commonly found on positions 2 and 6 on D-glucosamine as well as on position 2 on the L-iduronic acid unit [38, 39].
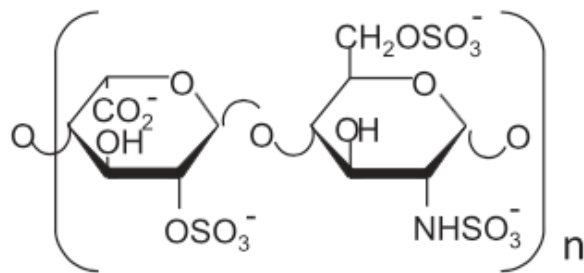

Figure 3. The disaccharide unit of heparin containing L-iduronic acid (left) and D-glucosamine (right) linked via α-(1→4) glycosidic linkages [39].

There is substantial variation within the sugar composition of heparins from different species and tissues [39]. Additionally, there is considerable variation among the length of heparin-like polysaccharide chains which can range anywhere from 3 to 30kDa.

Heparin vs heparan sulfate

Heparan sulfate (HS) is another GAG found in the extracellular matrix having similar sequence and backbone structure to heparin. One difference between HS and heparin is the contrasting proportions and arrangements of sugar saccharides and sulfation patterns [39, 40]. In

addition, HS is expressed more universally by all cells throughout the human body whereas heparin is only expressed by mast cells [40]. The primary difference is the degree of sulfation; glucosamine residues of HS are only 30-60% sulfated with clusters of the polysaccharide heavily sulfated and other portions unsulfated [40]. Heparin is 80-90% sulfated with no clustering of the sulfate groups.

Biosynthesis of heparin

Heparin is synthesized in the golgi apparatus in a series of steps involving many different enzymes; however, the first step begins with a serine residue of the core protein, serglycin, [40-42]. The biosynthesis continues with the sequential linkage of D-glucuronic acid (GlcA), glacatose (Gal), and xylose (Xyl) by various enzymes to form the non-sulfated tetrasaccharide substrate (-GlcA-Gal-Gal-Xyl-) (Fig. 3) [40]. Following the formation of this initial substrate is the elongation process, which begins with the addition of *N*-acetyl-D-glucosamine (GlcNAc) and continues with the alternating addition of GlcA and GlcNAc (Fig. 3) [40, 41]. Polymerization of the substrate is catalyzed by complexed EXT1 and EXT2 polymerases. Modifications involving the substitution of acetyl groups with sulfate groups are catalyzed by GlcNAc *N*-deacetylase / *N*-sulfotransferase enzymes [42]. Subsequently the epimerization of D-glycuronic acid units into L-iduronic acid is catalyzed by uronosyl C5-epimeraser, and O-sulfation on two positions in D-glucuronic acid and one position in L-iduronic is catalyzed by 2-O, 3-O and 6-O sulfotransferases (Fig. 3) [41, 42]. Incompletion of these reactions (particularly of the O-sulfation) yields a wide variety of unique polysaccharides, a characteristic of heparin-like molecules that regulates the biological activity of these GAGs.
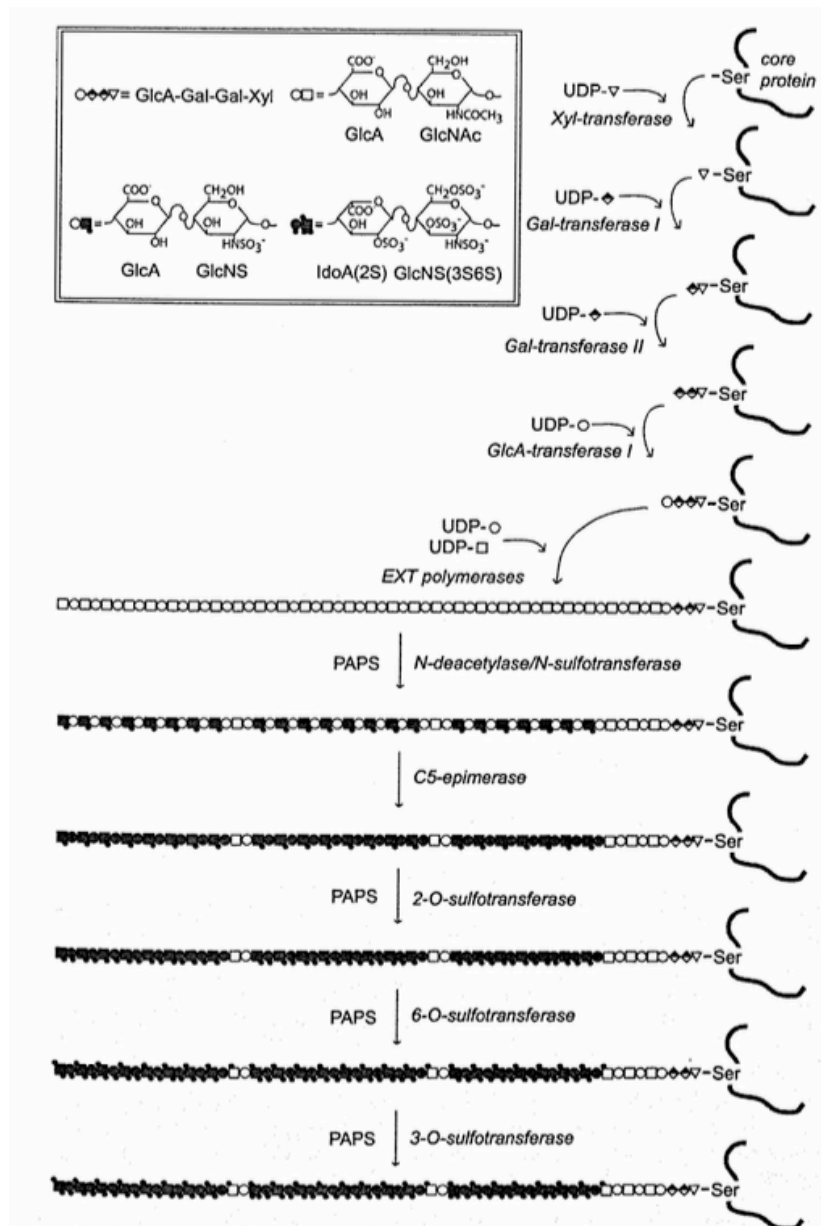
Figure 4. Biosynthesis of heparin.

Biological significance of heparin

Heparin is principally known for its biological activity as an anticoagulant by enhancing the inhibitory action of antithrombin. While heparin interacts with various serine protease inhibitors, also know as serpins, its most dominant interaction by far occurs with antithrombin.

Antithrombin has a high affinity for a specific pentasaccharide sequence within heparin

(αDGlcNAc(6S)-βDGlcA-αDGlcNS(3S, 6S)-αLIdoA(2S)-αDGlcNS(6S)) [43]. Upon binding, a

conformational change within antithrombin exposes a reactive loop that mimics the substrate of

the serine protease thrombin. When thrombin cleaves the sequence of the reactive loop on

antithrombin, the protease becomes locked in an inactive complex, preventing its succeeding

action on fibrinogen to initiate the clot forming process [43].

Beyond its interaction with serpins such as antithrombin, heparin binds to FGFs with high

affinity, and functions as a regulator of FGF movement and the duration of their biological half-

life. Thus heparin provides an interesting mechanism for organized growth and development of

complex systems and organisms [44]. As FGFs are highly involved in tissue repair following

injury, heparin also serves as a mediator of wound healing processes.

Heparin-hFGF1 interaction

The basis of the interaction between heparin and hFGF1 is electrostatic interactions,

which occur between the sulfate groups of heparin and the positively charged residues of the

heparin-binding pocket of hFGF1. The heparin-binding region of FGFs is composed of three

exposed loops. These loops form a confined pocket and contain several positively charged

residues located on beta strands 10 and 11 [3]. Site directed mutagenesis studies from the 1990's

report a reduction in the heparin-binding affinity specifically for charge reversal of lysine

residues toward the C-terminus (K132, K127, K114, and K115) [45]. This study was one of the

first attempts to characterize the heparin-binding region of hFGF1.

Full characterization of the heparin-hFGF1 interface has since been determined in detail

with the help of x-ray crystallography and multidimensional nuclear magnetic resonance. One of

the first hFGF1-heparin crystal structures was a hFGF1 dimer bound to a heparin decasaccharide (PDB 2AXM) [46]. This structure clearly confirms that C-terminal residues 126-142 of hFGF1 facilitate heparin binding. Interestingly the crystal structure contains no protein-protein interactions and each monomer binds the heparin sulfate groups on opposing sides of the polysaccharide [46]. Interestingly, DiGabriele and coworkers report that heparin binding does not induce any conformational change in hFGF1 structure.

An additional crystal structure composed of two 1:1 hFGF1-FGFR2 dimers shows that a helical heparin deasaccharide chain makes contacts with both hFGF1 monomers (denoted A and B) (PDB 1E0O) [47]. In this crystal structure, the hFGF1 residues facilitating heparin binding are K126, K127, N128, K132, R133, R136, and K142 [47]. Pellegrini and coworkers report that hFGF1 monomer A interacts with 6 monosaccharides of heparin, while hFGF1 monomer B interacts with only 5 heparin monosaccharides, and thus makes distinct contacts with heparin including a hydrogen bond which occurs between Trp121 and GlcN-1 [47]. Furthermore Pellegrini and coworkers report that the heparin chain exhibits a 34° kink between the second and third disaccharides and that, in addition to electrostatic interactions, van der Waals forces significantly contribute to hFGF1-heparin binding [47].

Further study of the positively charged residues in the heparin-binding region of hFGF1 emphasizes the importance of the conserved lysine at position 132, located in the base of the pocket toward the protein core. K132 is responsible for interacting with critical N-sulfate and 2-O-sulfate groups on the heparin iduronic acid sugar. Interaction with K132 induces a conformational change in the positioning of iduronic acid. This conformational change alters the backbone torsion angles of heparin and induces a "kink" in the ligand structure [48]. Repositioning of heparin induces formation of additional van der Waals forces that help to

achieve optimum binding with hFGF1 as previously noted [47, 48]. The spatial arrangement of these positively charged, heparin-binding residues are unique for each subfamily, and such deviations give each FGF a different affinity for different heparin-like GAGs.

Overlay of the Cα traces of residues in the heparin-binding region from five different FGF crystal structures (including hFGF1) resulted in very low rms values (0.45-0.75 A°), indicating that the structural arrangement of these loop regions correspond and are more rigid in character as previously mentioned [48]. However, comparison of the side chains positions of positively charged amino acids in the heparin binding loops from the same five crystal structures did not correspond well. This indicates that the spatial arrangement of these side chains for hFGF1 is unlike the arrangement for any other FGF, and provides a unique "signature" for its heparin-binding interface [48]. Furthermore, heparin binding with hFGF1 does not induce any conformational shift within the protein, which is demonstrated by biophysical characterization of the protein in the presence and absence of heparin.

Role of heparin in hFGF1-FGFR signaling

The role of heparin in hFGF1-FGFR interaction and subsequent activation has been a subject of debate. It is believed that heparin not only helps stabilize the protein, but also that the biological activity of hFGF1, including receptor binding and activation, is fully dependent on heparin [38, 47, 49, 50]. Thus heparin is thought to be essential to the biological function of hFGF1. This understanding was developed from the previously mentioned crystal structures. These structures demonstrate that both monomers of dimeric hFGF1 as well as the FGFR are linked to the same heparin chain, and therefore it was claimed that heparin is essential in the hFGF1 dimerization and FGFR activation process [47, 49]. Furthermore, based on the dimer

structure of these crystals, the hypothesis developed that hFGF1 dimerization is mandatory for subsequent receptor binding and activation.

In 2002, Kumar and coworkers used a molecular mimic of heparin, sucrose octasulfate (SOS), to study the biological activity of hFGF1 [51]. Their study shows that the binding of SOS to hFGF1 retains the protein in a monomeric form. Furthermore they demonstrate that monomeric hFGF1 bound to SOS was capable of substantial cell proliferation activity [51]. From this study they conclude that hFGF1 oligomerization is not mandatory for its biological activity with corresponding FGFRs.

Additional study from 2005 by Angulo and coworkers also demonstrates that hFGF1 dimerization is not essential for its biological activity, and furthermore they conclude that the sulfation pattern of heparin-like ligands has a substantial impact on the mitogenic activity of hFGF1 [52]. This study utilizes two synthetic sulfated hexasaccharides that bind and retain hFGF1 in its monomeric form as they cannot facilitate hFGF1 dimerization. These two ligands exhibit different sulfation patterns. The sulfate groups of both ligands span the length of the ligand molecule; however, one contains sulfate groups on both faces of the molecule and the other displays sulfate groups only on one side [52, 53]. It was shown that the ligand with sulfate groups oriented toward only one face of the molecule facilitated hFGF1-mediated cell signaling at the same level as natural heparin and therefore that dimerization of hFGF1 is not mandatory for biological activity [52, 53].

The claim that heparin is an absolute requirement for hFGF1 cell signaling has been revisited through multiple mutagenesis studies. From these studies, another belief has been developed that heparin is not essential for the biological activity hFGF1, but instead is useful primarily for stabilizing the inherently unstable protein, and for increasing the bioavailability of

the protein in reservoirs near the cell surface. hFGF1 is well known for its poor thermal stability and short half life *in vivo,* and is unstable at temperatures close to physiological [34, 54-56]. The poor stability of hFGF1 is thought to be a regulatory mechanism that protects against over active or unregulated FGF1 signaling, which can lead to tumorgenesis [57]. Those who believe that heparin is not essential for hFGF1 biological activity have hypothesized that hFGF1 could function independently of heparin if the thermal stability of the protein could be increased [56].

One interesting mutagenesis study found that the hFGF1 mutant, K132E, exhibits reduced heparin-binding, yet demonstrates complete FGF receptor binding and activation, and further was found to induce early-intermediate gene transcription [45]. Another study reports that substitution of serine for cysteine residues in three positions (30, 97, and 131) increases hFGF1's half-life from 0.26 hours up to 73 hours [55]. However, these mutants were found to be thermally destabilizing to the protein. Another study demonstrates its attempt to increase stability via mutations that increase the core-packing arrangement of hFGF1 [34]. Although most of the designed mutations were not successful towards generating more efficient core-packing arrangements, one mutation, L58F, was found to marginally increase the thermal stability of hFGF1 [34].

A more recent study utilized a sequence homology approach to rationally design the three mutations: H35Y, H116Y, F122Y [56]. While each individual mutation increased the thermal stability of hFGF1 by a couple of degrees, they were all ultimately combined with L58F to form the quadruple mutant H35Y/L58F/H116Y/F122Y. This quadruple mutant was found to increase thermal stability of hFGF1 by 7.8°C [56]. Furthermore, the biological activity of the quadruple mutant was equivalent to the wildtype protein. Following these studies, two additional stabilizing mutants Q54P and S61I were discovered, again through the sequence homology approach [58].

These two mutants were then combined with the previously described quadruple mutant as well as an additional stabilizing mutation, H107G, to form the septuplet mutant: H35Y/Q54P/S61I/L58F/H107G/H116Y/F122Y. These seven mutations collectively increase the thermal stability of hFGF1 by an astounding 27°C [58]. In the absence of heparin, the biological activity of this septuplet mutant, as well as the triple mutant Q54P/S61I/H107G, are six and ten times higher respectively than the wildtype hFGF1.

In 2009, Zakrzewska and coworkers revisited the K132E mutation (previously designed by Wong *et al.* in the early 90's) in an attempt to make a direct assessment on the role of heparin within hFGF1 activity. The charge reversal K132E mutation is known to reduce hFGF1's affinity for heparin due to its position within the heparin-binding pocket. Zakrzewska and coworkers additionally report the hFGF1 K132E mutant to be inactive toward DNA synthesis [59]. Interestingly, upon combination of the K132E mutant with the stabilizing triple mutant Q54P/S61I/H107G it was found that in the absence of heparin, the mitogenic activity of this quadruple mutant was fully recovered to the level of heparin-bound wildtype hFGF1 [59]. From these findings, the conclusion was made that heparin is not essential for hFGF1 binding and activation of its FGFR.

Another study from 2007, which notes that the N and C terminal flexible strands were only stabilized by hydrogen bonds, hypothesizes that the stability of hFGF1 could be increased if disulfide bonds were inserted into the N and C terminal tails. In effort to generate disulfide bonds, mutations K26C and P148C were designed, but were only found to increase thermal stability and mitogenic activity of hFGF1 under reducing conditions, with no disulfide bond formation. Interestingly, this study reports that the double mutant K26C/P148C is 30 times more active than the wildtype protein as measured by cell proliferation assays [60].

Overall, there have been numerous studies demonstrating the ability of hFGF1 to effectively facilitate cell signaling in a heparin independent manner; however, there still remains disagreement on the role of this ligand as current literature still characterizes heparin as mandatory for hFGF1 activity with FGFRs [2, 22, 61, 62]. Ultimately it is commonly recognized among all fields that heparin confers increased thermodynamic stability to hFGF1, thereby increasing the proteins physiological half-life while keeping the protein localized in the extracellular matrix.

FGF Receptors
FGFR gene evolution and isoforms

There are four known FGFR genes found in both humans and mice, all having approximately 810 amino acids with 56-71% sequence homology and identical exon-intron sequencing [1, 4]. These FGFR genes are scattered throughout the genome with no clustering, which suggests evolution from a common ancestral gene via two-fold genome duplication. There is no connection between the chromosomal gene distribution of FGFs and FGFRs. The variation among the four known FGFRs is a result of alternative splicing of the extracellular immunoglobin-like (Ig) domains giving rise to FGFRs with either two or three Ig domains [1]. The mechanism that regulates FGFR splicing is highly conserved throughout evolutionary history.

Alternative splicing of FGFRs 1, 2, and 3 gives rise to two different forms of Ig domain III (IIIb and IIIc). Ig domains II and III as well as the linker region between the two domains are dominantly responsible for the ligand-binding specificity of the receptor [63]. Overall, from the four known FGFR genes, there are seven different FGFR isoforms (1-IIIb, 1-IIIc, 2-IIIb, 2-IIIc, 3-IIIb, 3-IIIc, and 4) which all display unique ligand-binding specificity [4].

FGFRs consist of an extracellular domain composed of (up to) three Ig-like domains that facilitate ligand-binding, a single pass α helical transmembrane domain, and an intracellular tyrosine-kinase domain [4]. All receptor isoforms have similar molecular weights of approximately 90kDa and contain around 810 amino acids [2, 64]. The discrepancy within the splicing of Ig domain III (D3) (resulting in receptor isoforms b and c) is responsible for the diverse ligand specificity and tissue expression of the receptor isoforms [5]. FGFRb isoforms are expressed in epithelial cells and are activated by ligands expressed only in mesenchymal cell lines. Additionally, FGFRc isoforms are expressed in mesenchymal cells and are only activated by ligands expressed in epithelial cell lines [3, 65]. The reciprocal expression of FGFRs and their corresponding ligands coordinates the directional paracrine signaling of FGFs and also acts as a guard against aberrant autocrine FGF signaling [22].

Crystal structures of FGF ligands bound to FGFRs give molecular detail on how the splicing variation of the D3 domain regulates receptor-binding specificity. These structures reveal that splicing variation alters the sequence of critical binding residues and pockets that generate electrostatic as well as hydrogen bonds with FGF ligands [22]. For example FGF10 binding with FGFR2b and not FGFR2c is dependent on hydrogen bonding with a specific serine residue in FGFR2b. The corresponding position in FGFR2c is an alanine not a serine, thus critical hydrogen bonding is not facilitated with this receptor isoform. FGFR1 and FGFR2 equally express a high affinity for FGF1 and FGF2 with K_d values in the range of 100-500 pM [63]. FGFR3 and FGFR4 both demonstrate a higher affinity for FGF1 than for FGF2.

Study of the protein-receptor binding interface shows that hFGF1 makes contacts with Ig domains II (D2) and D3 of the receptor at the junction between the two domains [2]. Ig domain I (D1) as well as the acidic sequence of residues between D1 and D2 are reported to inhibit ligand binding, and recombinant receptor proteins lacking D1 are found to have a higher binding affinity for FGFs [2]. Overall the FGF1 ligand is more extensively bound to D3 making contacts with 23 residues, than with D2, as only 13 FGF1-D2 contacts are reported [66]. However, it is interestingly reported that the FGF1 residues involved in D2 binding are more highly conserved than FGF1 residues involved in D3 binding, [66]. Of FGF1 residues, 39 of 140 residues are involved in receptor binding, none of which include heparin-binding residues. One crystal structure of a heparin-bound FGF1 dimer complexed with an FGFR2 dimer (PDB E10O) specifically reveals that contacts between FGF1 and D2 of the receptor are mostly hydrophobic including residues Y29, G34, F36, Y108, L147, and L149 of FGF1 and residues K164, L166, A168, V169, and P170 of the receptor D2 [47]. Additional electrostatic interactions occur between residues R49 and R51 of FGF1 and E163 and D247 of the receptor D2, respectively. One critical interaction is a hydrogen bond between N109 of FGF1 and R251 which is located on the linker region between D2 and D3 of the receptor [47]. Critical interactions between FGF1 and D3 include an electrostatic interaction between E101 of FGF1 and R255 of D3, as well as hydrophobic interactions between I257 of D3 and L103 and H107 of FGF1. There is one splice form specific interaction between FGF1 and D3 that involves protein residue V65 and D3 residue F352. The lack of more distinct splice form interactions justifies the lack of specificity toward any particular receptor isoform demonstrated by FGF1 [47].

Study of the 1:1 FGF1:FGFR2 structure complex (PDB 1DJS) also reveals that the N and

C terminal ends which extend from the core of the FGF1 ligand make contacts with the D2-D3 linker region (Fig. 5). Figure 5 also shows the structure of a 2:2 FGF1:FGFR2 complex in the absence of heparin (PDB 1DJS). In this complex, the receptor D2 and D3 make contacts with both the ipsilateral and contralateral FGF1 ligands yet no ligand-ligand contacts are reported [66].

When present, heparin is dominantly bonded to the FGF1:FGFR complex through the heparin-binding region of FGF1; however additional contacts between heparin and receptor D2 are reported to occur between residues V175, H167, K164, T174, K176, R178, and K161 of D2 and the 9th and 10th saccharides of the heparin chain (Fig. 5) [47]. FGF-receptor dimer complexes with heparin can be classified as symmetrical, in which heparin makes contacts with both FGFs and both receptor chains, or asymmetrical, in which heparin makes contacts with both FGF ligands and only 1 receptor chain. Comparison of the FGF1-FGFR2 crystal structure in the presence (PDB 1E0O) and absence (PDB 1DJS) of heparin reveals two conformations for the receptor D3. In the structure with heparin present, D3 of the receptor is rotated around the D2-D3 linker region by an additional 170 Å. The two unique receptor conformations are hypothesized to represent a regulatory mechanism for receptor function [47].
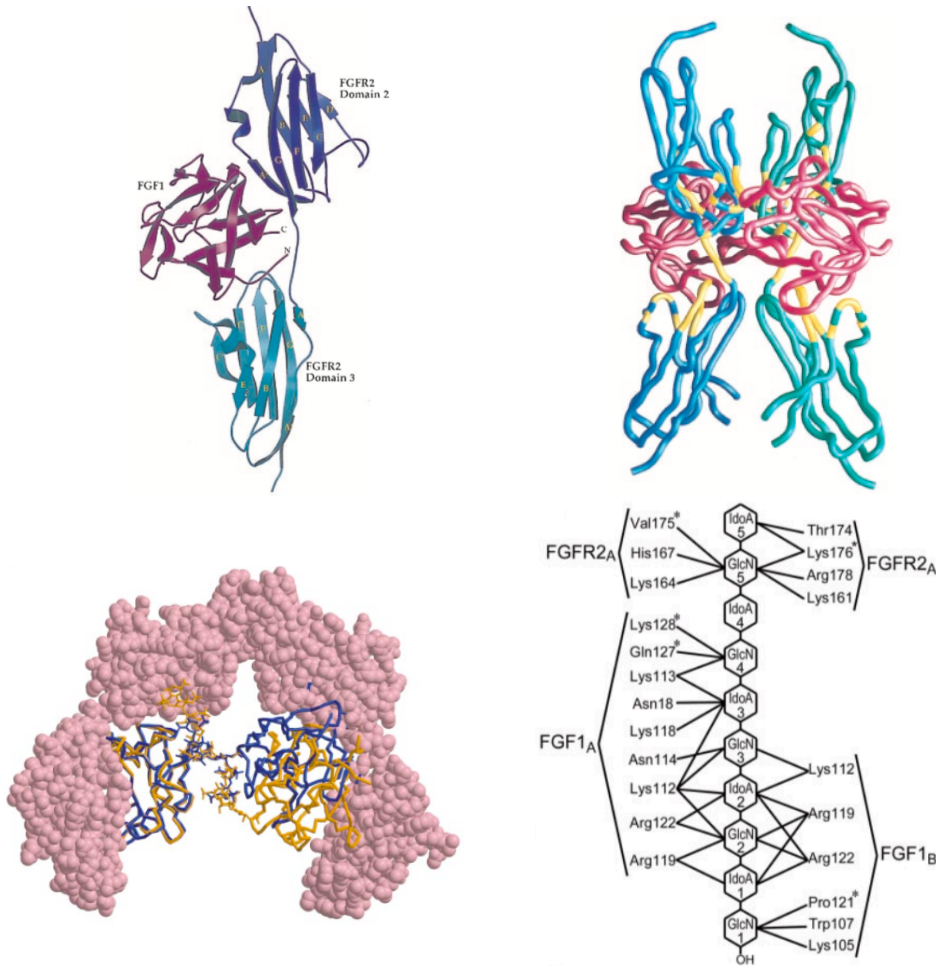
Figure 5. Top left, 1:1 FGF1:FGFR2 complex in the absence of heparin (PDB 1DJS). Top right, 2:2 FGF1:FGFR2 complex in the absence of heparin (D2 and D3 domains are colored in blue and green, FGF1 is colored in red, and receptor contacts with the FGF1 ligand are colored in yellow). Bottom left, 2:2 FGF1:FGFR2 complex in the presence of a heparin decasaccharide (FGFR2 is colored in pink, FGF1 ligand is colored in yellow and blue and heparin is in yellow stick formation) (PDB 1E0O). Bottom right, diagram of heparin contacts with FGF1 and D2.

Signaling cascades

Upon ligand binding, the extracellular domain of FGFRs facilitates receptor-ligand

complex dimerization. The FGF-FGFR dimerization brings the intracellular tyrosine kinase

domains of both receptors in proximity to each other. Juxtaposition of the intracellular domains

coordinates the phosphorylation of one domain by the kinase of the other and vice versa [5, 22].

The phosphorylation of a maximum of six tyrosine residues activates the receptor, and,

depending on the specificity of the FGF ligand, various signaling pathways are then activated. Specifically for FGFR1, the final phosphorylation of Y677 and Y766 induces substrate binding of STAT3, phospholipase Cγ (PCγ), and adaptor proteins such as FGFR substrate 2α. Once the receptor is activated, the receptor phosphorylates adaptor proteins for various intracellular signaling pathways. One of the known pathways is the PCγ pathway, which induces the cleavage of phospholipid phosphatidylinositol 4,5-bisphosphate (PIP2) into diacyl glycerol (DAG) and inositol 1,4,5-triphosphate (IP3). These agents mediate cell activity by activating protein kinase C and increasing intracellular calcium levels respectively.

Another pathway activated by FGFRs is the mitogen-activated protein kinase (MAPK) pathway, which mediates cell proliferation, survival, and mitosis through the activation of specific transcription factors that regulate target gene expression [2]. The third known signaling pathway is the Janus kinase (JAK)/signal transducer and activator of transcription (STAT) pathway, which mediates cell growth and differentiation, and is also reported to regulate immune response. The last major pathway associated with FGFRs is through activation of phosphoinositide 3-kinase and protein kinase B (PI3K-AKT). This pathway encourages cell survival through the inhibition of target molecules including pro-apoptotic effectors. The PI3K-AKT pathway also stimulates cell growth and proliferation by the phosphorylation and inactivation of molecules such as the cytosolic tuberous sclerosis complex 2 (TSC2).

FGF and FGFR regulation

As aberrant FGF/FGFR signaling is known to be involved in tumorgenesis and many other diseases, it is crucial for the signaling mechanisms to be under tight regulation [5]. One simple mechanism for signaling regulation is conducted by the interaction of ubiquitin ligase Cbl

to FGFRs, which results in internalization and degradation of the receptors [2]. Another type of regulation, involving phosphatases, controls the receptor kinase activity and downstream signaling. Growth factor receptor bound 2 (GRB2) is an adaptor protein that in dimeric form has been found to bind the C-terminal of FGFR2, thereby inhibiting complete phosphorylation. Binding of GRB2 also sterically hinders the down stream binding of other adaptor proteins necessary for MAPK and PI3K-AKT signaling pathways [2]. In addition, direct negative feedback loops within signaling pathways such as RAS-MAPK can inhibit the kinase activity of the receptor upon phosphorylation of specific C-terminus residues by ERK1 and ERK2 (downstream kinases activated by the pathway). MicroRNAs are another type of FGF-FGFR regulation that directly influences FGF and FGFR expression at the post-translational stage [2]. MicroRNAs are small noncoding RNAs and many studies have shown that suppression of particular microRNAs cause overexpression of particular FGFs and/or corresponding FGFRs. For example, microRNA-152 is known to down regulate FGF2 expression, and microRNA-198 is reported to down regulate FGFR1. In non-small-cell lung cancer, suppression of microRNAs 152 and 198 leads to the overexpression of FGF2 and FGFR1, which causes hyper proliferation and reduces apoptosis [2].

FGF secretion

As FGFs effectuate their biological properties through binding to cell surface receptors, they must be released from the cell into the extracellular matrix. Most all members of the FGF family except the prototypical members (FGF1 and FGF2) contain at least some type of signal peptide that directs for their secretion out of the cell. FGFs 3-8, 10, 17-19, 21, and 23 contain N-terminus peptides that signal for their secretion through the classical endoplasmic reticulum-

27

Golgi pathway [26]. Other FGFs (9, 16, and 20) have N-terminal hydrophobic sequences that regulate their secretion from the cell [1, 26]. Lastly, FGF1 and FGF2 are secreted non-classically as they do not contain signal peptides.

The secretion of FGF1 and FGF2 is induced by the stress response to various stimuli including heat shock and hypoxia [67]. Many studies on the non-classical release of FGF1 have revealed the order of prerequisites that lead to protein secretion. The first event is the formation of an FGF1 homodimer, which is induced by the oxidation of C30 on FGF1 (causing an intermolecular disulfide bond to form) by intracellular Cu^{2+}. After this, FGF1 associates with S100A13, a calcium binding protein that anchors the complex to the cell membrane. Lastly, FGF1 (as a part of the FGF1/S100A13 complex) binds to the C2A portion of the integral transmembrane protein, synaptotagmin, known as p40Syt1. Finally the ternary complex FGF1/S100A13/p40Syt1 is transported across the membrane.

FGF/FGFR diseases

As FGFs/FGFRs play critical roles throughout all stages of mammalian development, abnormal signaling caused by ligand and/or receptor mutation(s) have been identified in several diseases. One such mutation, D321A, occurring in FGFR2c, causes Pfeiffer syndrome, a disease characterized by irregular cranial bone formation. This mutation reduces FGFR2c binding with FGF2 and increases the aberrant autocrine signaling with FGF10 [22]. Additional mutations such as S252W (located in the linker region connecting D2 and D3) in FGFR2, N546K in FGFR1, N540K (located in the ATP-binding domain) in FGFR3, and G380R (located in the transmembrane domain) in FGFR3 are found to cause skeletal malformations that lead to dwarfism or abnormal cranial development [5, 26, 68]. These malformations are rare and occur

in approximately 1 out of every 5,000 birtheparin.

Kallmann syndrome, a form of hypogonadotropic hypogonadism, is a disease that has been associated with several different frameshift, nonsense, or donor splice mutations within various exons in FGFR1 coding genes [5]. The loss of function mutations leading to Kallmann syndrome, are marked by a lack of hormones needed for sexual development as well as impairment in sense of smell [69]. Without treatment, individuals with Kallmann syndrome will remain infertile. Mutation of P63 in the sterile acid motif of FGFR coding genes, reduces FGFR2 and FGFR3 transcription, and has been associated with Hay-Wells syndrome. This syndrome is a rare ectodermal dysplasia disorder resulting in abnormal development in skin, hair, nails, teeth, hands, and feet [5].

Due to their role in cell survival, growth, and migration, FGFs and their corresponding FGFRs have been associated with tumorgenesis in many kinds of cancers. Their role in the development of cancers occurs through different mechanisms including overexpression and amplification, mutations, gene fusions, and isoform switching/autocrine stimulation [5]. Studies indicate that FGFR1 and FGFR2 amplification across all cancers is 11% and 4% respectively [5]. Specifically, FGF2 is reported to be significantly overexpressed in prostate cancers within stromal fibroblasts and endothelial cells [70]. Additionally, FGFR3 amplification is reported within 45% of muscle invasive bladder cancers [5]. However, cancers in which FGFR amplification is identified are found to be more responsive to FGFR based therapies.

Mutations in FGFs and their receptors are also identified in many cancers. Gain-of-function mutations N546K and R576W in the kinase domain of FGFR1 have been found in glioblastoma brain tumors, and mutations outside of the kinase domain of FGFR1 including A429S and S125L have been associated with colorectal cancer and breast cancer respectively

[26, 68]. Single nucleotide polymorphisms within FGFR2c in stromal fibroblasts cause over expression of FGF10, which is associated with certain mutant related breast cancers [26]. Gain-of-function mutations in FGFR3 are found in multiple myeloma (white blood cell bone cancers), bladder cancers, as well as benign skin cancers [26]. FGFR4 mutations have been associated with a small percent of rhabdomyosarcoma, which occurs in connective muscle tissue [71].

Transforming acidic coiled-coil proteins have been identified as fusion partners specifically for FGFR1 and FGFR3, and ultimately function to increase cell proliferation by upregulating the kinase activity of and diminishing PLCγ binding to the intracellular receptor domain [5]. While additional transfusion proteins have also been determined for FGFRs 1, 2, and 3, cancers that contain these fusion proteins are all found to be suppressed by FGFR inhibitors [5]. Lastly, receptor expression of atypical isoforms in epithelial and stromal cells, known as isoform switching is reported to broaden the sensitivity of that particular tissue to different FGF ligands that ultimately increase cell proliferation and migration. Isoform switching has been reported in prostate cancers and many carcinomas [5]. Extensive review of FGF and FGFR related diseases is completed by Ornitz and Itoh [2].

Many drugs that function as FGFR selective tyrosine kinase inhibitors are in phase II and III clinical trials for treatment of cancers that exhibit FGFR mutations. Additional therapeutics targeting FGFR related cancers include (1) FGFR antibodies, which are isoform specific and avoid unwanted side effects, (2) FGF-ligand traps, which utilize the extracellular portion of an FGFR and target mitogenic FGFs, and lastly (3) allosteric molecules capable of limiting FGFR signaling have also shown promise toward reducing pancreatic cancer progression in mice [5].

Therapeutic applications of FGFs

There is a wide range of developing clinical applications for many different FGFs; however to stay relevant to the aims of this project, only those pertaining to hFGF1 will be examined. Due to its ability to induce cell proliferation, migration, differentiation, and angiogenesis, FGF1 is a critical proponent of regeneration for many tissues including skin, blood vessels, muscle, adipose, bone, and nerve. FGF1 has shown a lot of potential toward tissue regeneration particularly pertaining to cardiovascular disorders. Intramyocardial injection of FGF1 during bypass surgery has shown increased capillary proliferation as well as artery tissue regeneration [26]. FGF1 has been shown to improve peripheral circulation, and injection of FGF1 encoding plasmid is reported to help with ischemia in various parts of the body, which has reduced limb amputation for patients with critical limb ischemia [26]. FGF1 has also been tested with nerve injuries and has been shown to not only repair spinal injuries in rats, but has also helped regenerate motor functions in paralyzed limbs of a young boy [72, 73].

As FGF1 plays a large role through all phases of the wound healing process including inflammation, tissue regeneration, and re-modeling, it is a forerunner in the development of novel wound healing therapies. Acute and chronic wounds such as diabetic foot ulcers, pressure ulcers, and chronic venous leg ulcers are a serious problem in the United States health care system. A reported 71,000 patients with diabetic foot ulcers receive amputations each year, while a 68% mortality rate exists for patients with stage II or IV pressure ulcers [74]. Chronic wound care often requires extended stays at hospitals, and can cost up to hundreds of thousands of dollars per patient all the while diminishing the patient's quality of life through a very painful experience [74]. Studies administrating FGF1 have shown improved and accelerated wound healing in diabetic mice as well as in patients with burn wounds [75].

The delivery of FGF1 for effective tissue regeneration in the wound healing process is another critical component that has been well studied. Single injections of free FGF1 directly to the wound site have proven to be ineffective due to diffusion and inherent limitations of the protein, which lead to significant thermal unfolding and protease degradation [76]. Moreover, FGF1 is most effective when it is continuously applied to the defective area. In response to these issues, the application of FGF1 using delivery methods such as porous scaffolds, hydrogels, and nano-particulates has been well studied.

Porous scaffolds are most commonly made of natural polymers such as collagen, fibrin, and glycosaminoglycans, and FGF1 binds these polymers through electrostatic interactions that prolong the delivery of the protein by a slower release of the protein from the scaffold [76]. The use of self-hardening bioceramics, which includes materials such as calcium phosphates and glass ceramics, is also a developing field for the delivery of FGFs to hard tissues such as bone and teeth [76]. Hydrogels are another delivery method that resembles in *vivo* extracellular matrices better than other delivery methods, and are therefore recognized by cells with ease. FGFs fabricated into hydrogels are very secure and are released by enzymatic reactions or hydrolytic cleavages [76]. The release rate of FGFs from hydrogels can vary greatly depending on the charge characteristics and the biodegradability of the hydrogel material. Lastly nano particles such as micelles, liposomes, and nanospheres (or even microspheres) have gained interest for the specific delivery of FGFs via the blood stream or oral routes. Nano-particles can be made from a variety of natural materials such as gelatin or collagen, but synthetic materials have also been exploited with some success. The delivery rate of the encapsulated growth factor is determined by the composition and size of the nano-particle, which is easily manipulated [76].

Focus of this project and rationale for published paper style dissertation

Amongst all the members of the FGF family, it is the non-selective binding of hFGF1 to all FGFR isoforms that attracts interest towards this particular member for the development of tissue regeneration therapeutics [77]. However, one major drawback regarding the usefulness of hFGF1 for such therapeutics is the inherent instability of the free protein. hFGF1 is known to unfold at physiological temperature, increasing its susceptibility to proteolytic degradation, and thereby severely limiting its bioavailability. With respect to the instability of hFGF1 as well as the ongoing discourse regarding the exact role of heparin in hFGF1 cell signaling, this project contains three distinct aims. These aims are as follows: 1) to genetically engineer novel mutations that increase the inherent stability and cell proliferating activity of hFGF1, 2) to characterize the molecular basis for the stabilizing mutation, R136E, previously discovered in the Kumar group, and 3) to investigate the role of heparin towards hFGF1 facilitated cell signaling. To accomplish these aims, this project was divided into three unique studies. While the focal point of all three studies is hFGF1, each study takes a different approach toward influencing or understanding the stability of the protein and/or its interaction with the ligand heparin. Therefore the project is a compilation of multiple studies that each stand as a separate article.

The first study seeks to increase the inherent stability of hFGF1 via point mutations within the heparin-binding pocket at positions 135 and combined positions 135 and 136. These mutations involve the substitution of proline 135 with charged and polar residues including lysine, glutamate, and glutamine, and the charge reversal of arginine 136 with glutamate. It was anticipated that the introduction of negative charges within the heparin-binding pocket of hFGF1 would stabilize via electrostatic interactions the dense cluster of positive charge that constitutes the heparin-binding pocket in the native wildtype protein. Additionally, the intent of placing

positively charged as well as negatively charged amino acids within the heparin-binding pocket of hFGF1 is to generate variants that will exhibit either an increased or decreased binding affinity for the ligand heparin. Cell proliferation assays on hFGF1 mutants with varying binding affinities for heparin have shed light on the role of heparin within hFGF1 signaling.

The second study aims to further assess the role of heparin with an entirely different approach involving point mutations outside the heparin-binding pocket. In this study, we use site-directed mutagenesis to increase the magnitude of positive charge near the heparin-binding pocket (an area that is rationally believed to interact with long, biologically-relevant chain lengtheparin of heparin) with charge reversal mutations at positions D82 and D84. We then measure the heparin-binding affinity and cell proliferation activity of the hFGF1 mutants. If hFGF1 is dependent on heparin for receptor activation and downstream signaling, then by this premise, an increase in heparin-binding affinity should correlate to an increase in the bioavailability and consequently mitogenic activity of hFGF1 with its cell surface receptors.

The last study focuses on the hFGF1 mutant, R136E, which has been previously recognized for its increased thermostability, reduced affinity for heparin, and significantly increased cell proliferation activity compared to wildtype hFGF1. This study involves the use of two dimensional nuclear magnetic resonance spectroscopy and microsecond length molecular dynamics simulations followed by in-depth analysis to characterize the intramoleular interactions that generate robust characteristics ideal for novel hFGF1 tissue regeneration therapeutics.

Works Cited

1.   Itoh, N., Ornitz, D.M., Evolution of the Fgf and Fgfr gene families. Trends in Genetics, 2004. 20(11): p. 563-569.

2.   Ornitz, D.M., Itoh, N., The Fibroblast Growth Factor Signaling Pathway. WIREs Dev Biol, 2015. 4: p. 215-266.

3.   Ornitz, D.M., Itoh, N., Fibroblast growth factors. Genome Biology, 2001. 2(3): p. 1-12.

4.   Itoh, N., Ornitz, D.M., Fibroblast growth factors: from molecular evolution to roles in development, metabolism and disease. J. Biochem, 2011. 149: p.121-130.

5.   Carter, E.P., Fearon, A.E., Grose, R.P., Careless talk costs lives: fibroblast growth factor receptor signalling and the consequences of pathway malfunction. Trends Cell Biol., 2015. 25(4): p. 221-233.

6.   Miller, D., Ortega, S., Barhayan, O., Basilico, C., Compensation by Fibroblast Growth Factor 1 (FGF1) Does Not Account for the Mild Phenotypic Defects Observed in FGF2 Null Mice. American Society for microbiology, 2000. 20: p. 2260-2268.

7.   Hutley, L., Shurety, W., Fibroblast Growth Factor 1; A Key Regulator of Human Adipogenesis. Diabetes, 2004. 53: p. 3097-3106.

8.   Powers, C., McLeskey, S., Wellstein, A., Fibroblast growth factors, their receptors and signaling. Endocrine-Related Cancer, 2000. 7: p. 165-197.

9.   Zechel, S., Werner, S., Expression and Functions of Fibroblast Growth Factor 2 (FGF-2) in Hippocampal Formation. The Neuroscientist, 2010. 16(4): p. 357-373.

10.   Liao, S., Bodmer, J., Pietras, D., Azhar, M., Doetschman, T., Schultz, J.J., Biological Functions of the Low and High Molecular Weight Protein Isoforms of Fibroblast Growth Factor-2 in Cardiovascular Development and Disease. Developmental Dynamics, 2009. 238: p. 249-264.

11.   Giakoumopoulos, M., Golos, T., Embryonic stem cell-derived trophoblast differentiation: a comparative review of the biology, function, and signaling mechanisms. Journal of Endocrinology, 2013. 216: p. 33-45.

12.   Naiche, L., Holder, N., Lewandoski, M., FGF4 and FGF8 comprise the wavefront activity that controls somitogenesis. PNAS, 2011. 108(10): p. 4018-4023.

13.   Allerstorfer, S., et al., FGF5 as an oncogenic factor in human glioblastoma multiforme: autocrine and paracrine activities. Oncogene., 2008. 27(30): p. 4180-4190.

14. Drogemuller, C., Rufenacht, S., Wichert, B., Leeb, T., Mutations within the FGF5 gene are associated with hair length in cats. Animal Genetics, 2007 38(3): p. 218-221.

15. Armand A.S., Pariset, C., Laziz, I., Launay, T., Fiore, F., Della, G.B., Birnbaum, D., Charbonnier, F., Chanoine, C., FGF6 regulates muscle differentiation through a calcineurin-dependent pathway in regenerating soleus in adult mice. J. Cell Physiol., 2005. 204(1): p 297-308.

16. Guo, L., Degenstein, L., Fucheparin, E., Keratinocyte growth factor is required for hair development but not for wound healing. Genes & Development, 1996. 10: p. 165-175.

17. Fan, E.W., Li, C.C., Wu, W.J., Huang, C.N., Li, W.M., Ke, H.L., Yeh, H.C., Wu, T.F., Liang, P.I., Ma, L.J., Li, C.F., FGF7 Over Expression is an Independent Prognosticator in Patients with Urothelial Carcinoma of the Upper Urinary Tract and Bladder. The Journal of Urology 2015. 194: p. 223-229.

18. Tsai, S.M., Wang, W.P., Expression and Function of Fibroblast Growth Factor (FGF) 7 during Liver Regeneration. Cellular Physiology and Biochemistry, 2011. 27: p. 641-652.

19. Sekine, K., et al., FGF10 is essential for limb and lung formation. Nature Genetics, 1999. 21: p. 138-141.

20. Umemori, H., Linhoff, M.W., Ornitz, D.M., Sanes, J.R., FGF22 and Its Close Relatives Are Presynaptic Organizing Molecules in the Mammalian Brain. Cell, 2004. 118: p. 257-270.

21. Jarosz, M., Robbez-Masson, L., Chioni, A.M., Cross, B., Rosewell, I., Grose, R., Fibroblast Growth Factor 22 Is Not Essential for Skin Development and Repair but Plays a Role in Tumorigenesis. PLos-One, 2012. 7(6).

22. Goetz, R., Mohammadi, M., Exploring mechanisms of FGF signalling through the lens of structural biology. Nat Rev Mol Cell Biol 2013. 14(3): p. 166–180.

23. Crossley, P.H., Martin, G.R., The mouse Fgf8 gene encodes a family of polypeptides and is expressed in regions that direct outgrowth and patterning in the developing embryo. Development, 1995. 121: p. 439-451.

24. Olsen, S.K., Li, J.Y., Bromleigh, C., Eliseenkova, A.V., Ibrahimi, O.A., Lao, Z., Zhang, F., Linhardt, R.J., Joyner, A.L., Mohammadi, M., Structural basis by which alternative splicing modulates the organizer activity of FGF8 in the brain. Genes Dev., 2006. 20: p. 185-198.

25. Haque, T., Nakada, S., Hamdy, R.C., A review of FGF18: Its expression, signaling pathways and possible functions during embryogenesis and post-natal development. Histol Histopathol 2007. 22: p. 97-105.

26.   Beenken, A., Mohammadi, M., The FGF family: biology, pathophysiology and therapy. National Review Drug Discovery 2009. 8: p. 235-253

27.   Miyake, A., et al., Structure and Expression of a Novel Member, FGF-16, of the Fibroblast Growth Factor Family. Biochemical and Biophysical Research Communications, 1998. 243(1): p. 148-152.

28.   Itoh, N., Ohta, H., Roles of FGF20 in dopaminergic neurons and Parkinson's disease. Frontiers in Molecular Neuroscience., 2013. 6: p. 1-4.

29.   Smallwood, P., et al., Fibroblast growth factor (FGF) homologous factors: new members of the FGF family implicated in nervous system development. PNAS, 1996. 93: p. 9850-9857.

30.   Inagaki, T., et al., Fibroblast growth factor 15 functions as an enterohepatic signal to regulate bile acid homeostasis. Cell Metabolism, 2005. 2: p. 217-225.

31.   Kliewer, S.A., Mangelsdorf, D.J., Fibroblast growth factor 21: from pharmacology to physiology. American J Clinical Nutrition, 2010. 91: p. 254-257.

32.   Fukumoto, S., Physiological Regulation and Disorders of Phosphate Metabolism; Pivotal Role of Fibroblast Growth Factor 23. International Medicine, 2007. 47: p. 337-343.

33.   Bernett, M.J., Somasundaram, T., Blaber, M., An atomic resolution structure for human fibroblast growth factor 1. Proteins-Structure Function and Bioinformatics, 2004. 57(3): p. 626-634.

34.   Brych, S.R., Blaber, S.I., Logan, T.M., Blaber, M., Structure and stability effects of mutations designed to increase the primary sequence symmetry within the core region of a β-trefoil. Protein Science 2001. 10: p. 2587–2599.

35.   Zhu, X., Komiya, H., Chirino, A., Three-dimensional structures of acidic and basic fibroblast growth factors. Science, 1991. 251: p. 90-93.

36.   Sweet, R., et al., Crystal structure of the complex of porcine trypsin with soybean trypsin inhibitor (Kunitz) at 2.6 angstrom resolution. Biochemistry, 1974. 13: p. 4212– 4228.

37.   Murzin, A., Less, A., Chothia, C., β-Trefoil fold: Patterns of structure and sequence in the Kunitz inhibitors interleukins-1β and 1α and fibroblast growth factors. J Mol Biol, 1992. 223(2): p. 531-543.

38.   DePaz, J.L., et al., The Activation of Fibroblast Growth Factors by Heparin: Synthesis, Structure, and Biological Activity of Heparin-Like Oligosaccharides. ChemBiochem, 2001 2: p. 673–685.

39.   Casu, B., Naggi, A., Torri, G., Re-visiting the structure of heparin. Carbohydrate Research, 2015. 403: p. 60-68.

40.   Carlsson, P., Kjellen, L., Heparin Biosynthesis. Handbook of Experimental Pharamacology, 2012(207): p. 23-41.

41.   Jacobsson, K.G., Riesenfeld, J., Lindahl, U., Biosynthesis of Heparin, Effects of N-Butyrate on Cultured Mast Cells. J Biol Chem, 1985. 260(22): p. 12154-12159.

42.   Carlsson, P., Presto, J., Spillmann, D., Lindahl, U., Kjellen, L., Heparin/Heparan Sulfate Biosynthesis: Processive formation of N-Sulfated Domains. J Biol Chem, 2008. 283(29): p. 20008-20014.

43.   Gray, E., Hogwood, J., Mulloy, B., The Anticoagulant and Antithrombotic Mechanisms of Heparin. Handbook of Experimental Pharmacology, 2012(207): p. 43-61.

44.   Nugent, M.A., Heparin sequencing brings structure to the function of complex oligosaccharides. PNAS, 2000. 97(19): p. 10301-10303.

45.   Wong, P., Hampton, B., Szylobryt, E., Gallagher, A.M., Jaye, M., Analysis of Putative Heparin-binding Domains of Fibroblast Growth Factor-1. J. Biol. Chem., 1995. 270(43): p. 25805-25811.

46.   DiGabriele, A.D., Lax, I., Chen, D.I., Svahn, C.M., Jaye, M., Schlessinger, J., Hendrickson, W.A., Structure of a heparin-linked biologically active dimer of fibroblast growth factor. Nature, 1998. 393: p. 812-817.

47.   Pellegrini, L., et al., Crystal structure of fibroblast growth factor receptor ectodomain bound to ligand and heparin. Nature, 2000. 407(6807): p. 1029-1034.

48.   Raman, R., Venkataraman, G., Ernst, S., Sasisekharan, V., Sasisekharan, R., Structural specificity of heparin binding in the fibroblast growth factor family of proteins. PNAS, 2003 100: p. 2357–2362.

49.   Pellegrini, L., Role of heparan sulfate in fibroblast growth factor signalling: a structural view. Current Opinion in Structural Biology   2001. 11: p. 629–634.

50.   Harmer, N.J., Insights into the role of heparan sulfate in fibroblast growth factor signalling. Biochemical Society Transactions, 2006. 34(3): p. 442-445.

51.   Arunkumar, A.I., et al., Oligomerization of acidic fibroblast growth factor is not a prerequisite for its cell proliferation activity. Protein Science, 2002. 11: p. 1050-1061.

52.   Angulo, J., et al., Dynamic properties of biologically activity synthetic heparin-like hexasaccharides. Glycobiology, 2005. 15(10): p. 1008-1015.

53.   Canales, A., et al., Solution NMR structure of a human FGF-1 monomer, activated by a hexasaccharide heparin-analogue. Febs Journal, 2006. 273(20): p. 4716-4727.

54.   Chi, Y., Kumar, T.K., Wang, H.M., Ho, M.C., Chiu, I.M., Yu, C., Thermodynamic Characterization of the Human Acidic Fibroblast Growth Factor: Evidence for Cold Denaturation. Biochemistry, 2001. 40: p. 7746-7753.

55.   Culajay, J.F., et al., Thermodynamic characterization of mutants of human fibroblast growth factor 1 with an increased physiological half-life. Biochemistry, 2000. 39(24): p. 7153-7158.

56.   Zakrzewska, M., Krowarsch, D., Wiedlocha, A., Otlewski, J., Design of fully active FGF-1 variants with increased stability. Protein Engineering, Design & Selection, 2004. 17(8): p. 603-611.

57.   Blaber, S.I., Culajay, J.F., Khurana, A., Blaber, M., Reversible Thermal Denaturation of Human FGF-1 Induced by Low Concentrations of Guanidine Hydrochloride. Biophysical Journal, 1999. 77(1): p. 470-477.

58.   Zakrzewska, M., et al., Highly stable mutants of human fibroblast growth factor-1 exhibit prolonged biological action. J Mol Biol, 2005. 352(4): p. 860-75.

59.   Zakrzewska, M., et al., Increased Protein Stability of FGF1 Can Compensate for Its Reduced Affinity for Heparin. Journal of Biological Chemistry, 2009. 284(37): p. 25388-25403.

60.   Dubey, V.K., et al., Spackling the Crack: Stabilizing Human Fibroblast Growth Factor-1 by Targeting the N and C terminus β-Strand Interactions. J. Mol. Biol, 2007. 371: p. 256–268.

61.   Kanodia, J., Greg, F., Role of HEPARINGAGs in Regulation of FGF Signaling Pathway: Insights from Mathematical Modeling. Glycobiology, 2014. 4(1): p. 1000113.

62.   Kimura, H., Okubo, N., Chosa, N., Kyakumoto, S., Kamo, M., Miura, H., Ishisaki, A., EGF Positively Regulates the Proliferation and Migration, and Negatively Regulates the Myofibroblast Differentiation of Periodontal Ligament-Derived Endothelial Progenitor Cells through MEK/ERK- and JNK Dependent Signals. Cellular Physiology and Biochemistry 2013. 32: p. 899-914.

63.   Givol, D., Yayon, A., Complexity of FGF receptors: genetic basis for structural diversity and functional specificity. FASEB J., 1992. 6: p. 3362-3369.

64.   FGFR. Available from: https://www.sigmaaldrich.com/technical-documents/articles/biology/rbi-handbook/protein-serine-threonine-tyrosine-kinases/fgfr.html.

65.   Beenken, A., Eliseenkova, A.V., Ibrahimi, O.A., Olsen, S.K., Mohammadi, M., Plasticity in Interactions of Fibroblast Growth Factor 1 (FGF1) N Terminus with FGF Receptors Underlies Promiscuity of FGF1. J. Biol. Chem, 2012. 287(5): p. 30676-3078.

66.   Stauber, D.J., DiGabriele, A.D., Hendrickson, W.A., Structural interactions of fibroblast growth factor receptor with its ligands. PNAS, 2000. 97(1): p. 49-54.

67.   Kathir, K.M., et al., S100A13-lipid interactions - Role in the Non-classical Release of the Acidic Fibroblast Growth Factor. Biochim Ciophys Acta, 2007. 1768: p. 3080-3089.

68.   Rand, V., et al., Sequence survey of receptor tyrosine kinases reveals mutations in glioblastomas. PNAS, 2005. 102(40): p. 14344-14349.

69.   Dode, C. et al., Loss-of-function mutations in FGFR1 cause autosomal dominant syndrome. Nature Genetics, 2003. 33: p. 1-3.

70.   Giri, D., Ropiquet, F., Ittmann, M., Alterations in expression of basic fibroblast growth factor (FGF) 2 and its receptor in FGFR-1 in human prostate cancer. Clinical Cancer Research, 1999. 5: p. 1063-1071.

71.   Taylor, J.G., et al., Identification of FGFR4-activation mutations in human rabdomyoscarcomas that promote metastasis in xenotransplanted models. J. Clin. Invest., 2009. 119: p. 3395-3407.

72.   Cheng, H., Cao, Y., Olson, L., Spinal cord repair in adult paraplegic rats: partial restoration of hind limb function. Science, 1996. 273: p. 510-513.

73.   Lin, P.H., et al., Spinal cord implantation with acidic fibroblast growth factor as a treatment for root avulsion in obstetric brachial plexus palsy. J Chin Med Assoc, 2005. 68: p. 392-396.

74.   Barrientos, S. et al., Clinical Application of Growth Factors and Cytokines in Wound Healing. Wound Repair Regen., 2014. 22(5): p. 569-578.

75.   Borena, B.M., et al., Regenerative Skin Wound Healing in Mammals: State-of-the-Art on Growth Factor and Stem Cell Based Treatments. Cell Physiol Biochem, 2015. 36: p. 1-23.

76.   Yun, Y.R., Won, J.E., Jeon, E., Lee, S., Kang, W., Jo, H., Jang, J.H., Shin, U.S., Kim, H.W., Fibroblast Growth Factors: Biology, Function, and Application for Tissue Regeneration. Journal of Tissue Engineering, 2010. 2010: p 218142.

77.   Xia, X., Babcock, J.P., Blaber, S.I., Harper, K.M., Blaber, M., Pharmacokinetic Properties of 2nd-Generation Fibroblast Growth Factor-1 Mutants for Therapeutic Application. PLOS-One, 2012. 7(11): p. e48210.

Chapter 1

Probing the role of Proline -135 on the structure, stability, and cell proliferation activity of Human Acidic Fibroblast Growth Factor.

Julie Eberle Davis[1], Arwa Alghanmi[1], Ravi Kumar Gundampati[1], Srinivas Jayanthi[1], Ellen Fields[1], Monica Armstrong[1], Vanessa Weidling[1], Varun Shah[1], Bhanu prasanth Koppolu[2], David A. Zaharoff[2], Thallapuranam Krishnaswamy Suresh Kumar[1*]

1. Department of Chemistry and Biochemistry, University of Arkansas, 1 University of Arkansas, Fayetteville, AR 72701, USA

2. Joint Department of Biomedical Engineering, North Carolina State University and University of North Carolina-Chapel Hill, Raleigh, NC 27695, USA

*To whom all correspondence should be addressed: Prof. TKS Kumar

Email: sthalla@uark.edu

Phone: +1 479-575-5646

Abstract

Human acidic fibroblast growth factor 1 (hFGF1) is a protein intricately involved in cell growth and tissue repair. In this study, we investigate the effect(s) of understanding the role of a conserved proline (P135), located in the heparin binding pocket, on the structure, stability, heparin binding affinity, and cell proliferation activity of hFGF1. Substitution of proline-135 with a positively charged lysine (P135K) resulted in partial destabilization of the protein; however, the overall structural integrity of the protein was maintained upon substitution of proline-135 with either a negative charge (P135E) or a polar amino acid (P135Q). Interestingly, upon heparin binding, an increase in thermal stability equivalent to that of wt-hFGF1 was observed when P135 was replaced with a positive (P135K) or a negative charge (P135E), or with a polar amino acid (P135Q). Surprisingly, introduction of negative charge in the heparin-binding pocket at position 135 (P135E) increased hFGF1's affinity for heparin by 3-fold, while the P135K mutation, did not alter the heparin-binding affinity. However, the enhanced heparin-binding affinity of mutant P135E did not translate to an increase in cell proliferation activity. Interestingly, the P135K and P135E double mutations, P135K/R136E and P135/R136E, reduced the heparin binding affinity by ~3-fold. Furthermore, the cell proliferation activity was increased when the charge reversal mutation R136E was paired with both P135E (P135E/R136E) and P135K (P135K/R136E). Overall, the results of this study, suggest that while heparin is useful for stabilizing hFGF1 on the cell surface, this interaction is not mandatory for activation of the FGF receptor.

Keywords: fibroblast growth factor, heparin binding, charge-reversal, bioactivity, stability

Highlights:

- Mutation of residues P135 and R136 alters heparin-binding affinity of hFGF1.

- The cell proliferation activity of hFGF1 is not correlated to its heparin-binding affinity.

- Mutation R136E increases hFGF1 thermostability and activity independent of heparin.

Abbreviations[1]:

---

[1] human acidic fibroblast growth factor-1 (hFGF1); wildtype hFGF1 (wt-hFGF1); site directed mutagenesis (SDM); circular dichroism (CD); heteronuclear single quantum coherence (HSQC); American Type Culture Collection (ATCC); Visual Molecular Dynamics (VMD); isothermal titration calorimetry (ITC)

Introduction

hFGF1 is a member of a family of polypeptides recognized as powerful mitogens which are involved in cell proliferation, cell differentiation, and wound healing processes [1-5]. FGFs initiate these processes through activation of the tyrosine kinase cell surface receptors (FGFRs). [5-7]. Unlike other family members, human acidic fibroblast growth factor (hFGF1) binds to all four isoforms of FGFRs, rendering this molecule as an ideal target for therapeutic applications [4, 5, 8, 9]. The major caveat in using hFGF1 as a wound-healing agent is its poor inherent stability, which significantly shortens its bioavailability. In fact, a significant population of hFGF1 is known to exist in denatured state(s) at physiological temperatures [10-12].

Binding of hFGF1 to the heavily sulfated cell surface glycosaminoglycan, heparin, is known to confer structural stability leading to its increased physiological half-life [13-15]. Heparin binding occurs at the c-terminal domain of hFGF1 to a cluster of positively charged residues recognized as the heparin binding pocket [16]. Although there is a general agreement that heparin stabilizes hFGF1, the exact physiological role of heparin in hFGF1 mediated signaling is still a subject of debate. Heparin is widely believed to be mandatory for hFGF1 signaling. Crystal structures of the FGF-FGFR- dimeric complexes show that both hFGF1 and its FGFR appear to be associated through their interactions with heparin [17-21]. Site-directed mutagenesis studies have identified a number of mutations that stabilize hFGF1. Furthermore, some of these stabilized hFGF1 mutants have been shown to exhibit increased levels of cellular proliferation activity in the absence of heparin [22,23]. In another study, it has been shown that a charge reversal mutation, K132E, not only diminished heparin binding affinity, but also decreased the mitogenic activity of hFGF1. These studies suggest that heparin binding *per se* is not critical for the activation of the cell surface receptor of hFGF1 [24].

44

hFGF1 has been shown to be susceptible to thrombin action. The proteolytic enzyme has been shown to render hFGF1 inactive by specifically cleaving hFGF1 at the secondary cleavage site, R136 [25]. This aspect has been a significant bottleneck in FGF-based wound care therapeutics because both thrombin and FGF are simultaneously present at a wound site [25, 26]. In this context, we recently studied the effect(s) of a charge reversal mutation at position R136 on the structure, stability, heparin binding affinity and cell proliferation activity of hFGF1. Interestingly, the single point charge-reversal mutation, R136E, was found to reduce hFGF1's affinity to heparin while significantly increasing its cell proliferation activity [27]. In this context, here we examine if similar effects on the structure, stability, and cell proliferation activity can be achieved through substitution of the conserved proline-135 with charged residues.

Proline-135 (P135), located in the heparin-binding pocket is well conserved among the FGF1 family. Previously, using biophysical and molecular dynamics studies we showed that P135G mutation caused a subtle change in the solvent-exposed non-polar surfaces in the protein but it significantly increased the susceptibility of hFGF1 to trypsin protease [16]. In addition, it was found that P135G mutation resulted in the decrease in membrane permeability of hFGF1 and consequently the stress-induced release of the growth factor was significantly affected. In this background we examined the role of P135 on the stability, heparin-binding affinity, and cell proliferation activity of hFGF1. Results of this study for the first time showed that P135 alone and in conjunction with R136 contribute significantly to the heparin structure and bioactivity of hFGF1. In addition, the findings of this study demonstrate that heparin contributes to the stability of hFGF1 but the cell proliferation activity of the growth factor is not strictly dependent on its affinity to bind to heparin.

Results and Discussion

Conservation and spatial microenvironment Proline135 in the structure of hFGF1

The three-dimensional structure of the heparin – hFGF1 binary complex reveals that the c-terminal domain (residues, N120-H138) of the protein plays an important role in heparin binding [19, 28, 29]. Heparin binds to hFGF1 through electrostatic interactions with several positively charged residues (K126, K127, K132, R133, R136) located in this heparin-binding pocket [28]. These positively charged residues are primarily located in the flexible loops between beta strands X, XI, and XII. K127, K132, G134, and R136 are well conserved among different isoforms of FGF. Interestingly, alignment of amino acid sequences of FGF1 isolated from different species shows that the residues in the heparin-binding pocket, including residues 132 to 137, are highly conserved. The well-conserved P135 is located in the loop connecting β-strands XI and XII. P135 is positioned in the center of a triangle with the three positively charged residues (K119, R133 and R136) constituting the three corners of the triangle (Fig 1). Crystal structure of the heparin-hFGF1 binary complex (PDB 2ERM) shows that the Cα atom of P135 is positioned within 4 - 7 Å of the Cα atom(s) of K119, R133 and R136 [28, 29]. The structural rigidity imparted by P135 is believed to be critical for the orientation of the side-chains of the positively charged residues (R133, and R136) to optimally interact with the negatively charged heparin.
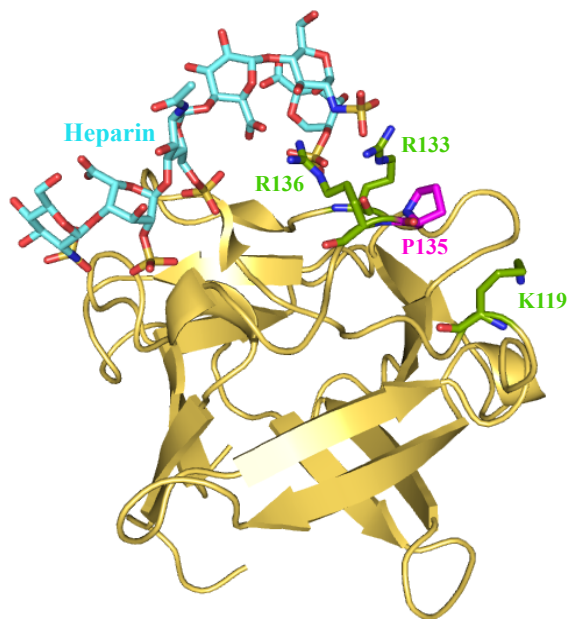
Figure 1: The spatial orientation of P135 (pink sticks) in the loop between beta strands XI and XII in relation to heparin (blue sticks) and charged residues K119, R133, and R136, of which, R133 and R136 are critically involved in heparin binding. The Cα atom of P135 is positioned 3.4Å and 6.2Å from the functional side chains of R133 and R136 respectively. It is 5.4Å from the side chain ε-amino group of K119 (PDB 2ERM) [28].

Mutations at position 135 modestly perturb the tertiary structure of hFGF1.

Wt-hFGF1 and all the designed mutants were purified to homogeneity using heparin Sepharose affinity chromatography (Fig. S1, Appendix 1). Except for the double mutant, P135E/R136E, all the other mutants eluted in high salt concentration (1500 mM NaCl) like wt-hFGF1. P135E/R136E eluted in 500 mM NaCl, suggesting decreased heparin binding affinity. The Far-UV circular dichroism (CD) spectra of the designed mutants of hFGF1 overlaid well with the wild type, exhibiting the characteristic positive ellipticity band in the wavelength range 220 - 240 nm, and a negative band in the region of 200 - 210 nm (Fig. 2). These spectral features indicate that the native β-trefoil conformation is not significantly perturbed due to the designed mutations (Fig. 2).
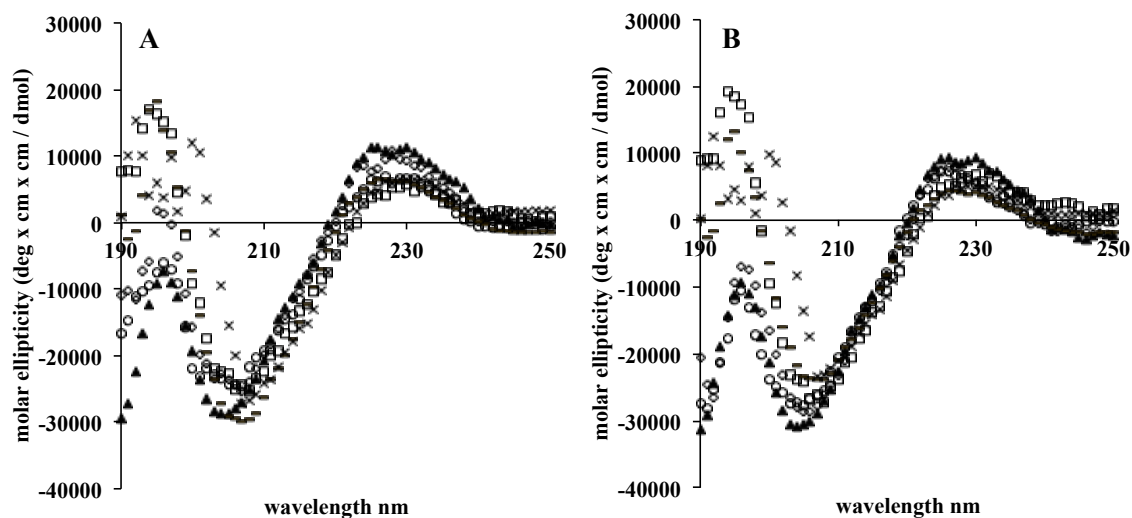
Figure 2: Far-UV CD spectra of wt-hFGF1 and all hFGF1 mutants in the absence (Panel-A) and presence (Panel-B) of heparin reveals that beta-barrel structure is not compromised by any of the designed mutations. Wt-hFGF1 (Δ), P135E (◇), P135K (●), P135Q (□), P135E/R136E (-), P135K/R136E (X).

Wt-hFGF1 contains eight tyrosine residues and a lone tryptophan residue (W121). The intrinsic fluorescence spectrum of native wt-hFGF1 conspicuously shows an emission maxima (at 308 nm) representative of the tyrosine fluorescence. The fluorescence of the single tryptophan residue (W121) is mostly quenched by lysine and proline residues that are in the spatial vicinity of W121 [30]. However, in the denatured state(s) of hFGF1, the indole ring of W121 is exposed to the polar environment, which is manifested by the appearance of the tryptophan fluorescence around 350 nm. Similar to wt-hFGF1, the intrinsic fluorescence spectra of all the designed mutants of hFGF1 showed the characteristic tyrosine emission maximum at 308 nm (Fig. 3). However, unlike wt-hFGF1, all designed hFGF1 P135 single mutants, and the P135/R136 double mutants exhibited, to varying degrees of emission intensity, a broad shoulder in the 350 nm region. The indole side chain of W121 is positioned ~3.5 Å from the pyrrole side chain of P135, thus introduction of a lysine, glutamine, or glutamate at position 135 appears to induce a plausible minor change in the local microenvironment causing an increased solvent exposure of

the indole ring of W121. Interestingly, the relative fluorescence intensity of W121 was modestly

different for each hFGF1 mutant, which could be attributed to local structural perturbations. In

the single mutants, P135E and P135Q, the 350 nm fluorescence intensity was moderately

increased, but the ratio of tyrosine fluorescence at 308 nm to tryptophan fluorescence at 350 nm

was still high (Fig. S2, Appendix 1). However, the 350 nm emission intensity of the P135K

variant was greater than for any other hFGF1 mutant and the 308/350 nm fluorescence ratio was

diminished. This indicates that introduction of a positively charged lysine at position 135 may be

generating charge repulsion with spatially close positively charged residues, K119, R133, and

R136, which might cause significant perturbation of the indole ring of W121. The fluorescence

spectrum of double mutant, P135E/R136E, revealed that the 350 nm emission intensity is

modestly increased in a similar manner as observed in the case of the P135E and P135Q mutants.

Interestingly, the fluorescence spectrum of the double mutant, P135K/R136E, is most similar to

wt-hFGF1. These results indicate that introduction of a negatively charged residue (via the

R136E mutation) appears to negate the destabilizing effects(s) of the P135K mutation.
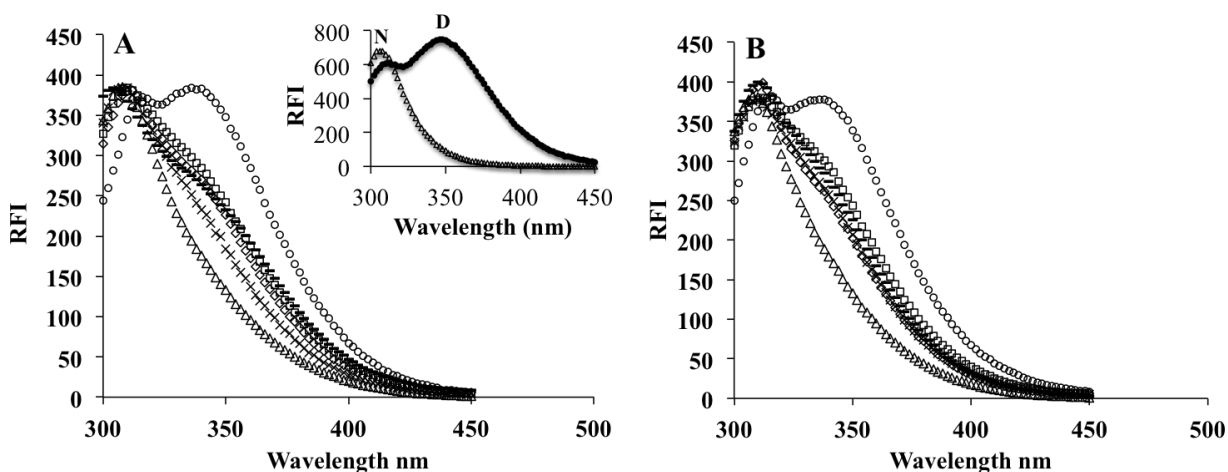

Figure 3: Intrinsic fluorescence spectra for wt-hFGF1 and all hFGF1 mutants in the absence
(Panel-A) and presence of heparin (Panel-B). wt-hFGF1 (Δ), P135E (◇), P135K (⬤), P135Q (
□), P135E/R136E (-), P135K/R136E (X). Inset figure in panel A depicts the fluorescence
spectra of native (N) and denatured (D) wt-hFGF1.

Introduction of positive charge at position 135 increases the structural flexibility of hFGF1

Anilino naphthalene 8- sulfonate (ANS) binding is commonly used to examine the tertiary structural changes in proteins [31]. In this context, we measured the changes in the ANS fluorescence to examine the structural perturbation(s) that was caused by mutations introduced at position 135. ANS is an extrinsic fluorescent probe that binds to solvent-accessible hydrophobic surface(s) in proteins [31]. As hydrophobic residues are typically buried in the protein core, increase in ANS fluorescence is suggestive of greater solvent-accessible hydrophobic surface(s). The ANS binding curves of mutants P135E, P135E/R136E, P135Q, and P135K/R136E are quite similar to wt-hFGF1, indicating the tertiary folding of the hFGF1 does not significantly change due to the introduced mutations (Fig. 4). However, the relative emission intensity of ANS (at 500 nm) upon binding to the P135K mutant is about two-fold higher than when bound to wt-hFGF1, indicating that introduction of positive charge at position 135 induces a modest conformational change causing an increase in the solvent-exposure of the hydrophobic surfaces(s). These results corroborate well with those obtained based on the changes in the intrinsic tryptophan fluorescence.
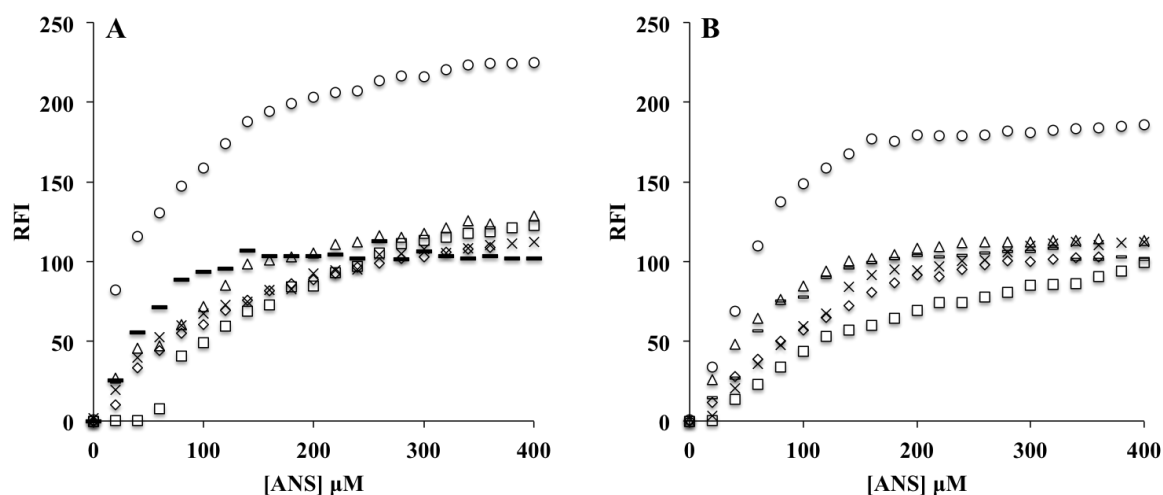

Figure 4: ANS binding curves for wt-hFGF1 and all hFGF1 mutants in the absence (Panel-A) and presence of heparin (Panel-B). wt-hFGF1 (Δ), P135E (◇), P135K (○), P135Q (□), P135E/R136E (-), P135K/R136E (X).

Trypsin, a serine protease, cleaves proteins at the c-terminal end of lysine and arginine residues. Therefore, limited trypsin digestion (LTD) assay is a useful technique to monitor the subtle changes in flexibility of the backbone caused by introduction of the mutations in the heparin-binding pocket of hFGF1 [32]. We performed LTD assay on hFGF1 and the designed mutations of hFGF1, in the presence and absence of heparin, to determine the effect(s) of the individual mutations on the conformational flexibility of hFGF1. Examination of the rate of digestion of wt-hFGF1 and the designed mutants by trypsin, in the absence of heparin, showed that after 40 minutes incubation with the enzyme, wt-hFGF1 and the P135E/R136E mutant are digested by 10% and 20% respectively (Fig. 5 and Fig. S3 Appendix 1). Unlike wt-hFGF1, the P135E, P135K/R136E, and P135Q mutants showed higher susceptibility to trypsin. Their original band intensity, after 40 minutes incubation with trypsin, decreased by ~50%, ~60%, and ~75% respectively (Fig.5A). Introduction of positive charge at position 135 drastically increases the susceptibility of hFGF1 to trypsin degradation, as interestingly, the P135K mutant is 80% digested after the first 10 minutes and is completely digested within 40 minutes exposure to trypsin (Fig. 5 and Fig. S3 Appendix 1). These results suggest that the introduction of an extra positive charge, via the P135K mutation, appears to enhance the flexibility of the backbone due to increased charge repulsions between the cluster of positively charged residues located in the heparin-binding pocket. Alternatively, it may be argued that the increased trypsin susceptibility of the P135K mutant is due to introduction of an additional trypsin cleavage site. However, this possibility is unlikely because the double mutant, P135K/R136E is relatively more resistant to the action of trypsin than the P135K mutant. The lower trypsin susceptibility of the double mutant, P135K/R136E as compared to the single mutant, P135K, appears to suggest that the negative charge introduced at position 136 partially nullifies the enhanced repulsions in the

heparin binding pocket caused by the addition of an extra positive charge via the P135K mutation. In summary, from analysis of the data presented so far, it appears that introduction of negative charge at position P135, individually and in tandem with mutation R136E does not seem to alter the backbone conformation of the protein but in fact appears to render the tertiary structure of hFGF1 more compact.
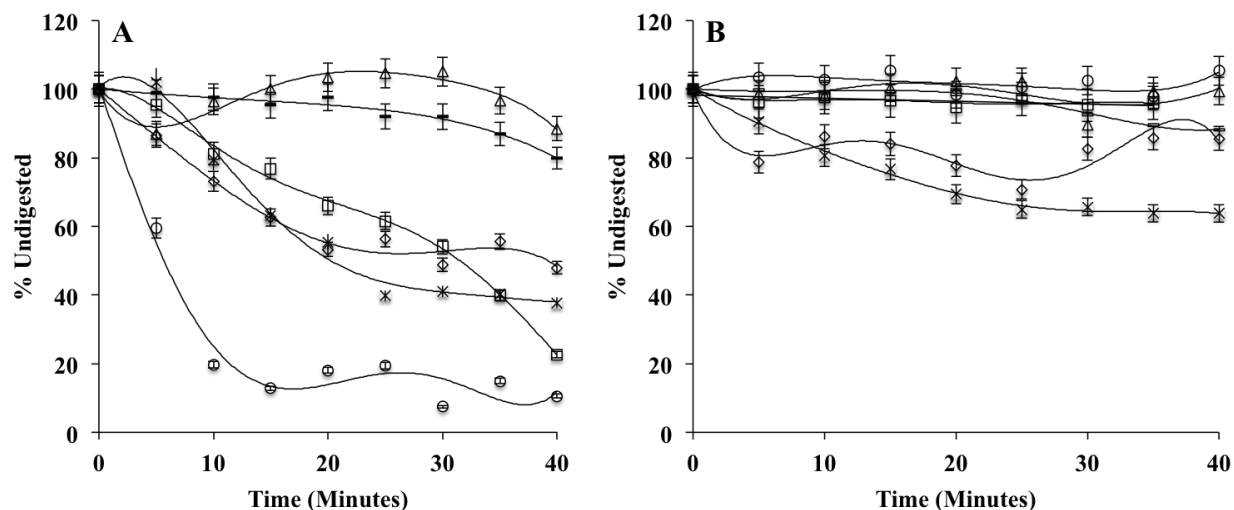

Figure 5: LTD of wt-hFGF1 and all hFGF1 mutants in the absence (Panel-A) and presence of heparin (Panel-B). wt-hFGF1 (Δ), P135E (◇), P135K (●), P135Q (□), P135E/R136E (-), P135K/R136E (X).

Mutations at position 135 only cause local structural changes

^{1}H-^{15}N Heteronuclear single quantum coherence (HSQC) spectroscopy is a two-dimensional NMR technique commonly employed to monitor atomic-level changes in the backbone conformation of proteins. Superimposition of the ^{1}H-^{15}N HSQC spectra of P135K on wt-hFGF1 and analysis of the ^{1}H-^{15}N chemical shift perturbation plot (Fig. 6A & B) indicated that introduction of positive charge at position 135 induces drastic shift in the crosspeak corresponding to G134, which is located in the heparin-binding pocket. In addition, residues T83 and G85, located in the disordered loop that is approximately ~6 Å from P135 were significantly perturbed. Similarly, analysis of the ^{1}H-^{15}N chemical shift perturbation data of the P135E mutant

also revealed that residues located in the heparin-binding pocket (G134, R133, R136, and Y139) expectedly showed significant ^{1}H-^{15}N chemical shift perturbation (Fig. 7A & B). Additionally, residues G85 and T83, which are in spatial proximity to position 135, are also significantly perturbed. The ^{1}H-^{15}N chemical shift perturbation observed for R133 and R136, upon introduction of negative charge at position 135 (P135E), may perhaps be due to the formation of favorable electrostatic interactions that plausibly reorient the positioning of these critical heparin-binding residues. Superimposition of the ^{1}H-^{15}N HSQC spectra of the double mutant P135E/R136E on that of wt-hFGF1 showed that G134 and R136 are the predominantly perturbed residues within the heparin-binding region. T83 and G85 are the most significantly perturbed residues outside of the ligand-binding pocket (Fig. S4 A & B Appendix 1). Overlay of the ^{1}H-^{15}N HSQC spectra of P135K/R136E with wt-hFGF1 indicated that the global structure of the protein is quite similar to wt-hFGF1 (Fig. S5 A & B Appendix 1). With the exception of L87 (which is located on beta strand XII in spatial proximity to position 135), the ^{1}H-^{15}N crosspeaks of most other residues in the protein showed minimal or no perturbation. The multidimensional NMR data obtained from the P135K/R136E double mutant suggests that introduction of a negative charge at position 136 helps to nullify the destabilizing interactions that come into play due to the introduction of an extra positive charge in the heparin binding pocket as a consequence of the P135K mutation. These results are quite consistent with the conclusions drawn from the intrinsic fluorescence, ANS binding, and LTD assays, which suggest that the structural integrity of the protein is maintained as well as the molecular dynamics simulation (MDS) analysis, which suggest that the stabilizing electrostatic interaction(s) are plausibly formed within the heparin-binding pocket as a result of the P135K/R136E mutations.
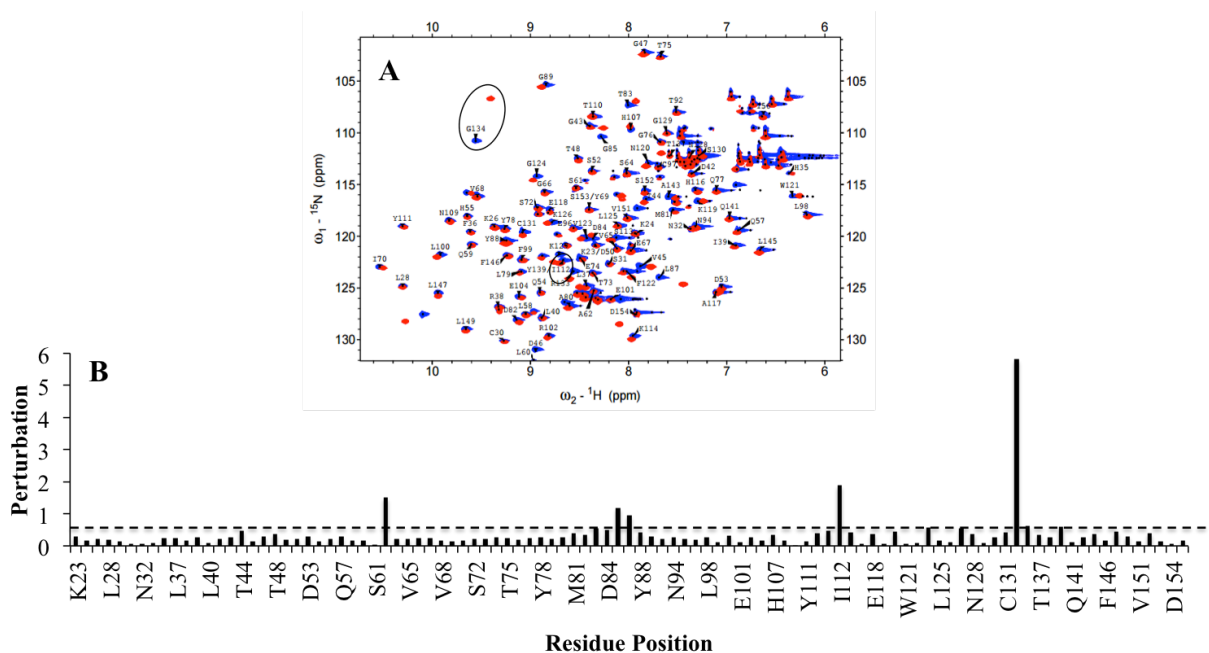
Figure 6: Panel – **A**, The ^{1}H-^{15}N HSQC of wtFGF (red) is superimposed onto P135K (blue). Panel – **B**, the chemical shift perturbation plot of the P135K mutant. The dashed line signifies an arbitrary threshold above which ^{1}H – ^{15}N chemical shift perturbations are considered significant. The ^{1}H-^{15}N chemical shift perturbation of individual residues were calculated using the formula, $(\sqrt{[(2\Delta\delta_{NH})^2 + (\Delta\delta_N)^2]})$.
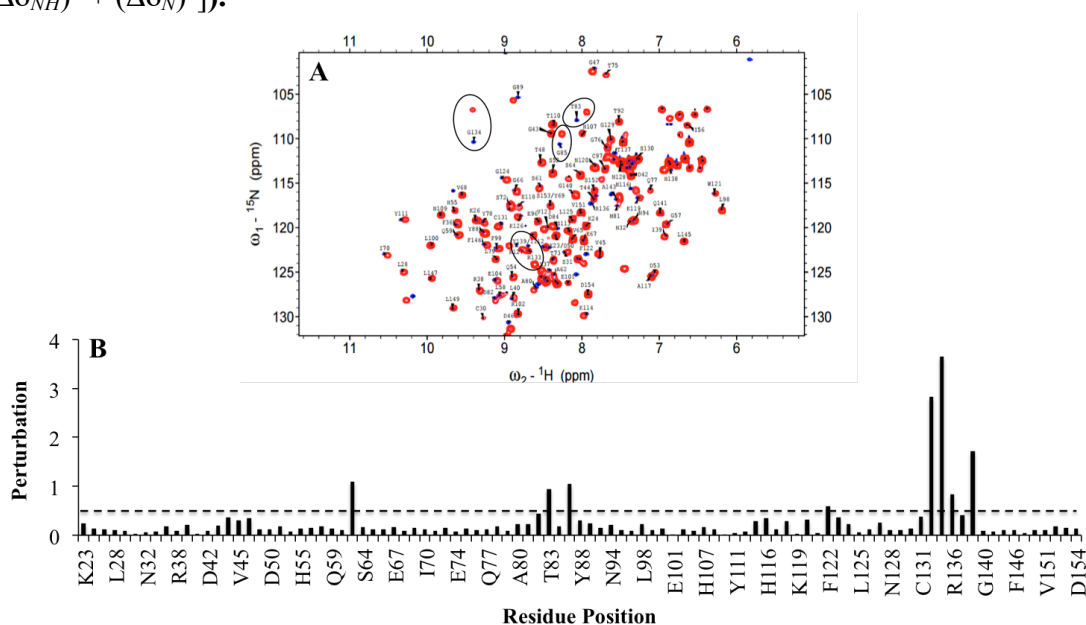

Figure 7: Panel – **A**, The HSQC of wtFGF (red) is superimposed onto P135E (blue). Panel – **B**, the chemical shift perturbation from the P135E mutant. The dashed line signifies an arbitrary threshold above which ^{1}H – ^{15}N chemical shift perturbations are considered significant. The ^{1}H-^{15}N chemical shift perturbation of individual residues were calculated using the formula, $(\sqrt{[(2\Delta\delta_{NH})^2 + (\Delta\delta_N)^2]})$.

Introduction of negative charge at position 135 and/or 136 introduces additional salt bridges and hydrogen bonding in the heparin-binding region of hFGF1.

Molecular dynamics simulations were performed on each of the designed mutants of hFGF1 to gather support for the conclusions drawn from the biophysical experiments. Simulations were performed using the crystal structure of wt-hFGF1 in the absence of heparin (Protein Data Bank code 1RG8). Movies of the simulations are provided in the supporting information (supplemental movie SM1, SM2, SM3, SM4, SM5, and SM6 respectively). From each trajectory, the interdomain distances of the Cα backbone atoms were measured as a function of time, showing no major differences between wt-hFGF1 and all the hFGF1 mutants (Fig. S6 A Appendix 1). Additionally, a comparison of the root mean square fluctuations (RMSF) of the Cα atoms of each mutant to wt-hFGF1 (Fig. S6 B Appendix 1) indicated no significant differences in the RMSF of mutant P135K from wt-hFGF1. The RMSF for mutant P135Q is decreased compared to wt-hFGF1 for certain residues between positions 30 to 80, corresponding to the flexible loop regions of the protein (Fig. S6 B Appendix 1). RMSF of P135E is modestly increased for residue L27 located on beta strand I, residue R49 located on the flexible loop region between beta strands III and IV, and residue K115 within the heparin-binding region. RMSF of double mutant P135E/R136E is modestly lower for residue Q59 as well as residues E67-Y69 found within beta strands IV and V, respectively, but is significantly higher for loop regions containing residue M81 and K115. The RMSF for double mutant P135K/R136E is significantly higher for residues L27, L58, Y69, found on beta strand I, IV and V respectively and is modestly increased for residues P93 and E95 located in the flexible loop region between beta strands VII and VIII.

Salt bridge and hydrogen bonding analyses were also performed on wt-hFGF1 and each

of the designed mutants. In the molecular dynamics simulation of P135K, it was observed that the side chains of R133, K135, and R136 are oriented in relatively opposite directions (Fig. S7 Appendix 1). The guanidinium head groups of the arginine residues were positioned away from each other, plausibly to minimize destabilizing electrostatic repulsion and steric hindrance. Overall, P135K had one fewer salt bridge than wt-hFGF1. Additionally, the P135K mutant contained no hydrogen bonds or salt bridges involving residues R133, K135, and R136 with any other residues located in the spatial vicinity of the heparin-binding region (Table S1 Appendix 1). The absence of any additional stabilizing interactions in the heparin-binding region is also supported by the fluorescence, ANS binding, trypsin digestion, and equilibrium unfolding data.

Similar to the P135K mutant, the P135Q mutant had only one less salt bridge than wt-hFGF1 (Table S1 Appendix 1). Hydrogen bonding analysis revealed the presence of stabilizing hydrogen bonds between the side chain amide group of Q135 and the carbonyl group on the backbone of D84 (Fig. S7 Appendix 1). In addition, hydrogen bonding also occurs between the carbonyl group on the side chain of Q135 and the amide group on the backbone of Q135. Substitution of glutamine for proline at position 135 did not induce stabilizing interactions with residues R136 or R133, which would leave these two critical heparin-binding residues available for interaction with the ligand. Therefore, this observation is consistent with the conclusions drawn from structure and stability data, which suggest that P135Q does not significantly alter the protein stability or interaction(s) with heparin.

Hydrogen bonding analysis of double mutant P135K/R136E revealed stabilizing bonds between the side chain amine group of K135 and the side chain carboxyl group of D84. The salt bridge pattern of double mutant P135K/R136E is identical to wt-hFGF1, which lends support to the conclusions drawn from equilibrium unfolding, ANS, and fluorescence experiments.

Interestingly, no salt bridge was observed to form between K135 and E136; however, E136 was found to be neutralized by a salt bridge formed between E136 and R133 (Fig S7 Appendix 1). Hydrogen bonding was also observed between the side-chain carboxyl group of E136 and the guandinium head group of the side chain of R133 as well as between the amide group on the backbone of E136 and the backbone carbonyl group of R133. These interactions between R133 and E136 may stabilize hFGF1 and diminish hFGF1 affinity for heparin.

Furthermore, one additional salt bridge in the heparin-binding region was observed for mutant P135E between residues E135 and R133. Several additional salt bridges were observed for double mutant P135E/R136E between residues E135 and R133, E136 and K132, and E136 and R133 (Table S1 Appendix 1). For mutant P135E, the interaction between E135 and R133 may plausibly reduce contact between R133 and heparin, consequently diminishing the overall increase in stability of P135E in the presence of heparin. This conclusion is consistent with the thermal stability data of heparin-bound P135E which is ~10 °C less stable than heparin-bound wt-hFGF1 (Table 1). Additionally, the multiple salt bridges formed within the heparin-binding region of P135E/R136E may increase the native protein's overall stability while diminishing the heparin-binding affinity as well as the ability of heparin to influence the thermal stability of this double mutant. These conclusions are consistent with the thermal stability data for P135E/R136E (Table 1).

Heparin binding increases the thermal stability of P135K but not of other hFGF1 mutations

The thermal stability of hFGF1 and the designed mutants, was measured by Far UV CD spectroscopy by monitoring ellipticity changes (at 228 nm). Analysis of the denaturation temperature, T_m (the temperature at which 50% of the protein population exists in the denatured

state(s)), revealed that in the absence of heparin, all the hFGF1 mutants except the double

mutants, P135E/R136E (T_m = 53°C ± 0.87) and P135K/R136E (T_m = 48.5°C ± 0.91), exhibited a

marginally lower thermal stability than wt-hFGF1 (T_m = 48.5°C ± 0.72) (Fig. 8A) (Table 1). In

the presence of heparin, all the designed hFGF1 mutants are less stable than wt-hFGF1.

Interestingly, heparin binding increased the thermal stability of P135K (ΔT_m = 20.8°C) to the

same extent as wt-hFGF1 (ΔT_m = 20.5°C). However, introduction of a negative charge (P135E)

or a polar functional group (P135Q) at position 135 modestly reduced the net increase in T_m

upon binding to heparin [(P135E ΔT_m = 15.3°C) and (P135Q ΔT_m = 16.2°C)] (Fig. 8A). The

total increase in T_m value of P135E/R136E upon binding to heparin was only very modest

~4.7°C. The T_m of the P135K/R136E mutant was not found to increase upon binding to heparin

(Table 1). The insignificant or no increase in stability upon binding to heparin for both the

double mutants (P135E/R136E and P135K/R136E) suggests that the charge reversal at position

136 has a unique effect of diminishing heparin binding affinity of the protein.

The stability of each mutant, in the absence and presence of heparin, was also measured

by urea-induced denaturation (Fig. 8B). In the absence of heparin, for all the designed hFGF1

mutations with the exception of the double mutants, (P135E/R136E (C_m = 1.8M ± 0.67) and

P135K/R136E (C_m = 1.8M ± 0.26), the C_m values (concentration of the denaturant at which 50%

of the protein population is in the denatured state(s) were lower than that of the wt-hFGF1 (C_m =

1.80M ± 0.11) (Table 1). Interestingly, in the presence of heparin, P135E (ΔC_m = 2.6M) was

stabilized to the same extent as wt-hFGF1. Heparin did not stabilize any of the other designed

mutants to the extent it stabilized wt-hFGF1 and P135E. Of the hFGF1 single mutants, P135K

and P135Q were stabilized by heparin the least (Table 1 and Fig. 8B). Lastly, the ΔC_m value(s)

for the double mutants, P135E/R136E (ΔC_m = 0.5M) and P135K/R136E (ΔC_m = 0.9M) were

significantly reduced compared to wt-hFGF1. The lack of heparin-induced stabilization for both double mutants is likely due to the additional stabilizing salt bridges formed within the heparin-binding region previously discussed in the MDS section.

Overall, the thermal and urea equilibrium unfolding data indicate that substitution of proline at position 135 with lysine or glutamine modestly reduced the ability of heparin to stabilize these mutants compared to wt-hFGF1. This may be due to a decrease in structural stability, which is observed from the fluorescence and trypsin digestion data. Furthermore, the presence of the charge reversal mutation at position 136 (R136E) significantly diminished the stabilizing effect(s) of heparin toward hFGF1, as observed with the double mutants P135K/R136E and P135E/R136E (Table 1). These conclusions are in good agreement with the conclusions drawn based on the thermal denaturation data.

Table 1. Thermostability of designed hFGF1 mutants and wt-hFGF1.

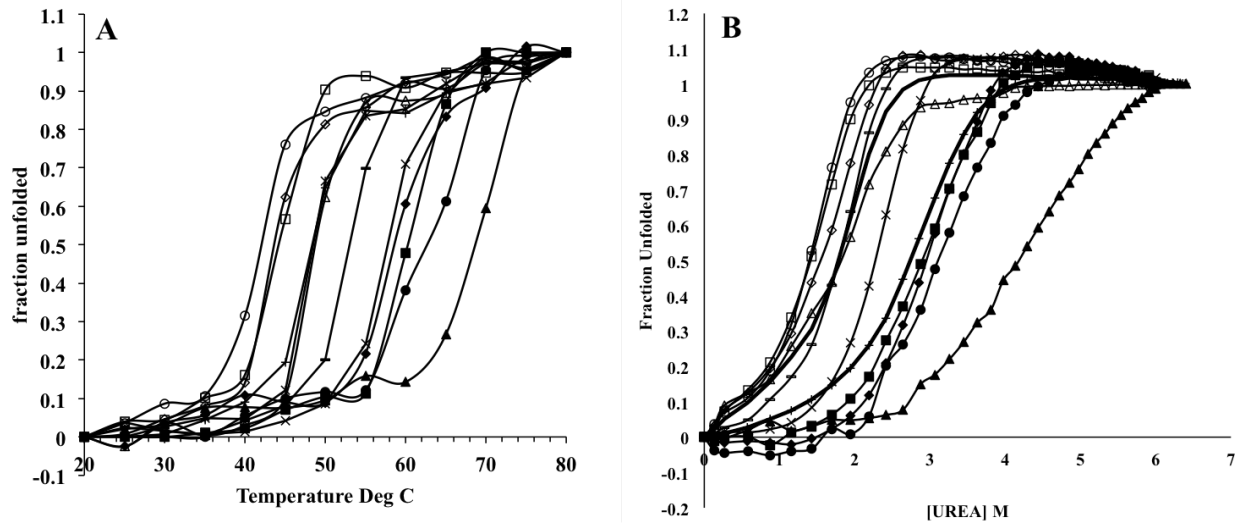|	T_m °C			C_m (M)		
	- heparin	**+ heparin**	**ΔT_m**	**- heparin**	**+ heparin**	**ΔC_m**
wt-hFGF1	48.5 ± 0.72	69 ± 0.68	20.5	1.8 ± 0.11	4.2 ± 0.09	2.4
P135E	43.5 ± 1.3	58.8 ± 0.43	15.3	1.5 ± 0.32	4.1 ± 0.17	2.6
P135K	42 ± 1.0	62.8 ± 0.81	20.8	1.4 ± 0.27	3.1 ± 0.28	1.7
P135Q	44 ± 0.40	60.2 ± 0.50	16.2	1.4 ± 0.27	2.9 ± 0.15	1.5
P135/ER136E	53 ± 0.87	57.7 ± 0.46	4.7	1.8 ± 0.67	2.3 ± 0.60	0.5
P135K/R136E	48.5 ± 0.91	48.5 ± 0.55	0	1.8 ± 0.26	2.7 ± 0.32	0.9

Figure 8: Thermal (Panel-**A**) and urea-induced (Panel-**B**) equilibrium unfolding of wt-hFGF1 and hFGF1 mutants in the presence and absence of heparin. Unfolding was monitored by intrinsic fluorescence and fraction of unfolded protein was determined from changes in fluorescence intensity of the ratio 308/350 nm. Unfolding profile in the absence of heparin: wt-hFGF1 (Δ), P135E (◇), P135K (O), P135Q (□), P135E/R136E (-), P135K/R136E (✳). Unfolding profile in the presence of heparin: wt-hFGF1 (▲), P135E (♦), P135K (●), P135Q (■), P135E/R136E (X), P135K/R136E (+).

Introduction of two negative charges in the heparin-binding pocket reduces heparin-binding

affinity

Isothermal titration calorimetry (ITC) is a useful technique for the determination of the thermodynamic binding parameters characterizing the ligand-protein interactions. Comparison of the binding affinity (K_d) values, representing the interaction of wild type hFGF1 and the P135K mutant with heparin, showed that introduction of positive charge at position 135 does not have any significant effect on the heparin-binding affinity, (P135K K_d = 1.58μM) (Fig. 9). On the contrary, introduction of negative charge at position 135 (P135E) increased the heparin-binding affinity three-fold (P135E K_d = 0.58μM) (Fig. 9). It was originally predicted that introduction of a positive charge at position 135 would increase binding affinity of hFGF1 for heparin and that introduction of a negative charge would likely reduce the affinity for the negatively charged

heparin. However, it appears that the side chain of E and K at position 135 are oriented away from the hFGF1-heparin binding interface because mutations at this site (P135) did not have the anticipated effect on heparin binding. Introduction of a polar functional group at position 135 modestly increased the heparin-binding affinity of hFGF1 (P135Q K_d = 1.02μM) (Fig. 9), which may be due to the slightly more compact structure of the mutant compared to wt-hFGF1 as measured by the ANS fluorescence experiment as well as RMSF values. Introduction of negative charge at combined positions 135 and 136 reduced the affinity of hFGF1 for heparin as expected (P135E/R136E K_d = 4.65μM). Therefore, it appears that the addition of the second negative charge at position 136 drastically reduces the affinity of the protein towards its ligand heparin. These results are in good agreement with the thermal and urea denaturation data. Finally, the double mutant, P135K/R136E, was also found to exhibit reduced binding affinity for heparin (P135K/R136E K_d = 5.56μM) despite introduction of a positive charge at position 135 (Fig. 9). As the single mutant, P135K, did not show increased binding affinity to heparin, the observed reduction in heparin-binding affinity of the double mutant P135K/R136E seems to be largely due to the charge reversal mutation at position 136 (R136E).
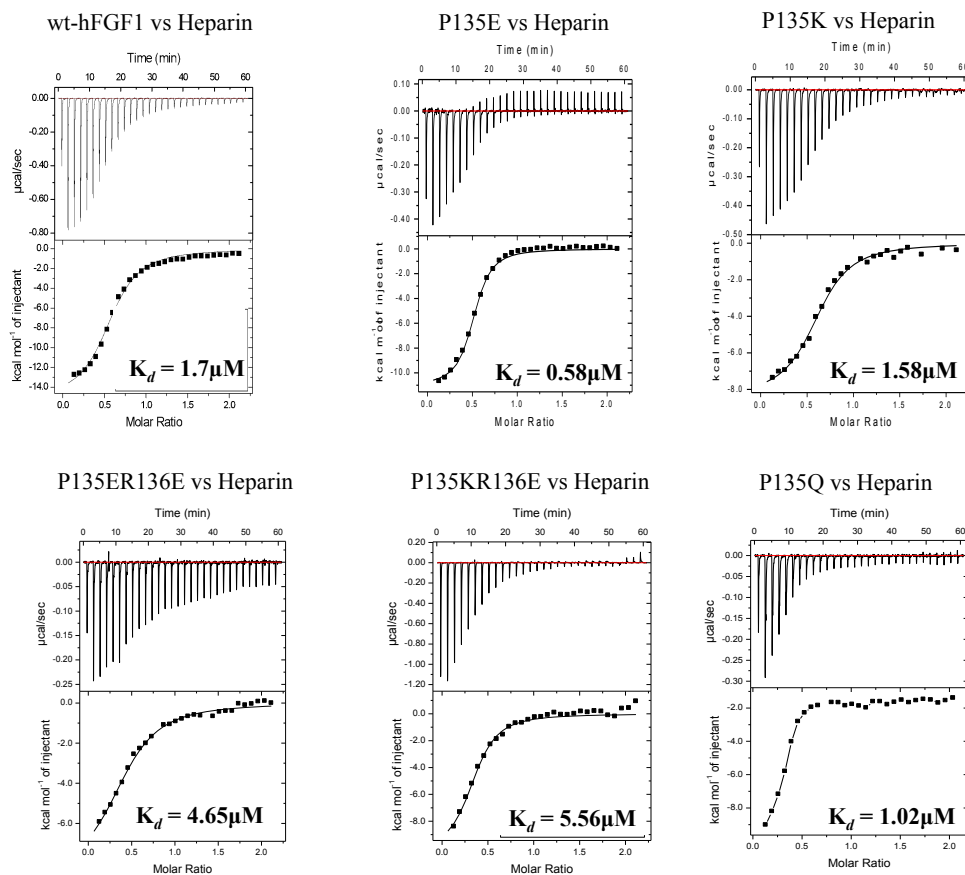
Figure 9: Isothermograms representing the titration of wt-hFGF1 and the individual designed mutants of hFGF1 with heparin. The top panel displays the raw heat changes of heparin-protein interaction and the bottom panel displays the best-fit of the binding curve using a one set-of-sites binding model [14]. All data have been corrected for heats of dilution.

ITC data provides valuable information on the thermodynamics governing protein-ligand interactions as well [14]. The change in enthalpy (ΔH) represents interactions including electrostatic, hydrogen bonding, and van der Waals [14]. The change in entropy (ΔS) represents changes in solvation as well as conformational changes within the protein upon binding with heparin [14]. The enthalpy values characterizing the interaction of heparin with the designed mutants [P135E (ΔH = -1.11 ± 0.2 k.cal mol^{-1}), P135Q (ΔH = -1.08 ± 0.6 kcal mol^{-1}), and P135K/R136E (ΔH = -1.04 ± 0.73 kcal mol^{-1})] of hFGF1 were about half of that compared to the ΔH values representing the wt-hFGF1-heparin interaction (ΔH = -2.14 ± 0.4 k.cal mol^{-1}). These

results suggest that the degree of contact between the designed hFGF1 mutants and heparin is reduced (Table S2). Additionally, the change in enthalpy observed for the interaction of heparin individually with P135K (ΔH = -0.85 ± 0.2 k.cal mol^{-1}) and P135E/R136E (ΔH = -0.85 ± 0.5 k.cal mol^{-1}) were approximately three-fold lower than the wt-hFGF1-heparin interaction, which indicates that the degree of contact between these mutants and heparin is significantly reduced (Table S2). The TΔS values for the interaction of heparin with the individual hFGF1 mutants are five- and ten-fold lower as compared to the interaction of the glycosaminoglycan with wt-hFGF1 (TΔS = -1.1 k.cal mol^{-1}). These results indicate that any conformational change(s) or desolvation occurring at the binding interface of the individual hFGF1 mutants, upon interaction with heparin, are minimized (Table S2). However, despite an increase in the entropic term, all entropic values are still negative and therefore favorable.

Binding affinity does not positively correlate with mitogenic activity

It is generally believed that heparin plays a critical role in the interaction of hFGF1 with its receptor. By this premise, it is likely that an increase in the binding affinity of hFGF1 to heparin would correlate with an increase in the growth factor-mediated mitogenic activity. If so, it can be expected that hFGF1 mutants that exhibit higher binding affinity to heparin than wt-hFGF1 would exhibit enhanced cell proliferation activity. In this context, we measured the proliferation of heparinase treated NIH3T3 cells by wt-hFGF1 and the designed mutants in the presence and absence of heparin (Fig. 10). Maximum cell proliferation with wt-hFGF1 was achieved at a heparin to protein ratio of 10:1, and therefore all cell proliferation assays were performed at this ratio. Fig. 10A shows that in the absence of heparin, mutants P135K and P135E exhibit modestly higher cell proliferation activity than wt-hFGF1. However, in the

presence of heparin, both P135K and P135E showed slightly lower activity than wt-hFGF1 (Fig. 10B). Reduced cell proliferation activity of P135K is perhaps due to the decreased structural stability ascribed to the protein as measured by fluorescence, LTD, and equilibrium unfolding experiments. Interestingly, the structural integrity of the P135E mutant is maintained as measured by fluorescence, LTD, and equilibrium unfolding experiments. In addition, the heparin-binding affinity of P135E is ~ 3-times higher than that of wt-hFGF1 but yet the cell proliferation activity of this mutant is lower than that exhibited by wt-hFGF1. These results suggest that the mitogenic activity of hFGF1 is not strongly correlated to its binding affinity to heparin. In addition, Figures 10 A & B indicate that both double mutants, P135E/R136E and P135K/R136E, in the presence and absence of heparin, exhibit higher cell proliferation activity than wt-hFGF1. We previously reported that the R136E mutation reduced hFGF1's affinity for heparin but increased its cell proliferation activity by about 10-fold [27]. As previously mentioned, ITC data suggests that both double mutants, P135E/R136E and P135K/R136E, have no or insignificant affinity to bind to heparin and the loss of heparin binding affinity is likely to be strongly associated with the introduction of a negative charge at position 136. Overall, the results of the cell proliferation experiments clearly indicate that the heparin binding is not a prerequisite for the mitogenic activity of hFGF1.
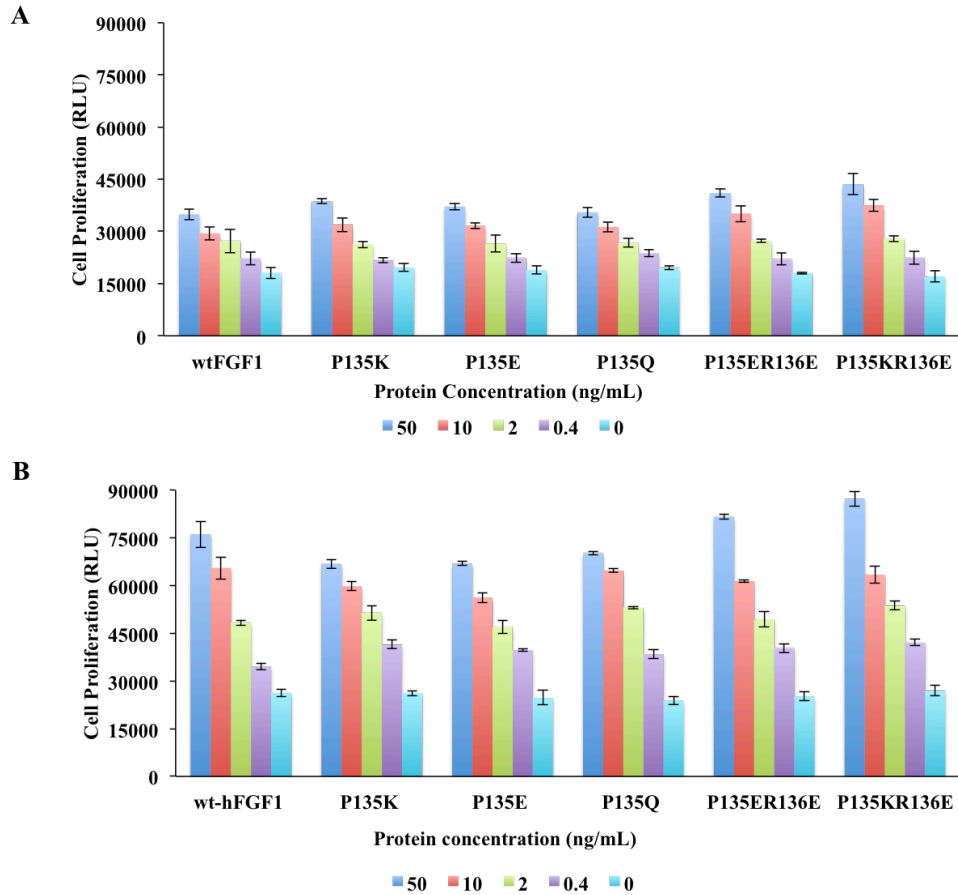
Figure 10: Proliferation of heparinase treated NIH 3T3 cells by wt-hFGF1 and the designed hFGF1 mutants in the absence (Panel-A) and in the presence (Panel-B) of exogenous heparin. Standard errors were determined from triplicate experiments.

The notion that heparin is not mandatory for hFGF1 activation of cell surface receptors has been previously reported [10, 12, 23, 33, 34]. Wong et al (1995) showed that charge reversal K132E did not alter the cell proliferation activity of hFGF1 despite its reduced affinity to heparin [35]. Similarly, Culajay et al (2000) demonstrated that substitution of the three cysteine residues with serine decreased heparin-binding affinity of hFGF1. Additionally, the cysteine to serine substitution(s) increased the physiological half-life of hFGF1 and also enhanced the cell proliferation activity of hFGF1 [12]. Furthermore, combination of mutations L58F, H35Y, H116Y, and F122Y revealed an increased thermal stability, even in the absence of heparin,

without any significant loss in the cell proliferation activity of hFGF1 [10]. Inclusion of mutations at additional sites on the quadruple mutant (L58F/H35Y/H116Y/F122Y) to generate a septuplet mutant (H35Y/Q54P/L58F/S61I/H107G/H116Y/F122Y) increased the stability of hFGF1 significantly [33]. Interestingly, the septuplet mutant was also found to exhibit six-fold higher cell proliferation activity than the wildtype protein in the absence of heparin [33]. In this context, the results of this study clearly show that heparin is not a pre-requisite for the cell proliferation activity of hFGF1. Heparin, present on the cell surface, serves plausibly as a reservoir to facilitate the accumulation of hFGF1 on the cell surface and also to increase the stability of the growth factor through electrostatic interactions.

Conclusion

An understanding of the structure-function relationship between hFGF1 and heparin is important for the design and development of FGF-based therapeutics for wound healing and tissue regeneration applications. The results of the equilibrium unfolding experiments clearly suggest that the primary role of heparin is to confer structural stability to hFGF1. ITC data in conjunction with cell proliferation assays using the double mutants P135E/R136E and P135K/R136E clearly demonstrate the ability of the protein to effectively induce cell proliferation in a heparin independent manner. In addition, the results obtained in this study conclusively suggest that increased affinity for heparin does not necessarily result in increased cell proliferation activity.

Materials and Methods

Materials: DNA plasmid isolation kits were purchased from Qiagen, USA and Quikchange II
XL mutagenesis kits were obtained from Agilent. Competent cells (DH5α and BL-21(DE3))
were sourced from Novagen Inc., USA. Lysogeny broth (LB) was obtained from EMD
Millipore, USA. Heparin sepharose was obtained from GE Healthcare, USA. VWR Scientific
Inc, USA was the supplier for all buffer components including Na_2HPO_4, NaH_2PO_4, NaCl, and
$(NH_4)SO_4$. Low molecular weight heparin sodium salt (~3kDa) was procured from Sigma and
MP Biomedicals LLC. NIH 3T3 cells were sourced from American Type Culture Collection
(ATCC) and additional cell culture reagents such as, DMEM media, fetal bovine serum (FBS),
and penicillin streptomycin were obtained from Thermo Fisher Scientific USA.

Molecular Dynamic Simulations: hFGF1 crystal structure (PDB 1RG8) was visualized using the
Pymol visualizing tool. All mutations were created using Pymol mutagenesis tool [36].
Structures were first energy-minimized for 2000 steps and then immediately solvated in a water
box of 12x12x12 $Å^3$. 0.150 M NaCl was then added to neutralize the solvent box. Following
solvation, the solvent molecules and ions as well as the protein backbone and side chains were
relaxed while hydrogen atoms were kept rigid. Relaxation was performed to prepare the system
for equilibration. Equilibration of the system was implemented in the NPT ensemble utilizing the
CHARMM36 force field and NAMD 2.9 [37, 38]. Side chains were relaxed for 10 picoseconds
(ps) with the backbone fixed in the absence of solvent molecules. Next, water molecules were
relaxed for 1,500 steps around the protein while protein atoms remained fixed. Relaxation of the
system was followed by 50 ps of dynamics. Finally, the solvent molecules were relaxed around
the protein with harmonic constraints using a force constant of 1 kcal/(mol $Å^2$). After relaxation

of the solvent molecules, the temperature of the system was increased in small increments (10 K per 2 ps) until a final temperature of 300 K was reached. Temperature adjustment was followed by 250 ps of dynamics. Temperature (300 K) was sustained by Langevin dynamics with a damping coefficient of 1 ps^{-1} and a pressure of 1 atmosphere with a 100 femtosecond (fs) period, and 50 fs decay time was sustained by the Langevin piston method [39]. Long-distance electrostatic interactions were determined using particle mesh Ewald (PME) method and periodic boundary conditions. Additionally, a switching function was applied to terminate electrostatic and Van der Waals interactions greater than 12 Å. Production runs of 100 nanoseconds (ns) were performed and protein stability was evaluated from the resulting simulations. Visual Molecular Dynamics (VMD) 1.9 was used to visualize the simulation(s) and to trace hydrogen bonding of the mutated residue [40].

Construction and purification of hFGF1 mutants: For site-directed mutagenesis, a form of hFGF1 without the first 14 N terminal residues (residues 15-154) was used. pET20b bacterial expression vector was the template for the site-directed mutagenesis. Agilent primer design software was used to design the desired primers, which were ordered from IDT DNA INC., USA. Instructions provided by the manufacturer for the QuikChange II XL kit were followed to conduct site directed mutagenesis (SDM). The heat shock technique was used to transform the plasmid into DH5α competent cells and the sequence of the plasmid was verified by the University of Arkansas Medical Science – DNA core sequencing facility [41]. Once the correct sequence was verified, overexpression of the wt-hFGF1 and designed mutants was achieved using BL-21(DE3) *Escherichia coli* host cells. Bacterial cells were incubated overnight at 250 rpm and 37°C in LB. It is recognized that hFGF1 overexpressed in *E. coli* lacks post-translational modification; however, no post-translational modification(s), which would alter its

heparin-binding properties in mammalian systems are known to occur to hFGF1,. Following

overexpression, bacterial cells were lysed *via* ultrasonication and the released proteins were

separated from the cell debris by centrifugation for 1 hour at 19,000 rpm. Purification of the

hFGF1 mutants was accomplished using heparin sepharose resin. Purification of hFGF1 was

achieved using a stepwise NaCl gradient in 10 mM sodium phosphate buffer (PB) containing

25mM $(NH_4)_2SO_4$ at pH 7.2 according to methods described previously [42]. Pure hFGF1

protein was typically obtained in the 1500 mM NaCl buffer fraction [10, 23, 33]. Protein purity

was analyzed using SDS-PAGE. Apparent molecular mass of the purified hFGF1 samples was

compared against a prestained standard protein molecular mass marker ranging 7 kDa -175 kDa.

Heparin-binding affinity of hFGF1 mutants: Isothermal titration calorimetry (iTC-200,

Malvern Inc.) was employed to determine the hFGF1–heparin binding affinity. Heat changes

were measured by titrating heparin (loaded in the syringe) into protein solution in the reaction

vessel. All protein and heparin samples were made in solution containing in 10 mM phosphate

buffer with 100 mM NaCl and 25 mM $(NH_4)_2SO_4$ (pH 7.2) and were degassed prior to titration.

A protein concentration of 50 μM and a heparin concentration of 500 μM was consistently used

to maintain a 1:10 ratio of protein to heparin in all ITC experiments. ITC experiment parameters

include a series of 30 titrations performed at 25°C with a stir speed of 1000 rpm. ITC binding

curves were best-fit to one set of sites binding model. Appropriate corrections were applied to

eliminate the contribution from the heats of dilution.

Fluorescence Spectroscopy and 8-Anilino-1-napthalenesulfonic acid (ANS) Binding: Intrinsic

fluorescence experiments and ANS binding assays were performed at 25°C on a Hitachi F-2500

fluorescence spectrophotometer. All fluorescence measurements were made using a slit width set

to 2.5 nm. A protein concentration of 0.1 mg/mL [in 10 mM phosphate buffer containing 100

mM NaCl, and 25 mM $(NH_4)_2SO_4$ (pH 7.2)] was used in all intrinsic fluorescence experiments.

For samples containing heparin, the glycosaminoglycan was present in 10-times molar excess of

the protein concentration to achieve saturated binding of heparin. All intrinsic fluorescence

measurements were acquired using an excitation wavelength of 280 nm and an emission

wavelength range of 300 nm – 450 nm. ANS binding assays were carried out with protein

concentrations of 0.25 mg/mL in 10 mM phosphate buffer containing 100 mM NaCl and 25 mM

$(NH_4)_2SO_4$ (pH 7.2). ANS binding measurements were performed by adding 1μL of ANS (from

a stock solution of 0.01 μM) into the protein solution such the concentration of the fluorescent

dye increased in 20 μM increments. After each titration, the reaction mixture was excited at 380

nm and the relative fluorescence intensity at 500 nm was recorded.

Circular Dichroism Spectroscopy: Far-UV CD measurements were performed using a protein

concentration of 0.5 μg/μL at 25 °C on a Jasco 1500 spectropolarimeter. Protein samples were

prepared in 10mM phosphate buffer containing 10 mM NaCl and 25 mM $(NH_4)_2SO_4$ (pH 7.2).

Far-UV CD spectra acquired in the presence of heparin, were performed with a protein to

heparin ratio of 1:10 to ensure complete heparin saturation of hFGF1. All data were normalized

using necessary background corrections and smoothed using the Savitzky-Golay algorithm. In

samples containing heparin, the contribution of excess heparin to the observed ellipticity was

normalized by making appropriate background corrections.

Limited Trypsin Digestion: For limited trypsin digestion (LTD) experiments, a 1:100 ratio of

enzyme (5 μg) to substrate (500 μg) was dissolved in 10 mM phosphate buffer containing 100

mM NaCl and 25 mM $(NH_4)_2SO_4$ at pH 7.2. LTD experiments completed in the presence of

heparin contained the glycosaminoglycan in ten times molar excess the protein concentration to

achieve complete protein saturation. hFGF1 samples, incubated at 37°C, were withdrawn at 5-

minute intervals and the reaction was stopped with the addition of 100% trichloroacetic acid prior to analysis on SDS PAGE. The percentage of hFGF1 sample digested by trypsin, at different time points, was calculated by densitometry [using UN-SCAN IT (Silk Scientific Inc., USA)] by comparison with the Coomassie blue stained band intensity of ~17 kDa protein withdrawn at the zero time point.

Equilibrium unfolding of hFGF1 mutants: Thermal and chemical denaturation experiments were completed using a Jasco-1500 spectropolarimeter equipped with fluorescence detector. For thermal unfolding, protein samples were made using a protein concentration of 0.5 mg/mL in 10 mM phosphate buffer containing 100 mM NaCl and 25mM $(NH_4)_2SO_4$ at pH 7.2. For spectra collected in the presence of heparin, a protein to heparin ratio of 1:10 was used. Spectra were collected in 5 degrees increments from 20°C to 80°C. T_m, temperature at which 50% of the protein molecules exist in the denatured state(s), was calculated from the plot of fraction of unfolded protein population *versus* temperature.

Urea-induced equilibrium unfolding of hFGF1 samples was measured using the fluorescence mode on the Jasco – 1500 spectropolarimeter. Urea-induced unfolding experiments were performed at a protein concentration of 3 μM protein in 10 mM phosphate buffer containing, 100 mM NaCl and 25mM $(NH_4)_2SO_4$ at pH 7.2. Far-UV CD and intrinsic fluorescence spectra were recorded individually on a protein sample at increasing concentrations of urea. At each concentration of urea both the molar ellipticity value at 228 nm and the ratio of the 308 nm /350 nm emission intensity was measured. The fraction unfolded of the proteins species, at each concentration of urea, was calculated from both sets of data. Spectra were collected as an average of 3 scans using a quartz cell of 1 cm pathlength.

Nuclear Magnetic Spectroscopy: NMR spectra were obtained on a Bruker 500 MHz NMR, equipped with a cryoprobe, using 2K x 256 data points. ^{1}H-^{15}N Heteronuclear single quantum coherence (HSQC) experiments were performed at 25°C using a protein concentration of at least 300 μM in 10 mM phosphate buffer containing 100 mM NaCl and 25 mM $(NH_4)_2SO_4$ (pH 7.2). Protein samples were isotopically labeled with ^{15}NH$_4$Cl and the samples prepared using well-established methods [43]. 2D NMR data were analyzed using Sparky 3.114 software [44]. Composite ^{1}H-^{15}N chemical shift perturbation for each residue was calculated using the equation, $\sqrt{[(2\Delta\delta_{NH})^2 + (\Delta\delta_N)^2]}$. ^{1}H-^{15}N chemical shift perturbations, in the presence of heparin, were carefully tracked by acquiring a series of ^{1}H-^{15}N HSQC spectra at various heparin: protein ratios. However, for a few residues, the ^{1}H-^{15}N chemical shift perturbation(s) could not be precisely monitored and these residues were not considered in the final presentation of the ^{1}H-^{15}N chemical shift perturbation data.

Cell proliferation activity: NIH 3T3 fibroblast cells (supplied by ATCC (Manassas, VA)) were cultured in DMEM supplemented with 10% FBS and 1% penicillin/streptomycin. When cells reached 80-90% confluency, they were incubated overnight in serum-free media at 37°C with 5% CO_2. Cell surface heparin was removed by treating the NIH 3T3 cells with 6 units of heparinase per 10,000 cells for 1 hour at 37°C. Cells were then washed twice with PBS and returned to complete DMEM.. Following heparinase treatment, an optimum heparin: protein ratio was determined by conducting the cell proliferation assays at different heparin concentrations and a fixed wt-hFGF1 concentration of 10 ng/mL (Fig. S8 Appendix 1). Maximum cell proliferation activity was achieved at a protein: heparin ratio of 1:10, and this ratio was used in all experiments wherein exogenous heparin was added. In brief, starved 3T3 fibroblasts were distributed in a 96-well plate at a density of 10,000 cells/well. wt-hFGF1 and

mutants were individually added at concentrations of 0, 0.4, 2, 10 and 50 ng/mL and incubated

for 24 hours. The CellTiter-Glo (Promega, Madison, WI) cell proliferation assay was used

following the manufacturer instructions to quantify the proliferation of NIH 3T3 cells.

Acknowledgements

Works Cited

1. Mason, I.J., The Ins and Outs of Fibroblast growth factors. Cell Press, 1994. p. 547-552.
2. Wilkie, A.O.M., Functions of fibroblast growth factors and their receptors. Cell Press, 1995. 5(5): p. 500-507.

3. Itoh, N., Fibroblast growth factors: from molecular evolution to roles in development, metabolism and disease. J. Biochem, 2011. 149: p. 121-130.

4. Ornitz, D.M., Itoh, N., The Fibroblast Growth Factor Signaling Pathway. WIREs Dev Biol, 2015. 4: p. 215-266.

5. Katoh, M., Therapeutics Targeting FGF Signaling Network in Human Diseases. Trends in Pharmacological Science, 2016. 37(12): p. 1081-1096.

6. Eswarakumar, V.S., Lax., Cellular Signaling by Fibroblast Growth Factor Receptors. Cytokine & Growth Factor Reviews, 2005. 16: p. 139-149.

7. Carter, E.P., Fearon, A.E., Grose, R.P., Careless talk costs lives: fibroblast growth factor receptor signalling and the consequences of pathway malfunction. Trends Cell Biol., 2015. 25(4): p. 221-233.

8. Miller, D., Ortega, S., Barhayan, O., Basilico, C., Compensation by Fibroblast Growth Factor 1 (FGF1) Does Not Account for the Mild Phenotypic Defects Observed in FGF2 Null Mice. Mol Cell Biol., 2000. 20: p. 2260-2268.

9.   Beenken, A., Eliseenkova, A.V., Ibrahimi, O.A., Olsen, S.K., Mohammadi, M., Plasticity in Interactions of Fibroblast Growth Factor 1 (FGF1) N Terminus with FGF Receptors Underlies Promiscuity of FGF1. J Biol Chem, 2012. 287(5): p. 30676-3078.

10.   Zakrzewska, M., Krowarsch, D., Wiedlocha, A., Otlewski, J., Design of fully active FGF-1 variants with increased stability. Protein Engineering, Design & Selection, 2004. 17(8): p. 603-611.

11.   Dubey, V.K., et al., Spackling the Crack: Stabilizing Human Fibroblast Growth Factor-1 by Targeting the N and C terminus β-Strand Interactions. J Mol Biol, 2007. 371: p. 256 – 268.

12.   Culajay, J.F., Blaber, S.I., Khyrana, A., Blaber, M., Thermodynamic characterization of mutants of human fibroblast growth factor 1 with an increased physiological half-life. Biochemistry, 2000. 39(24): p. 7153-8.

13.   Yu-Peng, H., et. al., Divergent Synthesis of 48 Heparan Sulfate-Based Disaccharides and Probing the Specific Sugar−Fibroblast Growth Factor - 1 Interaction. J American Chemical Society, 2012. p. 20722−20727.

14.   Brown, A., Robinson, C.J., Gallagher, J.T., Blundell, T.L., Cooperative Heparin-Mediated Oligomerization of Fibroblast Growth Factor-1 (FGF1) Precedes Recruitment of FGFR2 to Ternary Complexes. Biophys J, 2013. 104: p. 1720-1730.

15.   Hook, M., Kjelleʹn, L., Johansson, S., Robinson, J., Cell-surface glycosaminoglycans. Annu. Rev. Biochem 1984. 53: p. 847–869.

16.   Prudovsky, I., et al., Folding of Fibroblast Growth Factor 1 Is Critical for Its Nonclassical Release. Biochemistry, 2016. 55(7): p. 1159-67.

17.   Ornitz, D.M., Itoh, N., Fibroblast growth factors. Genome Biology, 2001. 2(3): p. 1-12.

18.   Harmer, N., Insights into the role of heparan sulphate in fibroblast growth factor signalling. Biochemical Society Transactions, 2006. 34(3): p. 442-445.

19.   Pellegrini, L., Burke, D.F., Von Deift, F., Blundell, T.L., Crystal structure of fibroblast growth factor receptor ectodomain bound to ligand and heparin. Nature, 2000. 407(6807): p. 1029-1034.

20.   Pellegrini, L., Role of heparan sulfate in fibroblast growth factor signalling: a structural view. Current Opinion in Structural Biology, 2001. 11: p. 629–634.

21.   DePaz, J.L., et. al., The Activation of Fibroblast Growth Factors by Heparin: Synthesis, Structure, and Biological Activity of Heparin-Like Oligosaccharides. ChemBiochem, 2001. 2: p. 673–685.

22.   Szlachcic, A., et al., Structure of a highly stable mutant of human fibroblast growth factor 1. Acta Cryst, 2009. 65: p. 67-73.

23.   Zakrzewska, M., et al., Increased Protein Stability of FGF1 Can Compensate for Its Reduced Affinity for Heparin. J Biol Chem, 2009. 284(37): p. 25388-25403.

24.   Arunkumar, A.I., et. al., Oligomerization of acidic fibroblast growth factor is not a prerequisite for its cell proliferation activity. Protein Science, 2002. 11: p. 1050-1061.

25.   Erzurum, V.Z., et al., R136K fibroblast growth factor-1 mutant induces heparin-independent migration of endothelial cells through fibrin glue. J Vascular Surgery, 2003. 37(5): p. 1075-1081.

26.   Duarte, M., et al., Thrombin induces rapid PAR1-mediated non-classical FGF1 release. Biochem Biophys Research Communications. 2006. 350: p. 604-609.

27.   Thallapuranam, S.K., Engineered Compositions of FGF and Methods of Use Thereof. Patent Application No. 15/474,268, filed March 30, 2017.

28.   DiGabriele, A., Structure of a heparin-linked biologically active dimer of fibroblast growth factor. Nature, 1998. 393: p. 812-817.

29.   Canales, A., et al., Solution NMR structure of a human FGF-1 monomer, activated by a hexasaccharide heparin-analogue. FEBS Journal, 2006. 273(20): p. 4716-4727.

30.   Callis, P., et. al., Binding phenomena and fluorescence quenching. II: Photophysics of aromatic residues and dependence of fluorescence spectra on protein conformation. J Mol Structure, 2014. 1077: p. 22-29.

31.   Gabellieri, E., Strambini, G.B., Perturbation of Protein Tertiary Structure in Frozen Solutions Revealed by 1-Anilio-8-Napthalene Sulfonate Fluorescence. Biophysical Journal, 2003. 85(5): p. 3214-3220.

32.   Lindh, E., et al., Increased Resistance of Immunoglobulin a Dimers to Proteolytic Degradation after Binding of Secretory Component. J Immunol, 1975. 114: p. 284-286.

33.   Zakrzewska, M., Krowarsch, D., Wiedlocha, A., Olsnes, S., Otlewski, J., Highly stable mutants of human fibroblast growth factor-1 exhibit prolonged biological action. J Mol Biol, 2005. 352(4): p. 860-75.

34.   Xia, X., et al., Properties of 2nd-Generation Fibroblast Growth Factor-1 Mutants for Therapeutic Application. PLOS-One, 2012. 7(11): p. e48210.

35.   Wong, P., Hampton, B., Szylobrgt, E., Gallagher, A.M., Jaye, M., Burgess, W.H., Analysis of Putative Heparin-binding Domains of Fibroblast Growth Factor-1. J. Biol. Chem., 1995. 270(43): p. 25805-25811.

36.   Bernett, M.J., Somasundaram, T., Blaber, M., An atomic resolution structure for human fibroblast growth factor 1. Proteins-Structure Function and Bioinformatics, 2004. 57(3): p. 626-634.

37.   Olsson, et al., Propka3: consistent treatment of internal and surface residues in empirical pKa predictions. J. Chem. Theory Comput., 2011. 7: p. 525-537.

38.   Best, et al., Optimization of the additive CHARMM all-atom protein force field targeting improved sampling of the backbone ϕ, ψ and side-chain $\chi 1$ and $\chi 2$ dihedral angles. J. Chem. Theory Comput., 2012. 8: p. 3257-3273.

39.   Martyna, G.J., Tobias, D.J. Klein, M.L., Constant pressure molecular dynamics algorithms. J. Chem. Phys., 1994. 101: p. 4177-4189.

40.   Humphrey, W., Dalke, A., Schulten, K., VMD: Visual Molecular Dynamics. J. Mol. Graph., 1996. 14: p. 27-28, 33-38.

41.   Froger, A., Hall, J.E., Transformation of Plasmid DNA into E. coli Using the Heat Shock Method. J. Visualized Experiments, 2007. 6: p. 253.

42.   Eberle Davis, J., et al., Effect of Extension of the Heparan Sulfate Binding Pocket on the Structure, Stability, and Cell Proliferation Activity of the Human Acidic Fibroblast Growth Factor. Biochemistry and Biophysics Reports, 2018. 13: p. 45-57.

43.   Marley, J., Lu, M., Bracken, C., A method for efficient isotopic labeling of recombinant proteins. J. of Biomolecular NMR, 2001. 20: p. 71-75.

44.   Goddard, T.K., DG., SPARKY 3. University of California, San Francisco.

Chapter 2

Effect of Extension of the Heparin Binding Pocket on the Structure, Stability, and Cell Proliferation Activity of the Human Acidic Fibroblast Growth Factor.

Julie Eberle Davis[1], Ravi Kumar Gundampati[1], Srinivas Jayanthi[1], Joshua Anderson[1], Abigail Pickhardt[1], Bhanu prasanth Koppolu[2], David A. Zaharoff[2], Thallapuranam Krishnaswamy Suresh Kumar[1*.]

1. Department of Chemistry and Biochemistry, University of Arkansas, 1 University of Arkansas, Fayetteville, AR 72701, USA

2. Joint Department of Biomedical Engineering, North Carolina State University and University of North Carolina-Chapel Hill, Raleigh, NC 27695, USA

*To whom all correspondence should be addressed: Prof. T. K.S. Kumar

Email: sthalla@uark.edu

Phone: +1 479-575-5646

Abstract

Acidic human fibroblast growth factor (hFGF1) plays a key role in cell growth and proliferation. Activation of the cell surface FGF receptor is believed to involve the glycosaminoglycan, heparin. However, the exact role of heparin is a subject of considerable debate. In this context, in this study, the correlation between heparin binding affinity and cell proliferation activity of hFGF1 is examined by extending the heparin binding pocket through selective engineering via charge reversal mutations (D82R, D84R and D82R/D84R). Results of biophysical experiments such as intrinsic tryptophan fluorescence and far UV circular dichroism spectroscopy suggest that the gross native structure of hFGF1 is not significantly perturbed by the engineered mutations. However, results of limited trypsin digestion and anilino naphthalene 8-sulfonate (ANS) binding experiments show that the backbone structure of the D82R variant is more flexible than that of the wild type hFGF1. Results of the temperature and urea-induced equilibrium unfolding experiments suggest that the stability of the charge-reversal mutations increases in the presence of heparin. Isothermal titration calorimetry (ITC) data reveal that the heparin binding affinity is significantly increased when the charge on D82 is reversed but not when the negative charge is reversed at both positions D82 and D84 (D82R/D84R). However, despite the increased affinity of D82R for heparin, the cell proliferation activity of the D82R variant is observed to be reduced compared to the wild type hFGF1. The results of this study clearly demonstrate that heparin binding affinity of hFGF1 is not strongly correlated to its cell proliferation activity.

Keywords: fibroblast growth factor, heparin binding, stability, cell proliferation

Highlights

- Extension of heparin pocket via point mutations increases ligand binding of hFGF1.

- hFGF1 cell proliferation activity is not well correlated to heparin binding affinity.

- Heparin confers stability to hFGF1 but is not vital for receptor signaling.

Abbreviations[2]

---

[2] human fibroblast growth factor-1 (hFGF1); site directed mutagenesis (SDM); circular dichroism (CD); heteronuclear single quantum coherence (HSQC); American Type Culture Collection (ATCC), Visual Molecular Dynamics (VMD), Isothermal titration calorimetry (ITC)

Introduction

FGFs are a family of polypeptides involved in a wide range of core signaling processes that govern cell growth, cell proliferation, cell differentiation, stress response and wound healing [1-7]. FGFs exert their action(s) by binding to their cell surface receptors (FGFRs) [1, 6-9]. FGF1 is the only member of the FGF family that binds with high affinity to all four types of FGFRs [10, 11]. Formation of the hFGF1/FGFR complex, initiates the processes of dimerization and autophosphorylation of the intracellular tyrosine kinase domain, ultimately triggering downstream signaling [12].

hFGF1-receptor interaction is believed to be highly dependent on heparin, a glycosaminoglycan that is commonly found in the extracellular matrix of mammalian cells at concentrations up to 10^6 units per cell [5, 13-15]. heparin consists of long, unbranched, helical chains of repeating disaccharide units, which are heavily sulfonated [13]. heparin is also believed to be critical for the biological activity of hFGF1 [16]. Crystal structures of the hFGF1/FGFR complex suggest that heparin directly contacts both hFGF1 and the receptor [16].

Crystal and solution structures of the heparin -FGF complex show that the glycosaminoglycan binds to a cluster of positively charges residues, which are located at the c-terminal end of the molecule. The residues involved in the putative heparin -binding pocket of hFGF1 include K126, K127, K132, R133, R136, and K142 [17]. These heparin -binding amino acids form a region of concentrated positive charge that renders hFGF1, in its unbound form, to be relatively unstable and prone to thermal and proteolytic degradation [4, 18-20]. Therefore, hFGF1 binding to heparin increases the stability of the growth factor [8, 9]. Furthermore, heparin's interaction with FGFRs stabilizes the hFGF1-FGFR binary complex [5, 16, 21, 22]. However, there has been a long-standing debate on whether heparin is obligatory for hFGF1

activity. The initial "dogma" describes heparin's role as a mandatory co-receptor that is critical for cell signaling events triggered by hFGF1 [14, 16, 23, 24]. However, there are significant reports to the contrary, which suggest that heparin is only necessary for stabilizing the growth factor [4, 12, 18, 20, 25, 26]. In this context, the debate on the exact role of heparin in the FGF1 signaling process is still an open question.

Several studies using a site-directed mutagenesis approach have identified several conserved residues, which, when appropriately mutated, increased the thermodynamic stability of hFGF1. In addition, several mutant forms of hFGF1 have exhibited mitogenic activity even in the absence of heparin [4, 12, 18-20, 25, 26]. One notable mutation is the charge-reversed substitution K132E in the heparin -binding pocket, which was found to reduce hFGF1's affinity for heparin [12]. Interestingly, it has been shown that introduction of thermally stabilizing mutations into hFGF1 variants with reduced affinity for heparin, such as K132E, have been shown to compensate for lack of heparin involvement in FGFR activation [12]. While these studies suggest that heparin binding to hFGF1 is not critical for the protein's mitogenic activity, heparin is still opined to have a critical role in hFGF1 receptor binding and signaling [9, 27-29].

One approach to assess the role of heparin that has yet to be investigated is the evaluation of hFGF1 activity using mutations that are predicted to increase heparin binding. In this context, we have studied the correlation between heparin-binding affinity and cell proliferation activity of hFGF1 by designing charge-reversal mutations in the vicinity of the heparin binding pocket involving the substitution of aspartic acid for arginine at position 82 and 84 (PDB 2ERM) [17]. Specifically, D82R and D84R mutations have been designed to extend the heparin-binding interface on hFGF1. Crystal structures of hFGF1, both with and without heparin, were used to measure the distance between the carboxyl side chain group of D82 and the guanidinium side

chain group of R133. Comparison of these measurements reveals that the position of D82 in the heparin-bound hFGF1 structure is 6 A° farther away from the heparin-binding region than it is in the native hFGF1 structure. D82N is also included as a control mutant to determine if a lack of negative charge at this position influences the protein's structure, stability, activity, and interaction differently than the D82R mutant.

Results of this study show that charge reversal at position 82 destabilizes hFGF1 structure. Furthermore, although charge reversals D82R and D84R increase heparin-binding affinity, they do not concomitantly increase the cell proliferation activity of hFGF1. The results obtained in this study strongly suggest that heparin merely increases the bioavailability of hFGF1 at the cell surface and thereby enhances the probability of a productive hFGF1-receptor interaction. For this study, all protein samples were derived from expression in *E. coli*, an expression system that lacks post-translational modification. However, hFGF1 is not known or predicted to undergo post-translational modification that would potentially affect the heparin binding.

Results and Discussion

Human acidic fibroblast growth factor (hFGF1) is a beta-barrel protein with 12 antiparallel beta-strands. The canonical heparin-binding pocket is located at the c-terminal end between beta strands 10 and 12. Positively charged residues densely populate the heparin-binding pocket in the protein. Site-directed mutagenesis studies have shown that the positively charged residues in the heparin-binding pocket are critical for the heparin binding affinity of hFGF1 [30, 31]. In this study, we have used low weight molecular heparin as it is well known that high molecular weight heparin is polydispersed, containing a heterogeneous mixture of

heparin molecules of varying chain lengtheparin. The high polydispersity poses significant

technical challenge in the interpretation of the NMR results. In addition, in our experience, the

high polydispersity also presented serious problems in calculating the average molecular weight,

which in-turn adversely influenced the heparin concentration determination(s). The low

polydispersity of the low molecular heparin significantly diminished the above-mentioned

technical difficulties. Furthermore, the low molecular weight (M_r~ 3000 Da) heparin used has

been estimated to be 8 to 12 units long and multiple studies have shown that heparin with a chain

length of 8-uints has been shown to be sufficient to facilitate optimal FGF-induced cell signaling

[13, 32, 33].

Spatial proximity of D82/D84 to the putative heaprin-binding pocket

Residues D82 and D84 are located on the protein surface within the linker region

connecting beta strands 6 and 7 (Fig. 1). In the folded conformation of hFGF1, both D82 and

D84 residues appear to be fully solvent-exposed [17]. Thus, neither amino acid is involved in the

inner core network of hydrogen bonding or electrostatic interactions stabilizing the three-

dimensional structure of the protein. The side chain carboxyl groups of D82 and D84 are located

within a spatial distance of 5 A° from T83, L86, L87, and Y88. Neither D82 nor D84 is a part of

the canonical heparin-binding pocket. The position of both D82 and D84 in relation to R133,

which is in the midst of the heparin-binding pocket, was measured using crystal structures of

native hFGF1 in the presence (PDB 2ERM) and absence of heparin (PDB 1RG8) [17, 32]. In the

absence of heparin, D82 and D84 are positioned ~6.9 Å and ~6.1 Å, respectively, away from the

critical heparin-binding residue R133 (PDB 1RG8) [32]. In the presence of a hexasaccharide

heparin chain (PDB 2ERM), D84 is shifted modestly closer to R133 (~5.8 Å) while D82 is measured at ~12.8 Å from R133.

Using the crystal structure of hFGF1-heparin-FGFR ternary complex (PDB 1E0O), as well as a structure of the symmetrical hFGF1 dimer bound to a decasaccharide heparin chain (PDB 1AXM), it was determined that D82 of each hFGF1 monomer is within 8 - 11 Å from the sulfate groups of the third unit (D-glucosamine) in the heparin chain [23]. Replacement of aspartic acid with arginine at position 82 (D82R) in both hFGF1 monomers would bring the side chain even closer to the sulfate groups of heparin. It is evident from the crystal structure(s) of both complexes (PDB 1E0O and 1AXM) that the heparin chain must be approximately ten saccharide units long to facilitate the heparin-induced dimerization of hFGF1 [23]. Furthermore, taking in to account the dynamic nature of the molecular interaction(s), the side chain of arginine at position 82 and 84 would be placed within 3 to 8 Å of the closest sulfate group on heparin. Thus, substitution of D82 and D84 with arginine apparently would result in the extension of the heparin-binding pocket in hFGF1 and consequently can be potentially expected to provide additional points of contacts for the glycosaminoglycan binding.

Brown *et al.* showed that heparin fragments smaller than the octasaccharide cannot facilitate dimerization and are not physiologically relevant. Furthermore, the binding between hFGF1 and heparin is shown to exhibit a positive cooperativity that preferentially forms oligomers instead of 1:1 complexes, thus suggesting that chain lengths of heparin longer than the octasaccharide are more pertinent to the biological activity of hFGF1 [13]. In addition, it was demonstrated that a single heparin chain of molecular mass ~16 kDa can bind up to fifteen hFGF1 molecules [13]. In addition, the alpha helical backbone of heparin is shown to undergo

conformational change(s) upon binding to hFGF1 [34]. Although heparin is a relatively rigid

molecule in solution, it tends to be kinked upon binding to hFGF1 with alterations in the

backbone torsion angles. The kinked backbone structure of heparin is conducive for favorable

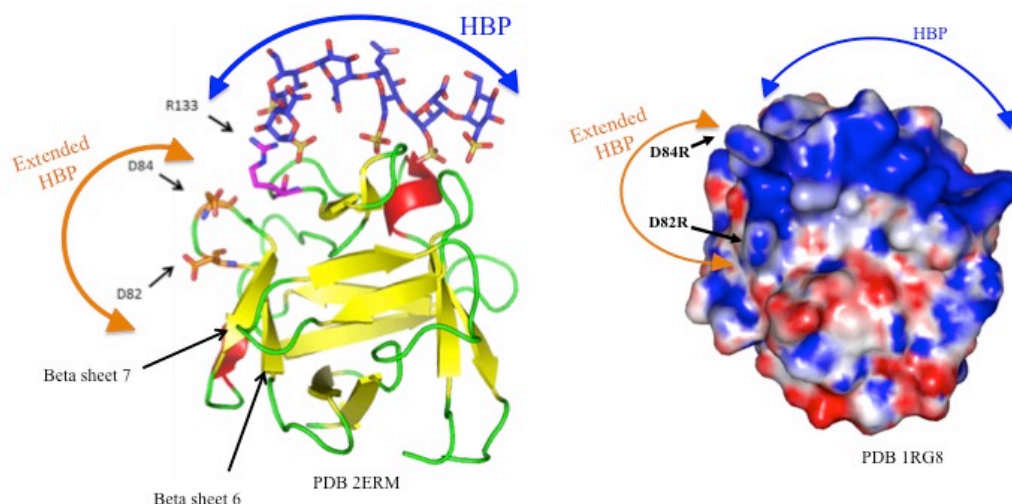electrostatic and van der Waals interactions with hFGF1 [13].

Figure 1: Left -Three-dimensional structure of hFGF1 (PDB 2ERM) depicting the side-chain of the positively charged residue R133 in the heparin-binding pocket. The heparin-binding pocket has been extended through reversal of charge on D82 (D82R) and D84 (D84R). Right - Representation of the electrostatic potential in the three-dimensional structure of hFGF1 showing that charge reversal(s) at D82 and D84 extends the heparin-binding region of hFGF1 (PDB 1RG8).

Individual charge reversals induce stabilizing hydrogen bonding

Molecular dynamic simulations were run to further assess the conclusions drawn from

fluorescence, trypsin digestion, and equilibrium unfolding experiments. All simulations were

completed using the crystal structure of hFGF1 in the absence of heparin (Protein Data Bank

code 1RG8). Still images of each simulation (Fig. S1, Appendix 2) as well as movies of each

simulation are provided in the supplementary material (SM 7-11). Interdomain distances of the

Cα backbone atoms were measured as a function of time for each trajectory and root mean

square fluctuation (RMSF) for the Cα atoms of each mutant were also determined (Fig. 2A and B). The root mean square deviation (RMSD) of mutant D82N and double mutant D82R/D84R are most similar to wt-hFGF1 showing no major jumps or significant fluctuations. RMSD calculations for D84R slowly increase over the course of the trajectory and reach a maximum of 1.4 Å between the 80-90 ns time mark. This maximum for D84R is modestly higher than the RMSD of wt-hFGF1 suggesting an increased level of flexibility. Increased flexibility within the D84R structure is also observed from RMSF calculations specifically for the loop within the heparin-binding region around residue G129 as well as for a solvent exposed loop outside of the heparin-binding region around residue E95 (Fig. 2B).

Interestingly the RMSD calculation for mutant D82R reveals a jump up to 2 Å around the 70 ns time mark, indicating increased flexibility compared to wt-hFGF1 (Fig. 2A). Furthermore, RMSF values for D82R also show increased flexibility compared to wt-hFGF1 among residues in the heparin-binding region (residues V109-G129). This data supports conclusions drawn from fluorescence and trypsin digestion experiments. RMSF calculations for mutant D82N and double mutant D82R/D84R both show overall reduced flexibility among several loop regions outside of the heparin-binding region of the protein. This data along with the RMSD measurements support conclusions drawn from fluorescence and trypsin digestion data that these respective mutations (D82N and D82R/D84R) result in a more compact protein structure.

Salt bridge and hydrogen bonding analysis were also completed for each hFGF1 mutant and wt-hFGF1. Analysis of the D82R trajectory reveals two additional salt bridges that are not present in wt-hFGF1 (Table 1). One salt bridge is formed between the guanidinium head group of R82 and the side chain carboxyl group of D84, which are both on the same loop region between beta strand 6 and 7, and therefore this salt bridge is not an interdomain stabilizing

interaction (Fig. 2A, Table 1). The other salt bridge occurs between the side chain carboxyl

group of D84 and the guanidinium head group of heparin-binding residue, R133. However,

despite the fact that this is an interdomain interaction, it does not increase the stability of the

protein in the presence of heat or the chemical denaturant, urea (Fig. 7A, B, Table 2). Similarly,

results of the molecular dynamics simulation of the D84R mutant reveal salt bridge formation

between the guanidinium head group of R84 and the side chain carboxyl group of D82 (Table 1).

Interestingly, these interactions are not present in wt-hFGF1 probably due to repulsion between

the closely placed negative charges of D82 and D84.

The molecular dynamics simulation of the D82N mutant indicates that hydrogen bonding

occurs between the backbone amide group of N82 and the backbone carbonyl group of L86 but

there is also additional hydrogen bonding between the side chain carbonyl group of N82 and the

backbone amino group of L86 (See supplementary movie). Analysis of salt-bridge formations for

the D82N mutant reveals an assessment identical to that of wt-hFGF1 (Table 1). Double charge

reversal at combined positions 82 and 84 does not induce the hydrogen bonding that is observed

with individual charge reversal mutations (See supplementary movie). In fact, analysis of the

results of molecular dynamics simulation of the double mutant, D82R/D84R reveal that the

guanidinium head groups of R82 and R84 are oriented away from each other. The side chain of

R84 appears moderately flexible while R82 is primarily locked into a rigid position due to

stabilizing hydrogen bonds formed between the guanindinium head group and the carboxyl side

chain of E96 located in the neighboring loop region. Analysis of salt bridge formations for

D82R/D84R reveals no significant difference compared to wt-hFGF1 except for the addition of a

stable bond between E118 and K119 within the heparin-binding region. Altogether, the results of

molecular simulations indicate that the introduction of positive charge at position 82 increases

the flexibility of the protein structure among loops in the heparin-binding region, and does not induce any stabilizing interdomain salt-bridges.
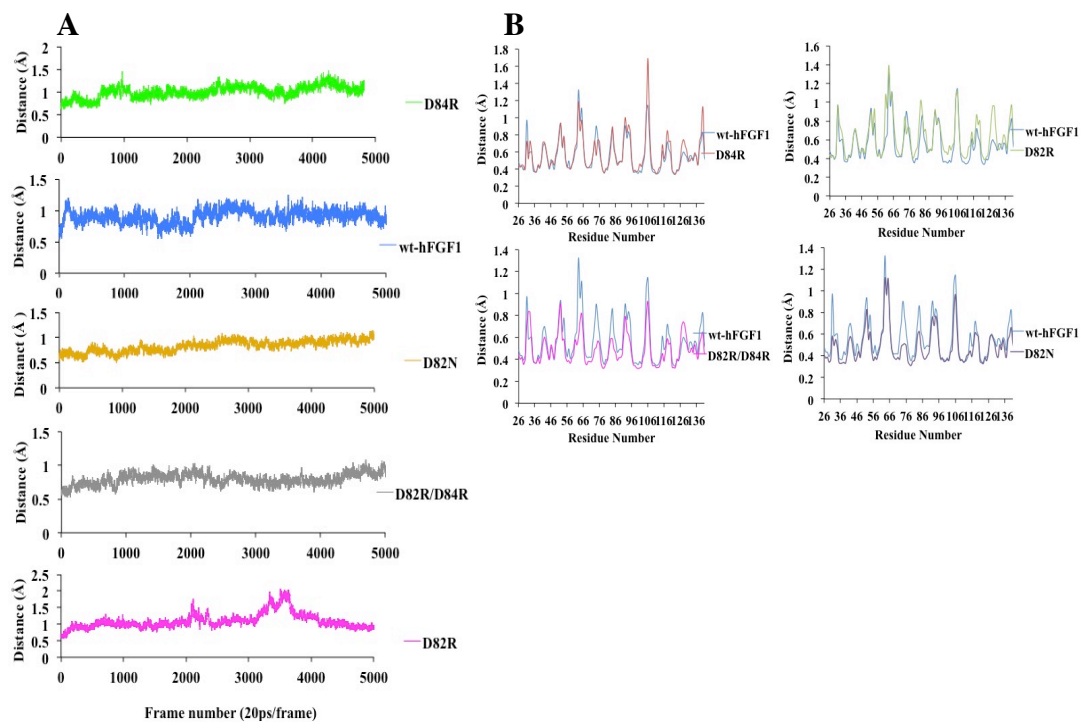

Figure 2: Panel-**A** Interdomain distances of the Cα backbone atoms as a function of time for each simulation. Panel-**B** overlay of RMSF values for each designed hFGF1 mutant with wt-hFGF1.

Table 1. Salt bridge analysis for each designed hFGF1 mutant and wt-hFGF1.

Stable Salt Bridges

wt-hFGF1	D46-R38	D53-R38			E67-K114	E95-K115	E105-K142	
D82R	D46-R38	D53-R38	D84-R82	D84-R133	E67-K114	E95-K115	E105-K142	
D84R	D46-R38	D53-R38	D82-R84		E67-K114	E95-K115		E118-K119
D82N	D46-R38	D53-R38			E67-K114	E95-K115	E105-K142	
D84R/D82R	D46-R38	D53-R38			E67-K114	E95-K114	E105-K142	E118-K119

D82R mutation causes a subtle change in the tertiary structure

Wt-hFGF1 and the designed mutant proteins were purified to homogeneity (Fig. S2, Appendix 2). D82R, D82N, and D84R mutants exhibit strong binding affinity to heparin and all of them are found to elute in 1500 mM NaCl from the heparin sepharose affinity column. The double mutant, D82RD84R, predominantly eluted in 800 mM NaCl along with some minor bacterial protein impurities and this mutant was subsequently passed over heparin sepharose again to obtain the pure protein (Fig. S2, Appendix 2). The yields of the purified wt-hFGF1 and single mutant proteins were in the range of 10 mg – 20 mg per liter of bacterial culture. D82RD84R was obtained at reduced yields of 3-5 mg per liter of bacterial culture.

Far UV circular dichroism is a useful technique to obtain reliable information on the secondary structure of proteins [35]. Comparison of the far-UV CD spectra of the hFGF1 mutants (D82R, D82N, and D84R) reveals that they superimpose well with wt-hFGF1 suggesting that the backbone of the protein is folded into the native beta-barrel structure and is not significantly perturbed due to substitution of the negative charge on D82 or D84 with positive charge (Fig. 3). The far-UV CD spectra of the double mutant D82RD84R, with and without heparin, yields the least pronounced positive band from 240-220nm as the wt-hFGF1 does, however the overall spectra of the mutant spectrum indicates that beta barrel structure is not significantly perturbed (Fig. 3).
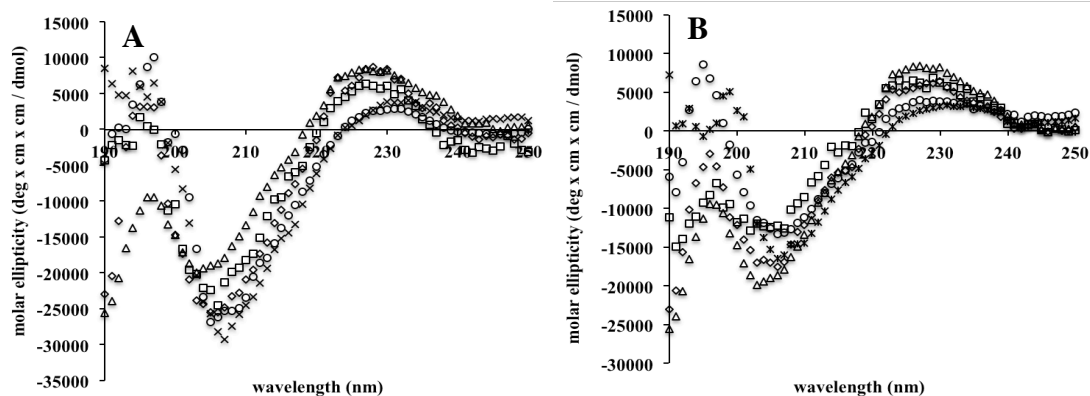
Figure 3: The Far-UV CD spectra of wt-hFGF1 and the engineered charge reversal mutations in the absence (Panel-**A**) and presence of heparin (Panel-**B**). wt-hFGF1 (Δ), D84R (◇), D82R (●), D82N (□), D82R/D84R (x).

hFGF-1 contains a lone tryptophan residue at position 121. The intrinsic fluorescence of the lone tryptophan is significantly quenched by the lysine and proline residues, which are located at close spatial proximity to the indole ring [36]. As a consequence, wt-hFGF-1 in its native conformation shows an emission maximum at 308 nm corresponding to the eight tyrosine residues in the protein. However, the quenching effects on the indole ring of Trp121 are completely relieved in the denatured state(s) of the protein and wt-hFGF1 shows the characteristic tryptophan emission peak at 350 nm. Intrinsic fluorescence spectra of wt-hFGF1 and all hFGF1 mutants in the presence and absence of heparin show a maximum emission at 308 nm, a characteristic feature of the native conformation of the protein (Fig. 4). However, the fluorescence spectra of D82R and the double mutant (D82RD84R) show a small hump at 350 nm in addition to the emission maximum at 308 nm. These spectral features suggest that a subtle perturbation of the tertiary structure occurs due to these mutations.
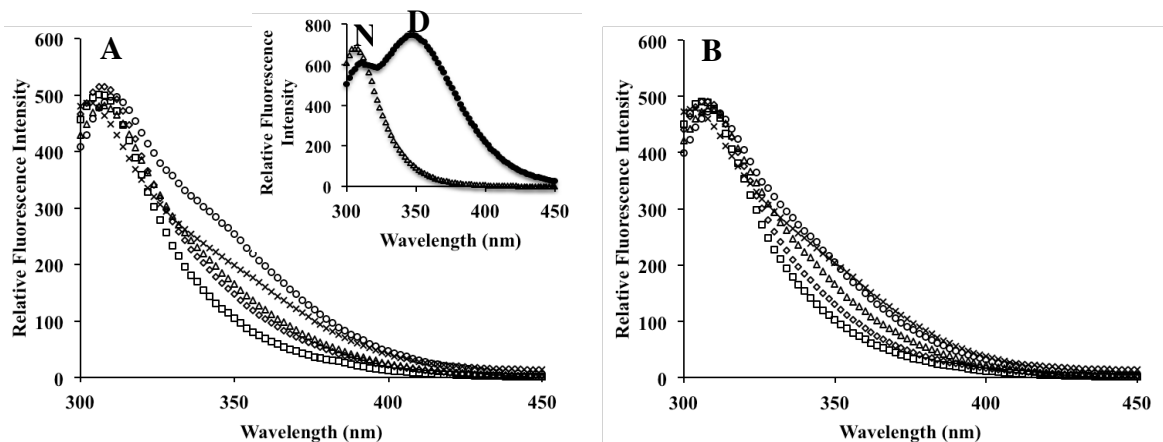
Figure 4: Intrinsic fluorescence spectra of wt-hFGF1 and the charge-reversal mutants in the absence (Panel-**A**) and in the presence (Panel-**B**) of HEPARIN. wt-hFGF1 (Δ), D84R (◇), D82R (●), D82N (□), D82R/D84R (x). Inset figure in panel A depicts the fluorescence spectra of native (N) and denatured (D) wt-hFGF1.

ANS is a non-polar dye that is commonly used to assess the presence of solvent-exposed hydrophobic surface(s) in proteins. ANS, when bound to wt-hFGF1, and the designed mutants, shows an emission maximum of 520 nm. Comparison of the ANS saturation curves reveals that the relative fluorescence intensity for D84R and D82N mutants is lower than that of wt-hFGF1 (Fig. 5A,B). These results indicate that the charge-reversal at position 84, and the loss of charge mutation at position 82 (D82N) only induce marginal changes in the solvent-exposed hydrophobic surface(s) of the protein. The observed decrease in ANS emission intensity suggests that the structure of the D84R mutant of hFGF1 appears to become more compact upon binding to heparin and consequently the solvent accessibility of the non-polar surface(s) in the protein decreases (Fig. 5). Interestingly, the emission intensity of ANS upon binding to the D82R and D82RD84R mutants, both in the presence and absence of heparin, is about two-fold higher than that observed for the wild type under similar conditions (Figs. 5A,B). These results indicate that charge-reversal at position 82 causes a subtle conformational change resulting in the increased solvent-exposure of non-polar surfaces in the protein. These observations pertaining to the

tertiary structure(s) of the D82R and D82RD84R mutants corroborate well with the conclusions

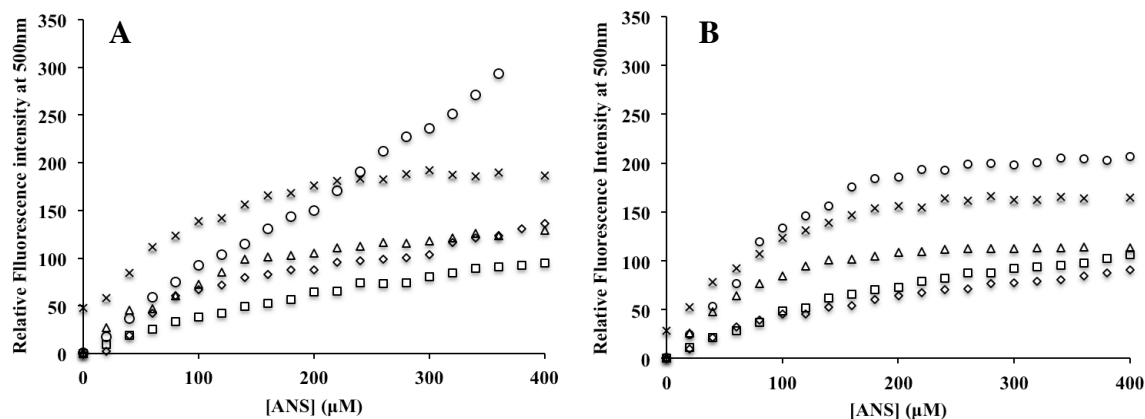drawn from the intrinsic tryptophan fluorescence data.

Figure 5: ANS binding curves of the wild type and the charge reversal mutations of hFGF1 in the absence (Panel-**A**) and presence (Panel-**B**) of HEPARIN. Wt-hFGF1 (Δ), D84R (◇), D82R (**O**), D82N (□), D82R/D84R (x).

Limited trypsin digestion is a commonly used method for probing the flexibility of

proteins and provides low-resolution information of structural changes (Fig. 6 and Fig. S3,

Appendix 2). D82R is quickly degraded by trypsin (85% of the protein is digested in 10

minutes). After 40 minutes of incubation with trypsin at 37°C, the 16 kDa band corresponding to

D82R is completely digested. In comparison, at the 40-minute time point, wt-hFGF1, D82N and

D84R are digested to 15%, 30% and 50%, respectively. Further, D82RD84R mutant of hFGF1 is

digested to 25% after 40 minutes of exposure to trypsin (Fig. 6A). The results of the limited

trypsin digestion experiments suggest that the backbone of the D82R mutant, in the absence of

heparin, is significantly more flexible than wt-hFGF1 and the D84R mutant. The observed

increase in trypsin susceptibility of the D82R mutant is unlikely due to incorporation of an

additional trypsin cleavage site in the protein because both D84R and the double mutant

(D82RD84R) exhibit lower susceptibility to trypsin action despite containing additional trypsin

cleavage site(s). In the presence of heparin, D82R, D84R, and D82RD84R mutants are strongly

resistant to limited trypsin digestion (Fig. 6B). Even after 40 minutes exposure to trypsin, these

three mutants remain completely undigested. These results suggest that the charge reversal

indeed increases the heparin binding of hFGF1. The observations regarding the flexibility of the

hFGF1 mutants, particularly the increase in structural flexibility of the D82R mutant, are

consistent with the conclusions drawn from both the intrinsic fluorescence and ANS binding

data.
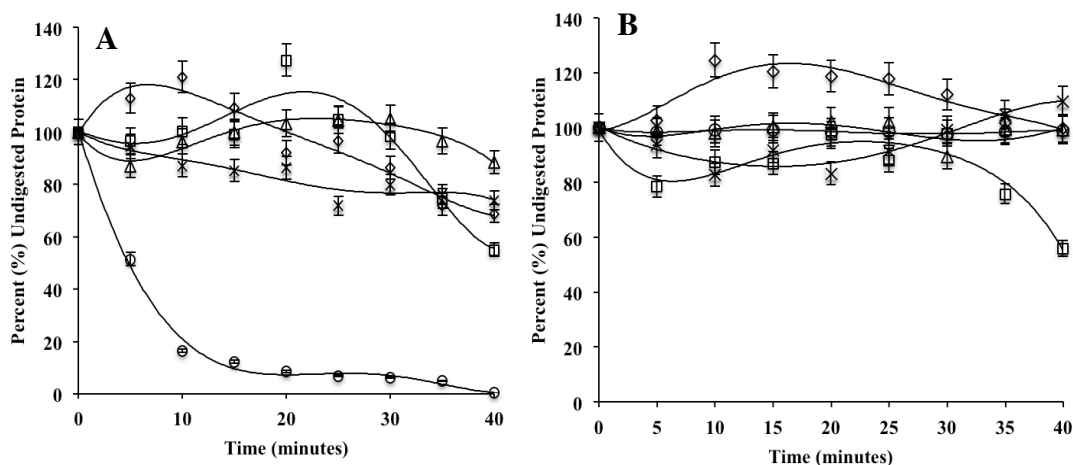
Figure 6: Densitometric analysis of the section of the SDS PAGE gel depicting the resistance of wild type and charge reversal mutants of hFGF1 to limited trypsin digestion in the absence (Panel-**A**) and presence (Panel-**B**) of heparin. Wt-hFGF1 (Δ), D84R (◇), D82R (**O**), D82N (□), D82R/D84R (x).

Heparin effectively increases stability of charge-reversal hFGF1 mutants

Thermal denaturation of hFGF1 was monitored by far-UV CD and the T_m values

[temperature wherein which 50% of the protein population exists in the denatured state(s)] were

calculated from the thermal unfolding curves (Fig. 7A, Table 2). The thermal stability data reveal

that, in the absence of heparin, both D82R ($T_m = 45°C \pm 0.59$) and D84R ($T_m = 42°C \pm 0.96$) are modestly *less* stable than wt-hFGF1 ($T_m = 48°C \pm 0.72$) (Table 1). In contrast, the stability of D82N ($T_m = 49°C \pm 0.72$) remains similar to that of wt-hFGF1. Interestingly, D82RD84R ($T_m = 53°C \pm 0.24$) is about 4°C more stable than wt-hFGF1 (Table 2). The thermal stability of wt-hFGF1 and the designed charge-reversal mutants effectively increases in the presence of heparin. The thermal stability of heparin-bound D84R ($T_m = 72°C \pm 0.51$) is approximately 3°C higher than that of wt-hFGF1 ($T_m = 69°C \pm 0.68$) (Table 2). The total change in thermal stability for D84R due to heparin binding ($\Delta T_m = 30°C$) is 10°C higher than that observed for wt-hFGF1 ($\Delta T_m = 20°C$) in the presence of heparin. The T_m for the D82R-heparin binary complex is about 5°C lower than the melting temperature for wt-hFGF1. The total increase in thermal stability of D82R ($\Delta T_m = 19°C$) upon binding to heparin is in the similar range as observed for wt-hFGF1 (Table 2). Furthermore, the large increase in thermal stability observed for D84R agrees well with ANS binding and limited trypsin digestion data demonstrating that heparin binding causes a conformational change in D84R that renders the protein molecule more compact and resistant to trypsin cleavage.

The T_m values for D82N and D82RD84R bound to heparin are 2°C to 3°C lower than the T_m measured for wt-hFGF1 in the presence of heparin. Overall, the ΔT_m for D82N ($\Delta T_m = 18°C \pm 0.72$) is very similar to the ΔT_m measured for wt-hFGF1 and the ΔT_m for D82RD84R ($\Delta T_m = 13°C \pm 0.72$) (Table 2) is approximately 8 degrees lower than wt-hFGF1. The diminished ΔT_m for D82RD84R suggests that heparin binding does not increase its thermal stability as effectively as it does for both the single mutants (D82R and D84R). The discrepancy in the ΔT_m value for the double mutant may be due to possible repulsion generated between the

guanindinium head groups at positions 82 and 84. The molecular dynamic simulation data of the double mutant suggested that the R82 and R84 side chains are oriented away from each other to minimize charge-charge repulsion. The altered orientation of the side chains may induce a conformational change that diminishes any contact between heparin and the side chains at position 82 and 84. This inference, pertaining to the D82RD84R mutant, is in good agreement with the conclusions drawn from the far-UV CD, intrinsic fluorescence, and the ANS saturation data, which indicate that introduction of two positive charges at positions 82 and 84 perturb the secondary and tertiary structure of the protein and consequently render the hydrophobic surface(s) in the protein to be more solvent-exposed.

The stability of wt-hFGF1 and each hFGF1 mutant was examined using urea-induced equilibrium unfolding (Fig 7B, Table 2). In the absence of heparin, the C_m values [the concentration of urea at which 50% of the protein population is denatured] for both D82R (C_m = 1.3M ± 0.14) and D84R (C_m = 1.6M ± 0.2) are similar to wt-hFGF1 (C_m = 1.8M ± 0.11) (Table 2), which indicates that these charge-reversal mutations do not significantly alter the stability of the protein. On the other hand, the C_m of D82N (C_m = 2.2M ± 0.08) (Table 2) was observed to be about 0.4 M higher than that of wt-hFGF1. This indicates that loss of charge at position 82 slightly increases the stability of the protein in the presence of urea. Once again in the presence of heparin, D82R (C_m = 4.4M ± 0.02) and D84R (C_m = 4.3M ± 0.08) are as stable as wt-hFGF1 (C_m = 4.2M ± 0.09) (Table 2). These results confirm that the charge reversals at positions 82 and 84 do not significantly alter the stability of the protein. Furthermore, the stability (C_m = 4.2M ± 0.04) conferred by the binding of heparin to the D82N mutant is similar to that observed for wt-hFGF1 bound to heparin. Overall, the ΔT_m and ΔC_m values determined for D82R, D84R, and

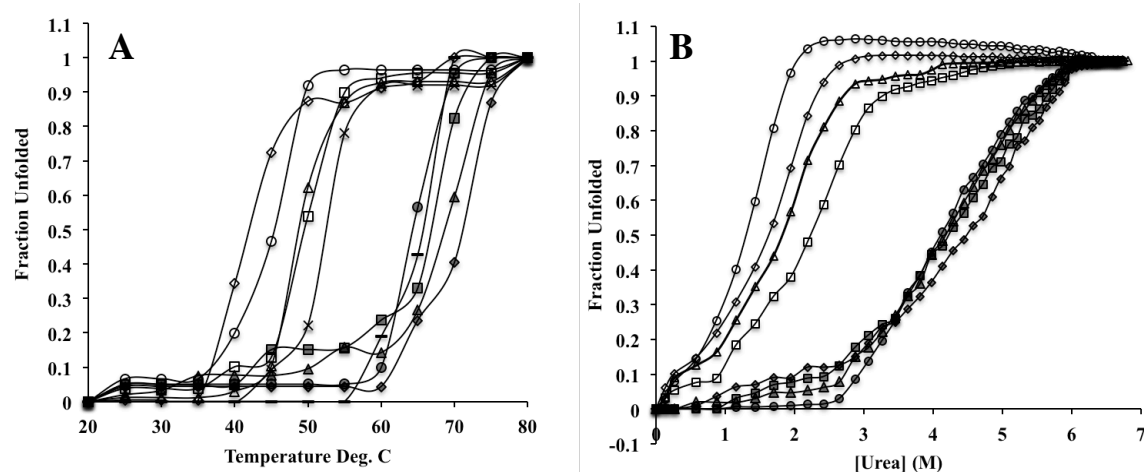D82N suggest that heparin effectively stabilizes these mutants to the same degree as that of wt-hFGF1.

Figure 7: Thermal (Panel-**A**) and urea-induced (Panel-**B**) equilibrium unfolding curves of wild type and the designed mutants of hFGF1 in the presence and absence of HEPARIN. The unfolding curves were monitored by changes in the ratio of the intrinsic fluorescence intensity at 308 nm/350 nm. Absence of heparin: wt-hFGF1 (△), D84R (◇), D82R (O), D82N (□), D82R/D84R (x). Presence of heparin: wt-hFGF1 (▲), D84R (♦), D82R (●), D82R/D84R (-).

Table 2. Thermodynamic stability of wt-hFGF1 and the designed mutants

Protein	T_m °C			C_M (M)		
	No heparin	With heparin	ΔT_m	No heparin	With heparin	ΔC_M
Wt-hFGF1	48.5 (±0.72)	68.7 (±0.68)	20.2	1.8 (±0.11)	4.2 (±0.09)	2.4
D82R	45.4 (±0.59)	64.3 (±1.40)	18.9	1.3 (±0.14)	4.4 (±0.02)	2.8
D84R	42 (±0.96)	71.6 (±0.51)	29.6	1.62 (±0.20)	4.3 (±0.08)	2.68
D82N	49.3 (±0.72)	67.0 (±1.12)	17.7	2.24 (±0.08)	4.2 (±0.04)	1.96
D82RD84R	52.6 (±0.24)	65.9 (±0.60)	13.3			

Increase in heparin-binding affinity of hFGF1 mutants

ITC is an extremely valuable tool for measuring the binding between two interacting molecules. The K_d value measured here for the interaction between heparin and wt-hFGF1 (K_d = 1.7µM) is comparable to the one reported by Brown and coworkers (Fig. 8) [13]. Identical K_d values are observed for the interaction of heparin with hFGF1 mutants D84R and D82N (K_d = 1.28µM), and this value is not significantly different from that obtained for wt-hFGF1 (Fig. S4, Appendix 2). Interestingly, the K_d value for the interaction of heparin with hFGF1 mutant, D82R, (K_d = 0.17µM) is approximately one log-fold lower than that exhibited by wt-hFGF1 (Fig. 8). This is expected because introduction of positive charge on the protein surface in proximity to the heparin-binding pocket can be predicted to increase the protein affinity to bind to heparin. The higher binding affinity of the D82R mutant for heparin does not appear to result in a concomitant increase in the thermodynamic stability of the mutant as evidenced by the results of the equilibrium unfolding experiments (Table 2). This may be attributed to the inherent lower stability of the D82R mutant. Comparison of the ΔT_m values (Table 2**)** indicate that heparin is able to stabilize the D82R mutant and the wild type protein to similar extent(s). The K_d values for both D84R and D82N indicate only a modest increase in affinity for heparin compared to wt-hFGF1 (Fig. 8). In contrast, the heparin binding affinity for the double mutant D82RD84R is reduced (K_d = 3µM) compared to wt-hFGF1 indicating that the behavior of the individual charge reversal mutants is not additive.
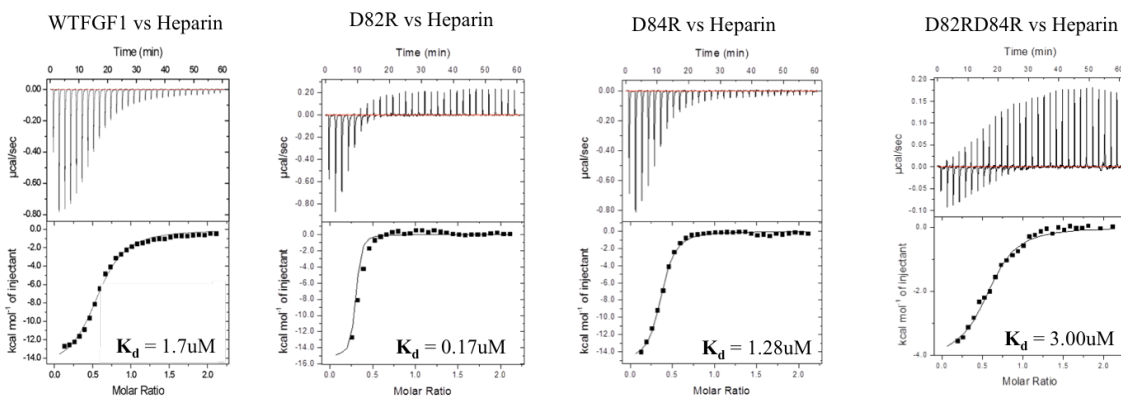
Figure 8: Isothermograms representing the titration of wild type and the designed mutants with heparin. The upper panels represent the raw heat changes that accompany the binding of the protein to heparin. The lower panels represent the best-fit of the binding curve(s) to a one-site binding model. All ITC data have been corrected for heats of dilution.

ITC measurements can also provide valuable information on the thermodynamics of interactions between molecules. The interactions between heparin and hFGF1 that contribute to the enthalpy term include electrostatic interactions, van der Waals forces, and hydrogen bonding. Interactions contributing to the entropic value include conformational changes as well as solvation changes accompanying hFGF1- heparin interaction [13]. For all hFGF1 mutations, the enthalpy value is negative, which indicates favorable binding of hFGF1 to heparin (Table 3). The change in enthalpy associated with D82R-heparin binding ($\Delta H = -1.5 \pm 2.4$ kcal mol^{-1}) is modestly lower than that observed for the wt-hFGF1-heparin binding ($\Delta H = -2.14 \pm 0.4$ kcal mol^{-1}) (Table 3). The change in enthalpy value characterizing the D84R-heparin interaction ($\Delta H = -1.6 \pm 0.32$ kcal mol^{-1}) is also modestly lower than that observed for the wt-hFGF1-heparin interaction, which suggests the degree of contact between this mutant and heparin is marginally reduced.

The change in entropy value for the D82R-heparin interaction (ΔS = -0.5 kcal mol^{-1}) is

lower than that for wt-hFGF1-heparin interaction (ΔS = -1.1 kcal mol^{-1}) (Table 3), but is still

favorable to promote interaction(s). The lower change in entropy value is likely due to the

desolvation occurring at the hFGF1-heparin binding interface. The change in enthalpy value for

the D84R-heparin interaction (ΔH = -1.6 ± 0.32 kcal mol^{-1}) is modestly lower than that of wt-

hFGF1-heparin binding. A lower enthalpy value for this mutant may be due to a conformational

change, which increases compactness of the tertiary structure.

The thermodynamic values for D82N-heparin interaction (ΔH = -2.04 ± 0.2 kcal mol^{-1},

ΔS = -1 Kcal mol^{-1}) (Table 3) closely correspond to the values determined for wt-hFGF1-

heparin binding. Lastly, the change in enthalpy value accompanying D82RD84R-heparin

interaction (ΔH = -4.1 ± 0.2 Kcal mol^{-1}) is larger than that observed for the wt-hFGF1-heparin

interaction, which appears to suggest greater degree of contact between this mutant and heparin.

However, the change in entropy value determined for D82RD84R-heparin binding (ΔS = 0.3

kcal mol^{-1}) (Table 3) is unfavorable.

The drastic increase in heparin binding affinity observed for the D82R mutant but not for

the D82N is likely due to the presence of the additional positive charge and not due to the

neutralization of the negative charge at this position (D82). The lack of drastic increase in

affinity of D84R for heparin could be due to local repulsion with the closely placed R133 (PDB

2ERM) [37]. R82 is positioned farther (12.5 Å) away from the canonical heparin-binding residue

R133. As the side chain of R82 is positioned on the surface of the protein, the D82R mutation

extends the range of positive charge and therefore might accommodate longer heparin chains that

span this distance more favorably than the D84R mutant.

Table 3. Thermodynamics of the heparin- hFGF1 interaction

Protein	ΔH (kcal/mol)	-TΔS (kcal/mol)
wt-hFGF1	-2.14 ± 0.4	-1.1
D82R	-3.91 ± 0.1	-0.5
D84R	-1.6 ± 0.32	-0.6
D82N	-2.04 ± 0.2	-1
D82RD84R	-4.1 ± 0.2	0.3

Charge reversal does not significantly perturb the structure of hFGF1

^{1}H ^{15}N HSQC is a versatile two-dimensional NMR experiment routinely used to obtain

structural information at the individual amino acid level. The structure of wt-hFGF1 has been

solved previously and the complete set of assigned resonances is available [17, 38]. The ^{1}H-^{15}N

chemical shift perturbations, upon addition of heparin, were monitored based on chemical shifts

assignments published by our group and others [17, 38]. Our results compare well with published

assignments and therefore assignments can be considered as accurate. Superimposition of HSQC

spectra of wt-hFGF1 and D84R mutant and the D82N mutant reveals modest chemical shift

perturbations (Fig. S5A and Fig. S6A, Appendix 2). The calculated ^{1}H-^{15}N chemical shift

perturbations indicate that, in both cases (D84R and D82N), most of the significant perturbation

occurs in the spatial region close to the location of the mutation site (Fig. S5B and Fig. S6B).

However, calculated chemical shift perturbations of D82R determined from the overlay of

HSQC spectra of D82R and wt-hFGF1 reveals that the most significant perturbation occurs not

only in residues in proximity to the site of the mutation (D84, G85, G89) but also among several

residues in the heparin-binding region (K115, K127, K132, and G134) (Fig. 9A & B).

The effect(s) of heparin on the global structure of D82R is determined from the overlay of the HSQC spectra of D82R in the presence and absence of HEPARIN (Fig. 10A). The ^{1}H-^{15}N chemical shift perturbation plot of D82R, in the presence and absence of HEPARIN, reveals significant perturbations throughout the protein sequence both in proximity to the site of the mutation (M81, D84, G85), and in the heparin-binding region (K126, K127, G129, S130, C131, R136, Q141, A143, L145) (Fig. 10B). These perturbations indicate involvement of these residues in the interaction with heparin.

The heparin binding to the D84R mutation increases the compact nature of the tertiary protein fold, thereby increasing the protein's thermal stability as well as its stability in the presence of the denaturant, urea. However, charge reversal at position 84 does not alter the overall structure of the protein and only marginally increases hFGF1 affinity for heparin. On the other hand, charge reversal at position 82 induces a conformational change that reduces the compact nature of the tertiary fold and increases the protein's flexibility without altering the protein's secondary structure. However, interestingly, charge reversal at position 82 significantly increases hFGF1's affinity for heparin. Loss of charge at position 82 (D82N) seems to have little to no effect on structure, stability, and heparin-binding affinity of hFGF1. While heparin binding to D82N modestly increases the compact character of the protein's tertiary fold. However, no significant changes in stability and heparin-binding affinity were observed due to this mutation. We could not obtain a quality HSQC spectrum of the double mutant, D82RD84R due to aggregation of the sample during data collection. This aspect precluded us from assessing the change(s) caused in the structure due to the double mutation.
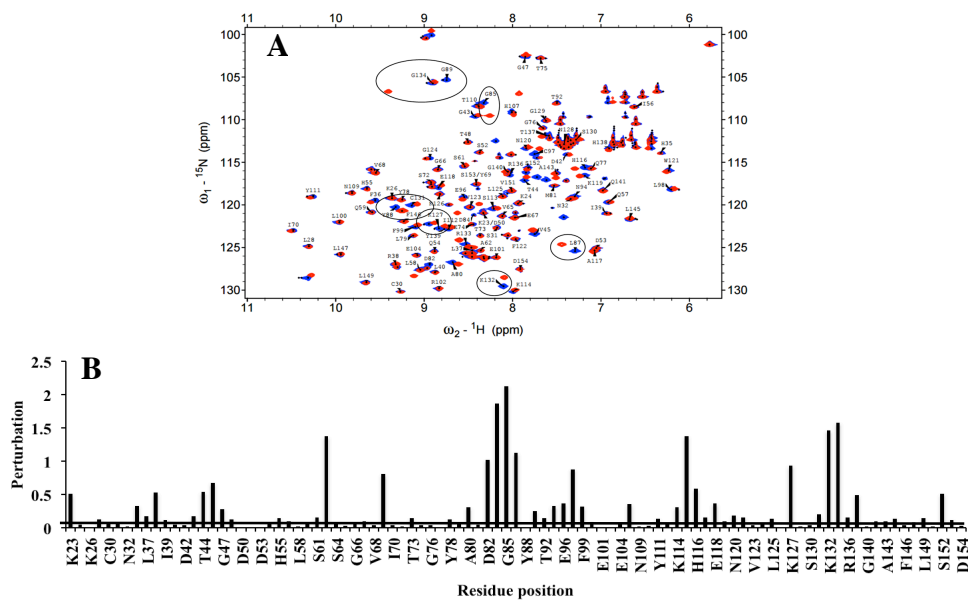
Figure 9: Panel–**A**, Overlay of the ^{1}H-^{15}N HSQC of wild type (red) and the D82R (blue) mutant of hFGF1. Panel-**B**, ^{1}H-^{15}N chemical shift perturbation observed due to the D82R mutation. The horizontal line represents the arbitrary threshold above which the ^{1}H-^{15}N chemical shift perturbation(s) was considered as significant. The ^{1}H-^{15}N chemical shift perturbation of individual residues were calculated using the formula, ($\sqrt{[(2\Delta\delta_{NH})^2 + (\Delta\delta_N)^2]}$)
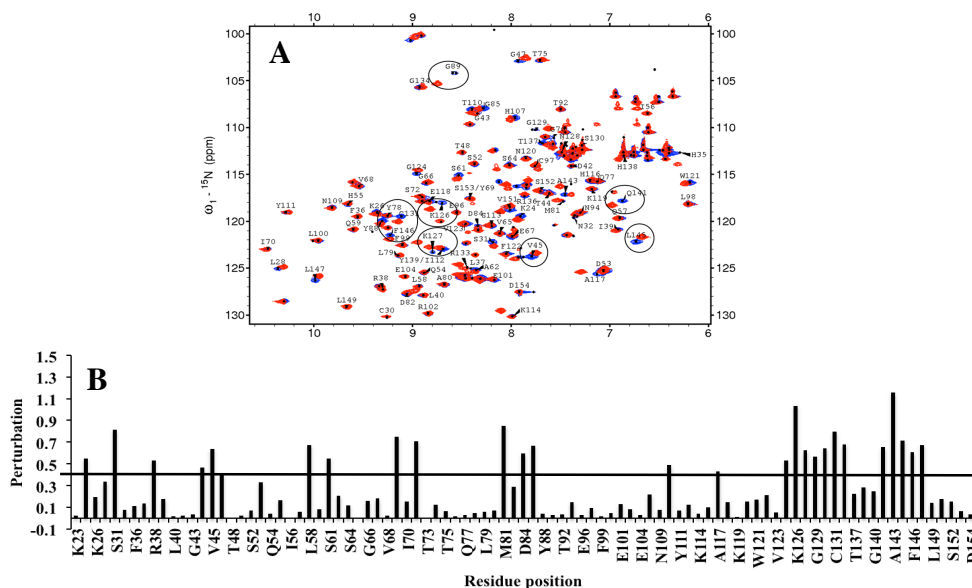
Figure 10: Panel –**A**, Overlay of the ^{1}H-^{15}N HSQC of D82R mutant of hFGF1 in the presence (blue) and absence of heparin (red). Panel-**B**, ^{1}H-^{15}N chemical shift perturbation observed due to the D82R mutation. The horizontal line represents the arbitrary threshold above which the ^{1}H-^{15}N chemical shift perturbation(s) was considered as significant. The ^{1}H-^{15}N chemical shift perturbation of individual residues were calculated using the formula, ($\sqrt{[(2\Delta\delta_{NH})^2 + (\Delta\delta_N)^2]}$).

Increased heparin binding affinity does not correlate with cell proliferation activity

It is believed that heparin is critical for FGF receptor activation. In this context, increased heparin binding affinity of the charged reversed hFGF1 mutants D82R and D84R is expected to result in increased activation of the receptor. The net consequence being increased cell proliferation activity. Cell proliferation study to optimize the heparin: protein ratio was performed on heparinase treated NIH 3T3 cells by varying the concentration of heparin with a fixed concentration of wt-hFGF1 (Fig. S7, Appendix 2). Optimum cell proliferation was achieved with a heparin: protein ratio of 10:1. Further cell proliferation experiments were then carried out for wt-hFGF1 and each designed hFGF1 mutant using a 10:1 ratio of heparin: protein.

Panel A of Fig. 11 indicates that at the highest protein concentration (50 ng/mL), the level of wt-hFGF1 is not significantly higher than mutant D84R or double mutant D82RD84R, but is does display a statically higher level of activity compared to single mutants D82R and D82N. Wt-hFGF1 also displays statistically higher cell proliferation activity than D82R at a protein concentration of 10 ng/mL. (No significant statistical differences are observed between wt-hFGF1 and other hFGF1 mutants at protein concentrations below 50 ng/mL) (Fig. 11 Panel-A, Supplemental Table 1, Appendix 2). Overall, the cell proliferation data indicate that both mutants (D82R and D84R), despite their increased heparin binding affinity, show similar levels of cell proliferation activity as the wt-hFGF1 in the presence of exogenous heparin (Fig. 11A, Supplemental Table 1, Appendix 2). In panel B of Fig. 11, in the absence of exogenous heparin, D82R and D84R are observed to have similar levels of activity as wt-hFGF1 at most all protein concentrations with no statistical differences. D82N and D82RD84R also display similar levels of activity, but D82RD84R is statistically less active than wt-hFGF1 at the highest protein

concentration (50 ng/mL) and D82N is statically less active than wt-hFGF1 at 2 ng/mL. Data produced from bioactivity experiments performed without preliminary heparinase treatment using the same 10:1 heparin: protein ratio yielded the same results as experiments in which heparinase treatment was applied. Altogether, this data again suggests that increased heparin binding does not result in a concomitant increase in the cell proliferation activity of hFGF1.

The notion that heparin's interaction with fibroblast growth factors is not essential for its biological activity has been well documented in the published literature. Two separate groups, Moscatelli and coworkers and Saksela and coworkers, observed that heparin bound human basic FGF (hFGF2) and free hFGF2 interact with its receptor in identical fashion [39]. In another study of hFGF1 mutants, changing two or all three cysteine residues in hFGF1 to serine were shown to have an increased physiological half life and also the biological activity of the mutant proteins was enhanced in a heparin independent manner compared to that of wt-hFGF1 [40]. Wong and coworkers also reported that substitution of K132 to glutamic acid reduces hFGF1 affinity towards heparin, yet they observe full receptor activation as well as early-intermediate gene transcription for the hFGF1 mutant [31]. In addition, several mutagenesis studies have shown that an increase in the thermal stability of hFGF1 confers increased mitogenic activity to the protein in the absence of heparin. Further, L58F and H107S hFGF1 mutations were found to marginally increase the thermal stability by approximately by 3°C to 7°C [18, 26]. Similarly, Zakrzewska et al generated several heat stable mutants of hFGF1, which exhibit significantly enhanced heparin-independent cell proliferation activity compared to wt-hFGF1 [4, 12, 20]. These studies clearly support our conclusions that an increase in heparin binding affinity, through extension of the heparin-binding pocket, does not translate into an increase in the cell proliferation activity of hFGF1. It appears that the primary roles of heparin on the cell surface

are: 1.) To enhance the stability of hFGF1 through electrostatic interactions with the densely populated positively charged residues in the heparin binding pocket and 2.) To serve as a reservoir to attract the growth factor molecules to the cell surface and consequently promote FGF-receptor interaction. The results of this study appear to clearly support earlier studies, which suggest that binding of heparin to hFGF1 is not mandatory for its cell proliferation activity.
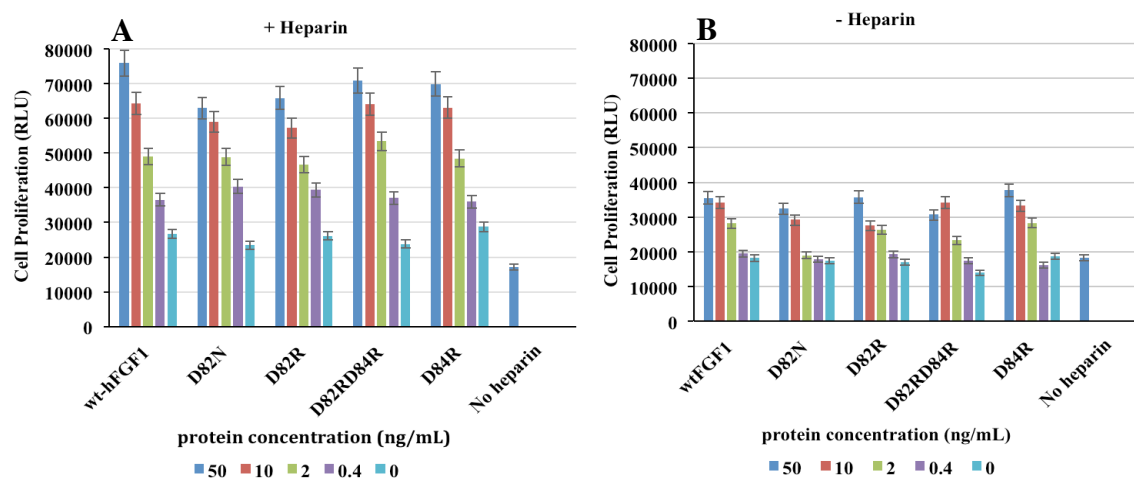

Figure 11: Panel-A, Proliferation of heparinase treated NIH 3T3 cells in the presence of wild type and the designed mutants of hFGF1 bound to heparin. Panel-B, Proliferation of heparinase treated NIH 3T3 cells in the presence of wild type and the designed mutants of hFGF1 without exogenous heparin. The standard errors were calculated from triplicate measurements (Supplemental Table 1).

Conclusions

Proteoglycans located on the cell surface help extend the half-life and modulate interaction of many ligands to their corresponding receptors [41]. Particularly, the interaction between hFGF1 and heparin has been studied extensively and overall there are two contrasting views that exist. Initially there has existed a general belief within literature that heparin is critical

for binding of hFGF1 to its receptors [14, 23]. This belief was developed from the study of crystal structures of heparin bound hFGF1 dimers in the presence and absence of FGFRs. From these structures, it is observed that the central heparin chain makes contacts with both hFGF1 monomers and one monomer of FGFR. These studies claimed that these ternary complexes are the structural basis for the belief that heparin is essential for hFGF1 signaling and further that hFGF1 dimerization is essential for signaling [23, 42]. Recent studies using isothermal titration calorimetry indicate that the oligomerization of hFGF1 to heparin is characterized by positive cooperativity and that an octasaccharide heparin is the shortest length capable of mediating hFGF1 dimerization [13]. However, studies from 2002 and 2005 of monomeric hFGF1 bound to the heparin mimic, sucrose octasulfate (SOS), as well as to a synthetic heparin-like hexasaccharide, have found hFGF1 fully capable of FGFR activation and cell proliferation [43, 44]. Both studies suggest that oligomerization of the protein is not mandatory for hFGF1 signaling. In this study we were able to show that enhancing the heparin binding property of growth factor hFGF1 through site-directed mutagenesis did not increase the mitogenic activity. This supports the assertion that hFGF1-FGFR interaction for activation of downstream signaling cascades does not critically depend on the binding of either ligand or receptor to the proteoglycan.

Materials and Methods

Materials: The Quikchange II XL mutagenesis kit was from Agilent and the DNA plasmid isolation kit was from Qiagen Inc., USA. DH5α and BL-21(DE3) competent cells were obtained from Novagen Inc., USA. Lysogeny broth is a product of EMD Millipore, USA. HEPARIN sepharose resin is from GE Healthcare, USA. Buffer components (Na_2HPO_4, NaH_2PO_4, NaCl, and $(NH_4)SO_4$) were acquired from VWR Scientific., USA. Low molecular weight (~3000 Da)

heparin sodium salt was obtained from Sigma and MP Biomedicals LLC. NIH 3T3 cells were

obtained from ATCC and all the cell culture reagents including, DMEM media, fetal bovine

serum (FBS) and penicillin streptomycin were purchased from Thermo Fisher Scientific

(Waltham, MA). All measurements of the spatial distance between residues within hFGF1 were

made using Pymol viewing software and were measured as the distance between side chain

functional groups (carboxyl groups for D82 and D84, guanidinium group for R133, R82, and

R84).

Molecular Dynamic Simulations: All mutations were created in Pymol viewing system using

the PDB structure 1RG8 [37]. Protein structures were minimized and then solvated with a

margin of 10 Å between the protein and the border of the solvent box. The solvent box was

neutralized with NaCl at a working concentration of 0.150 M. While hydrogen atoms were kept

rigid, the protein backbone, side chains, and solvent molecules/ions were relaxed to prepare the

system for equilibration, which was performed in the NPT ensemble utilizing NAMD 2.9

molecular dynamics code and the CHARMM36 force field. First, side chains were minimized for

10,000 steps (each step being 1fs) while the backbone was held rigid in the absence of solvent

molecules. Next, with all protein atoms fixed, water molecules were relaxed around the protein

over the course of 1,500 minimization steps followed by 50 ps of dynamics. A final relaxation

step was implemented to relax the solvent molecules around the protein harmonic constraints

using a force constant of 1 kcal/(mol Å^2). The last operation was the incremental increase of

temperature (10 K per 2 ps) to a final temperature of 300 K. Following the temperature increase,

the structure was allowed to freely move for 250 ps. Langevin dynamics with a damping

coefficient of 1 ps^{-1} was used to sustain a temperature of 300 K, and Langevin piston method

was used to sustain a pressure of 1 atm with a period of 100 fs and a decay time of 50 fs. Long-

range electrostatic interactions were determined using particle mesh Ewald method as well as

periodic boundary conditions and a switching function was applied to cut both electrostatic and Van der Waals interactions beyond 12 Å. 100 ns simulations with a time step of 2 fs were performed. Simulations were visualized and hydrogen bonding of the mutated residue was traced in VMD.

Construction and purification of hFGF1 mutants: A truncated form of hFGF1 (residues, 15-154) was cloned into pET-20b bacterial expression vector was used as a template for site-directed mutagenesis. Primers were designed using an Agilent primer design program and ordered from IDT DNA Inc. Site-directed mutagenesis (SDM) was performed using a QuikChange II XL kit followed by polymerase chain reaction (PCR) as per the protocol provided by the vendor. The plasmid was then transformed into DH5α competent cells. After obtaining confirmation of the plasmid sequences, each mutant protein was overexpressed in BL-21(DE3) *Escherichia coli* cells cultured in lysogeny broth (LB) at 37°C with agitation of 250 rpm. Overexpressed cells were lysed using ultrasonication (with ~15 watts output power) and the desired cell lysate was separated from the cell debris using ultra centrifugation at 19,000 rpm. hFGF1 mutants were then purified on a heparin Sepharose column using a stepwise salt gradient in 10mM sodium phosphate buffer containing 25mM $(NH_4)_2SO_4$ pH 7.2 [4, 12, 20]. The purity of the wt-hFGF1 and the mutant hFGF1 proteins were checked by 15% sodium dodecyl sulfate-polyacrylamide gel electrophoresis (SDS-PAGE) using a prestained protein molecular weight ladder of range 7 kDa-175 kDa. Protein bands were visualized by staining the gels with coomassie brilliant blue.

Isothermal Titration Calorimetry: The heparin binding affinity of wt-hFGF1 and each mutant were measured using isothermal titration calorimetry (ITC). Protein samples were prepared with

10 mM sodium phosphate buffer containing 100 mM NaCl and 25 mM $(NH_4)_2SO_4$ pH 7.2. All samples were degassed prior to loading. A 1:10 ratio of protein to ligand (50 μM protein: 500 μM heparin) was applied on a MicroCal iTC200 (Malvern Inc.) in which heparin was titrated into hFGF1 samples. The average molecular mass of heparin used is approximately ~3000 Da, which corresponds to a degree of polymerization anywhere from 8 to 12 saccharides [32]. For each experiment, a series of 30 titrations were performed at 25°C with a stir speed of 1000 rpm. The data for wt-hFGF1 and the mutants were best-fit to one set of sites and any excess heats of dilution given from heparin were appropriately subtracted out. The binding stoichiometry defined as the maximal number of heparins bound to a hFGF1 molecule can be determined from the inflection point of the titration plot [13].

Fluorescence Spectroscopy and 8-Anilino-1-napthalenesulfonic acid (ANS) binding: All intrinsic and extrinsic fluorescence measurements were performed on a Hitachi F-2500 spectrophotometer at 25°C using a slit-width of 2.5 nm and a 10mm quartz cuvette. Intrinsic fluorescence experiments were performed with protein concentration of 0.1mg/mL in a 10mM sodium phosphate buffer containing 100 mM NaCl and 25 mM $(NH_4)_2SO_4$ (pH 7.2). hFGF1 samples were excited at a wavelength of 280 nm and the emission spectra was recorded from 300 nm to 450 nm. ANS binding assays were performed using a protein concentration of 15μM. Experiments in the presence of heparin were performed at a heparin to protein ration of 10:1. Stock ANS was made such that 1 μL titrations into protein sample would increase ANS concentration by 20 μM increments. Fluorescence measurements were made between each titration until saturation was reached. Samples were excited at 380 nm and emission was measured at 520 nm.

Circular Dichroism Spectroscopy: Far-UV circular dichroism (Far-UV CD) experiments were performed using a protein concentration of 0.5μg/μL in 10 mM sodium phosphate buffer containing 10 mM NaCl and 25 mM $(NH_4)_2SO_4$ (pH 7.2) on a Jasco-1500 spectrophotometer at 25°C. Experiments performed in the presence of heparin were completed at a heparin to protein ratio of 10:1. For analysis of samples in the presence of heparin, the ligand was added in 10-fold's molar excess of the protein to ensure complete saturation of binding. Necessary background corrections were made and the data was subjected to a smoothing function via application of the Savitzky-Golay algorithm.

Equilibrium unfolding: Thermal and chemical unfolding of hFGF1 mutants were performed on a Jasco-1500 spectrophotometer through which intrinsic fluorescence and far-UV CD measurements can be made simultaneously. Equilibrium unfolding experiments were performed using a protein concentration of 0.5 mg/mL in 10mM sodium phosphate buffer containing 10 mM NaCl and 25 mM $(NH_4)_2SO_4$ at pH 7.2. Experiments including heparin were performed at a heparin to protein ratio of 10:1. Far UV CD data was acquired using a 1 mm quartz cuvette. Spectra were collected every 5 degrees from 20-80°C. Molar ellipticity values were recorded at 228 nm and the fraction unfolded was plotted as a function of temperature. The denaturation temperature (T_m) was determined as the temperature at which 50% of the protein population was denatured.

Urea-induced equilibrium unfolding experiments were conducted at a protein concentration of ~0.05mg/mL. Urea was titrated in consistent volumes into the sample up to a concentration of 6 M. Protein unfolding was monitored by both CD and fluorescence and the fraction unfolded was determined using molar ellipticity values at 228nm and the ratio of the tyrosine and tryptophan fluorescence (308/350nm) respectively.

Limited Trypsin Digestion: Limited trypsin digestion experiments were performed in the presence and absence of heparin. The initial reaction mixture included 500 μg of protein and 5 μg trypsin in 10 mM sodium phosphate buffer containing 100 mM NaCl, and 25 mM $(NH_4)_2SO_4$ at pH 7.2. Experiments performed in the presence of heparin were completed with a heparin to protein ratio of 10:1. A second identical sample was prepared with the addition of exogenous heparin in ten times molar excess the protein concentration to ensure saturation of the protein. Trypsin digestion was carried out at 37 °C and a portion of the reaction mixture was removed, at specified time intervals, and the reaction was arrested with the addition of 100% trichloroacetic acid. The reaction products were analyzed by 15% SDS-PAGE and the gels were stained using Coomassie Brilliant Blue (Sigma Aldrich). The percentage of proteolytic digestion was estimated from the band intensity, on the SDS PAGE gel, using UN-SCAN it densiometric software. Intensity of hFGF1 samples not subjected to proteolytic digestion was used as the control representing 100% protection from enzymatic degradation.

Nuclear Magnetic Spectroscopy: Heteronuclear single quantum coherence (HSQC) spectroscopy was performed on a Bruker 500 MHz NMR equipped with cryoprobe. The protein samples were isotopically labeled with ^{15}N as a result of expression in M9 minimal media containing $^{15}NH_4Cl$. All NMR experiments were acquired at 25°C using a protein concentration of 300 μM using 2K x 256 data points. Protein samples were prepared in 90% H_2O 10% D_2O solution containing 10 mM sodium phosphate buffer containing100 mM NaCl and 25 mM $(NH_4)_2SO_4$ (pH 7.2). The total chemical shift perturbation per residue ($\Delta\delta_{total}$) was calculated using the following equation : $\sqrt{[(2\Delta\delta_{NH})^2 + (\Delta\delta_N)^2]}$. All NMR data was analyzed using Sparky 3.114 software [37]. ^1H-^{15}N chemical shift perturbation at the residue level, caused due to binding of heparin, were carefully tracked by acquiring a series of ^1H-^{15}N HSQC spectra at

different heparin to protein ratio's. Despite our efforts, we could not unambiguously follow the ^{1}H-^{15}N chemical shift perturbation of few residues and these residues were not considered in the final ^{1}H-^{15}N chemical shift perturbation data presented.

Cell proliferation assay: 3T3 fibroblast cells obtained from ATCC (Manassas, VA) were cultured in complete media consisting of DMEM supplemented with 10% FBS and 1% penicillin/streptomycin. Cells were grown to 80-90% confluency and were incubated overnight at 37 °C with 5% CO_2 in serum free media before further use. Pretreatment of cells with heparinase was performed at a concentration of 6 units of enzyme per 10,000 cells. Cells were incubated with heparinase enzyme for 1 hour at 37 °C. Following incubation with heparinase, cells were centrifuged for 2 minutes at 6000rpm and then washed twice with hyclone buffer to remove any remaining trace of enzyme and returned to DMEM media with 10% FBS. The cell proliferation activity of hFGF1 was determined by quantifying the increase in cell number after the cells had been incubated with hFGF1 at varying concentrations. Starved 3T3 fibroblasts were collected and seeded in a 96-well plate at a seeding density of 10,000 cells/well. Cells were then co-incubated individually with wild type and mutant hFGF1 at concentrations of 0, 0.4, 2, 10, and 50 ng/mL. The cell proliferation assays were performed in the absence and presence of an optimized 1:10 ratio of hFGF1 : heparin. After 24 hours of incubation, 3T3 cell proliferation was assessed by the CellTiter-Glo (Promega, Madison, WI) cell proliferation assay.

Acknowledgements

Works Cited

1.   Lin, X., Buff, E.M., Perrimon, N., Michelson, A.M., Heparan sulfate proteoglycans are essential for FGF receptor signaling during, Drosophila Embryonic Development, 1999. 126: p. 3715-3723.

2.   Mason, I.J., The Ins and Outs of Fibroblast growth factors, Cell Press, 1994. p. 547-552.

3.   Wilkie, A.O.M., Morriss-Kay, GM., Jones, E.Y., Heath, J.K., Functions of fibroblast growth factors and their receptors, Cell Press, 1995. 5(5): p. 500-507.

4.   Zakrzewska, M., Krowarsch, D., Wiedlocha, A., Otlewski, J., Design of fully active FGF-1 variants with increased stability. Protein Engineering, Design & Selection, 2004. 17(8): p. 603-611.

5.   Yu-Peng, H., et. al., Divergent Synthesis of 48 Heparan Sulfate-Based Disaccharides and Probing the Specific Sugar−Fibroblast Growth Factor 1 Interaction, J American Chemical Society, 2012. p. 20722−20727.

6.   Itoh, N., Ornitz, D.M., Fibroblast growth factors: from molecular evolution to roles in development, metabolism and disease, J Biochem, 2011. 149: p.121-130.

7.   Ornitz, D.M., Itoh, N., Fibroblast growth factors, Genome Biology, 2001. 2(3): p. 1-12.

8.   Carter, E.P., Fearon, A.E., Grose, R.P., Careless talk costs lives: fibroblast growth factor receptor signalling and the consequences of pathway malfunction. Trends Cell Biol., 2015. 25(4): p. 221-233.

9.   Goetz, R., Mohammadi, M., Exploring mechanisms of FGF signalling through the lens of structural biology, Nat Rev Mol Cell Biol. 2013. 14(3): p. 166–180.

10.   Miller, D., Ortega, S., Barhayan, O., Basilico, C., Compensation by Fibroblast Growth Factor 1 (FGF1) Does Not Account for the Mild Phenotypic Defects Observed in FGF2 Null Mice, Mol Cell Biol, 2000. 20: p. 2260-2268.

11.   Beenken, A., Eliseenkova, A.V., Ibrahimi, O.A., Olsen, S.K., Mohammadi, M., Plasticity in Interactions of Fibroblast Growth Factor 1 (FGF1) N Terminus with FGF Receptors Underlies Promiscuity of FGF1, J Biol Chem, 2012. 287(5): p. 30676-3078.

12.   Zakrzewska, M., et al., Increased Protein Stability of FGF1 Can Compensate for Its Reduced Affinity for Heparin, J Biol Chem, 2009. 284(37): p. 25388-25403.

13.   Brown, A., Robinson, C.J., Gallagher, J.T., Blundell, T.L., Cooperative Heparin-Mediated Oligomerization of Fibroblast Growth Factor-1 (FGF1) Precedes Recruitment of FGFR2 to Ternary Complexes, Biophys J, 2013. 104: p. 1720-1730.

14.   Harmer, N.J., Insights into the role of heparan sulfate in fibroblast growth factor signalling. Biochem Soc Trans, 2006. 34(3): p. 442-445.

15.   Hook, M., Kjelleń, L., Johansson, S., Robinson, J., Cell-surface glycosaminoglycans, Annu Rev Biochem, 1984. 53: p. 847–869.

16.   Pellegrini, L., Role of heparan sulfate in fibroblast growth factor signalling: a structural view, Current Opinion in Structural Biology, 2001. 11: p. 629–634.

17.   Canales, A., et al., Solution NMR structure of a human FGF-1 monomer, activated by a hexasaccharide heparin-analogue, FEBS Journal, 2006. 273(20): p. 4716-4727.

18.   Culajay, J.F., Blaber, S.I., Khyrana, A., Blaber, M., Thermodynamic characterization of mutants of human fibroblast growth factor 1 with an increased physiological half-life. Biochemistry, 2000. 39(24): p. 7153-7158.

19.   Dubey, V.K., et al., Spackling the Crack: Stabilizing Human Fibroblast Growth Factor-1 by Targeting the N and C terminus β-Strand Interactions, J Mol Biol, 2007. 371: p. 256 – 268.

20.   Zakrzewska, M., Krowarsch, D., Wiedlocha, A., Olsnes, S., Otlewski, J., Highly stable mutants of human fibroblast growth factor-1 exhibit prolonged biological action, J Mol Biol, 2005. 352(4): p. 860-75.

21.   Schlessinger, J., et al., Crystal structure of a ternary FGF–FGFR–heparin complex reveals a dual role for heparin in FGFR binding and dimerization, Mol Cell, 2000. 6 p. 743-750.

22.   Saxena, K., et al., Influence of Heparin Mimetics on Assembly of the FGF J Biol Chem, 2010. 285(34): p. 26628-26640.

23.   Pellegrini, L., Burke, D.F., Von Deift, F., Blundell, T.L., Crystal structure of fibroblast growth factor receptor ectodomain bound to ligand and heparin, Nature, 2000. 407(6807): p. 1029-1034.

24.   DePaz J.L., et al., The Activation of Fibroblast Growth Factors by Heparin: Synthesis, Structure, and Biological Activity of Heparin-Like Oligosaccharides, ChemBioChem, 2001 2: p. 673–685.

25.   Szlachcic, A., et al., Structure of a highly stable mutant of human fibroblast growth factor 1, Acta Cryst, 2009. D65: p. 67-73.

26.   Brych, S., Blaber, S.I., Logan, T.M., Blaber, M., Structure and stability effects of mutations designed to increase the primary sequence symmetry within the core region of a β-trefoil, Protein Science, 2001. 10(12): p. 2587–2599.

27.   Ornitz, D.M., Itoh, N., The Fibroblast Growth Factor Signaling Pathway. Wiley Interdiscip Rev Dev Biol , 2015. 4(s): p. 215-266.

28.   Kanodia, J., Greg, F., Role of heparin GAGs in Regulation of FGF Signaling Pathway: Insights from Mathematical Modeling, J Glycobiology, 2014. 4(1). doi:10.4172/2168-958X.1000113

29.   Kimura, H., Okubo, N., Chosa, N., Kyakumoto, S., Kamo, M., Miura, H., Ishisaki, A., EGF Positively Regulates the Proliferation and Migration, and Negatively Regulates the Myofibroblast Differentiation of Periodontal Ligament-Derived Endothelial Progenitor Cells through MEK/ERK- and JNK Dependent Signals. Cell Physiol Biochem, 2013. 32: p. 899-914.

30.   Burgess, W.H., et al., Possible Dissociation of the Heparin-binding and Mitogenic Activities of Heparin-binding (Acidic Fibroblast) Growth Factor-1 from Its Receptor-binding Activities by Site-directed Mutagenesis of a Single Lysine Residue, J Cell Biol, 1990. 111: p. 2129-2138.

31.   Wong, P., Hampton, B., Szylobrgt, E., Gallagher, A.M., Jaye, M., Burgess, W.H., Analysis of Putative Heparin-binding Domains of Fibroblast Growth Factor-1. J Biol Chem, 1995. 270(43): p. 25805-25811.

32.   Fu, L., Zhang, F., Li, G., Onishi, A., Bhaskar, U., Sun, P., Linhardt, R.J., Structure and Activity of a New Low Molecular Weight Heparin Produced by Enzymatic Ultrafiltration, J Pharm Sci, 2014. 103(5): p. 1375-1383.

33.   Robinson, C.J., Harmer, N.J., Goodger, S.J., Blundell, T.L., Gallagher, J.T., Cooperative Dimerization of Fibroblast Growth Factor 1 (FGF1) upon a Single Heparin Saccharide May Drive the Formation of 2:2:1 FGF1·FGFR2c·Heparin Ternary Complexes, J Biol Chem, 2005. 280 (51): p. 42274-42282.

34.   Raman, R., Venkataraman, G., Ernst, S., Sasisekharan, V., Sasisekharan, R., Structural specificity of heparin binding in the fibroblast growth factor family of proteins, PNAS, 2002. 100(5): p. 2357-2362.

35.   Micsonai, A., Wien, F., Kernya, L., Lee, Y.H., Goto, Y., Refregiers, M., Kardos, J., Accurate secondary structure prediction and fold recognition for circular dichroism spectroscopy, PNAS, 2015. 112(24): p. 3095-3103.

36.   Callis, P.R., Binding phenomena and fluorescence quenching. II: Photophysics of aromatic residues and dependence of fluorescence spectra on protein conformation, J Mol Structure, 2014. 1077: p. 22-29.

37.   Bernett, M.J., Somasundaram, T., Blaber, M., An atomic resolution structure for human fibroblast growth factor 1, Proteins:Structure Function and Bioinformatics, 2004. 57(3): p. 626-634.

38.   Chi, Y.H., et al., Investigation of the structural stability of the human acidic fibroblast growth factor by hydrogen-deuterium exchange, Biochemistry, 2002. 41(51): p. 15350-15359.

39.   Rifkin, D.B., Moscatelli, D., Recent Developments in the Cell Biology of Basic Fibroblast Growth Factor, J Cell Bio, 1989. 109: p. 1-6.

40.   Ortega, S., et al., Conversion of Cysteine to Serine Residues Alters the Activity, Stability, and Heparin Dependence of Acidic Fibroblast Growth Factor, J Biol Chem, 1991. 266(9): p. 5842-5846.

41.   Nugent, M.A., Heparin sequencing brings structure to the function of complex oligosaccharides, PNAS, 2000. 97(19): p. 10301-10303.

42.   DiGabriele, A.D., Lax, I., Chen, D.I., Svahn, C.M., Jaye, M., Schlessinger, J., Hendrickson, W.A., Structure of a heparin-linked biologically active dimer of fibroblast growth factor, Nature, 1998. 393(6687): p. 812-817.

43.   Arunkumar, A.I., et al., Oligomerization of acidic fibroblast growth factor is not a prerequisite for its cell proliferation activity, Protein Science, 2002. 11(5): p. 1050-1061.

44.   Angulo, J., et al., Dynamic properties of biologically activity synthetic heparin-like hexasaccharides, Glycobiology, 2005. 15(10): p. 1008-1015.

Chapter 3

Introduction of a negative charge in the heparin-binding pocket significantly increases the stability and cell proliferation activity of the Human Acidic Fibroblast Growth Factor

Julie Eberle Davis[1], Jeevapani J. Hettige[1], Mahmoud Moradi[1], Thallapuranam Krishnaswamy Suresh Kumar[1*].

1. Department of Chemistry and Biochemistry, University of Arkansas, 1 University of Arkansas, Fayetteville, AR 72701, USA

*To whom all correspondence should be addressed: Prof. T. K.S. Kumar

Email: sthalla@uark.edu

Phone: +1 479-575-5646

Abstract

Human fibroblast growth factor 1 (hFGF1) is a potent signaling molecule, whose role in cell growth, differentiation, and migration has made it an excellent candidate for wide ranging biomedical applications. hFGF1 is a heparin sulfate binding protein and the proteoglycan has been shown to stabilize hFGF1, and furthermore is considered to play a critical role in the growth factor–induced cell signaling. Recently, a charge-reversal mutation, R136E, in the heparin-binding pocket has been shown to significantly decrease the heparin binding affinity of hFGF1, but yet has been demonstrated to exhibit increased stability and remarkably enhanced cell proliferation activity. However, the structural basis for the observed changes, due to the R136E mutation, is not yet fully understood. In this context, here the microsecond-level molecular dynamics (MD) of the R136E mutation as well as the wild type hFGF1 have been characterized. Microsecond molecular dynamics (MD) simulations performed here show that wild type hFGF1 undergoes a conformational change in which a significant portion of the heparin-binding region (HBR) including residues K126 to Q141 entirely unfolds from the native protein structure. Interestingly no conformational change is observed within the mutant, R136E, hFGF1 MD simulation. Analysis of the all-atom MD simulations suggests that the increased structural stability of the mutant hFGF1 is due to several electrostatic interactions in the HBR between residues E136 and R133, E136 and K132, as well as E136 and K126. Additionally several stabilizing hydrogen bonds involving residues within the HBR (S130-N128 and K127-N32) as well as residues throughout the protein structure (Q91-Q77, T48-D53, T75-S72) are unique to the mutant protein, and are also hypothesized to contribute to the increased inherent stability of the R136E mutant. Two-dimensional nuclear magnetic resonance (NMR) experiments have also identified 14 residues whose amide proton do not undergo exchange with

D_2O in the mutant structure only, and are thus hypothesized to contribute to the robust inherent stability observed in equilibrium unfolding experiments. Overall the results of this study suggest that the increased stability of the R136E mutant structure is due to several unique electrostatic interactions as well as hydrogen bonds, which are not present in the wild type hFGF1.

Keywords: fibroblast growth factor, molecular dynamics simulation, cross correlation map, stability

Abbreviations: human fibroblast growth factor-1 (hFGF1); heteronuclear single quantum coherence (HSQC); hydrogen-deuterium exchange (HDX), molecular dynamics simulation (MDS), American Type Culture Collection (ATCC), Visual Molecular Dynamics (VMD).

Introduction

hFGF1 is a member of a family of 22 growth factors whose signaling facilitate the regulation of key cellular responses including cell growth and proliferation, angiogenesis, and cell differentiation and migration [1, 2]. FGFs elicit a cellular response upon binding to their respective cell surface, tyrosine kinase receptors (FGFRs). hFGF1 is unique from the other members of the FGF family in its ability to activate all the different isoforms of FGFRs [3, 4]. Owing to its role in a wide range of cell signaling processes, hFGF1 has enormous potential as a wound-healing agent [5-8].

Despite its important role as a signaling molecule, hFGF1 is inherently unstable and is known to exist in partially unfolded state(s) at physiological temperatures [9-11]. hFGF1 is a heparin binding protein and exhibits high binding affinity to the proteoglycan ($K_d \sim 1.5$ μM). The proteoglycan is believed to increase the in vivo stability of hFGF1 and consequently increase the probability of its productive interaction with the corresponding FGFR. Heparin/heparin sulfate (HS) binds to a cluster of positively charged residues located at the C-terminal end (residues K126 to Q141) of hFGF1 [12, 13]. hFGF1 has been shown to be prone to thrombin cleavage [14]. Although hFGF1 lacks the typical thrombin recognition and cleavage site (-LYPRGS-), the protease has been shown to specifically cleave hFGF1 at R136 and render the growth factor molecule biologically inactive. This aspect significantly limits the therapeutic use of hFGF1 as a wound-healing agent [15].

Recently, a charge reversal mutation in the HS-binding pocket (R136E) was reported to overcome the susceptibility of hFGF1 to the action of thrombin. The R136E mutation has been shown to significantly increase the thermal stability of the growth factor [16]. In addition, the susceptibility of the R136E mutant to proteases such as thrombin and trypsin, is also drastically

lower than wild type hFGF1 (wt-hFGF1) [16]. More importantly, the cell proliferation activity, due to the R136E mutation, enhanced seven-fold more than that exhibited by wt-hFGF1 [16]. Interestingly, despite the significant differences in the stability, resistance of proteases, and enhanced cell proliferation activity, the gross structure of hFGF1 was not found to be discernably perturbed due to the charge reversal mutation, R136E, in the HS-binding pocket. In this context, effort has been made in this study to understand the structural basis for the extraordinary properties introduced due to the R136E mutation. The results of the study indicate that the introduction of a negative charge, via the R136E mutation, introduced new electrostatic interactions and hydrogen bonds that are responsible for the increased stability and enhanced cell proliferation activity of hFGF1. The results of this study for the first time indicate that the stability and the cell proliferation activity of hFGF1 can be modulated through specific alterations in the HS-binding pocket.

Results and Discussion

R136E mutation effectively increases stability of hFGF1

To assess the thermal stability of both mutant and wt-hFGF1, changes in secondary structure were monitored by far UV circular dichroism (CD) by observing the changes in the 250-190 nm ellipticity. T_m, is the temperature at which 50% of the protein population is in the unfolded state. Analysis of the thermal stability data showed that, in the absence of HS, the R136E mutant ($T_m = 60°C \pm 0.9$) was ~7 °C more stable than wt-hFGF1 ($T_m = 53°C \pm 0.5$) (Fig. 1A and Table 1A). In the presence of HS, the thermal stability of wt-hFGF1 ($T_m = 61.5°C \pm 1.5$) and the R136E ($T_m = 62.5°C \pm 1.5$) were mostly similar. Interestingly, the increase in thermal stability of wt-hFGF1 ($\Delta T_m = 8.5°C$) upon HS binding was four times larger than that observed

for the mutant, R136E (ΔT_m = 2.5°C) (Table 1A). Additionally, as two-dimensional NMR experiments were performed in both H_2O buffer spiked with 10% D_2O as well as 100% D_2O buffer, the denaturation of the mutant and wt-hFGF1 proteins was also monitored in D_2O buffer to determine if the buffer alone influenced the structural stability of the protein. The thermal stability experiments performed in D_2O buffer showed the same trend observed for experiments performed in H_2O buffer. In the absence of HS, R136E was (T_m = 63°C ± 0.8) ~6 °C more stable than wt-hFGF1 (T_m = 57°C ± 0.2) (Table 1A). However, the thermal stability of the R136E (T_m = 63°C ± 1.7) mutant did not change significantly in the presence of HS compared to wt-hFGF1 (T_m = 64.2°C ± 1.7) (Fig. 1B and Table 1A).

Chemical denaturant (urea) – induced equilibrium unfolding of hFGF1, in the presence and absence of HS, was monitored by changes in the emission intensity from 300-450 nm. C_m (the concentration of denaturant at which 50% of the protein population is in the unfolded state) value of the wt-FGF1, denatured by urea, was 1.8 M ± 0.4 (Fig. 1C). However, R136E (C_m = 2.8 M ± 0.4, Fig. 1C and Table-1B) was significantly more resistant to urea-induced denaturation. As expected, the C_m value of the wt-hFGF1 (2.9 M ± 0.33) increased by 1.1 M urea in the presence of HS. The marked contrast for the mutant, R136E, was observed as the C_m (2.9 M ± 0.3) value did not show any discernable change in the presence of heparin. A similar trend was again observed when the urea-unfolding experiments were performed in D_2O (Fig. 1D & Table - 1 B). The results of the thermal and urea-induced equilibrium unfolding experiments clearly suggest that heparin confers significant stability to wt-hFGF1 but not to the R136E mutant.
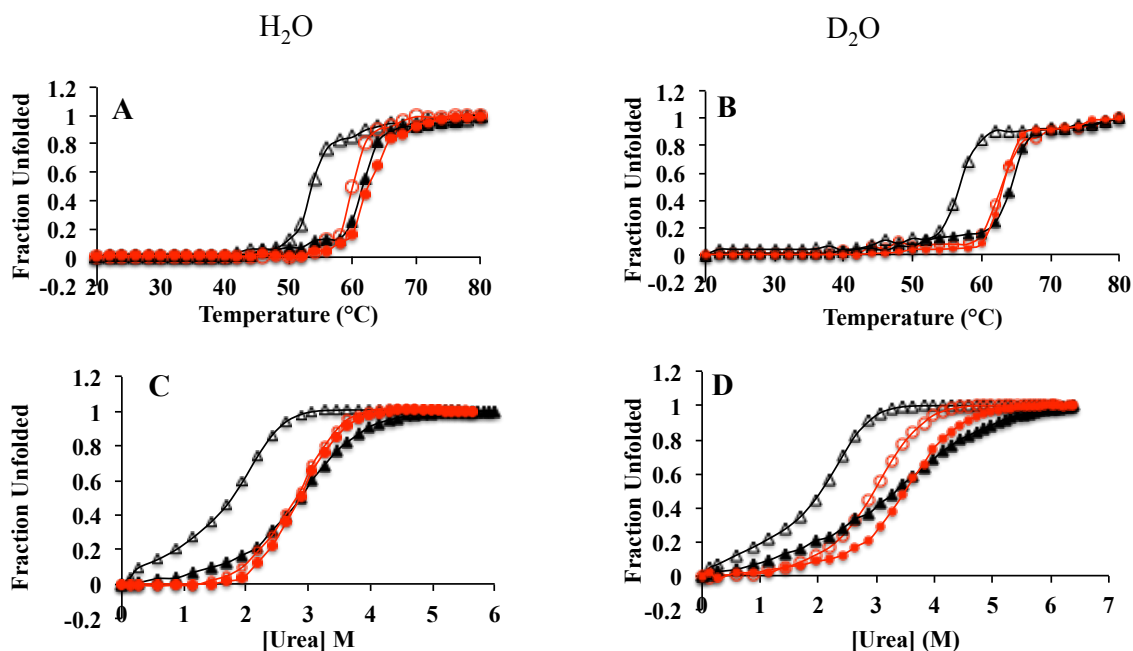
Figure 1. Thermal equilibrium unfolding curves of wt-hFGF1 and the designed mutants of hFGF1 in the presence and absence of heparin in H_2O buffer (Panel-**A**) and D_2O buffer (Panel-**B**). Urea-induced equilibrium unfolding for wt-hFGF1 and mutant, R136E, in the presence and absence of heparin obtained in H_2O buffer (Panel-**C**) and D_2O buffer (Panel-**D**). The unfolding curves were monitored by changes in the 228 nm ellipticity as well as the 308 nm / 350 nm fluorescence ratio. Absence of heparin sulfate: wt-hFGF1 (Δ), R136E (○). Presence of heparin sulfate: wt-hFGF1 (▲), R136E (●).

Table 1. Thermodynamic stability of wt-hFGF1 and mutant, R136E determined from thermal denaturation (Panel-**A**) and urea denaturation (Panel-**B**).

A.	T_m °C (in H_2O)			T_m °C (in D_2O)		
	- Heparin	**+ Heparin**	**ΔT$_m$**	**- Heparin**	**+ Heparin**	**ΔT$_m$**
wt-hFGF1	53.5 ± 0.5	61.5 ± 1.5	8.5	57 ± 0.2	64.2 ± 1.7	7.2
R136E	60 ± 0.9	62.5 ± 1.5	2.5	63 ± 0.8	63 ± 1.7	0

B.	C_m [M Urea] (in H_2O)			C_m [M Urea] (in D_2O)		
	- Heparin	**+ Heparin**	**ΔC$_m$**	**- Heparin**	**+ Heparin**	**ΔC$_m$**
wt-hFGF1	1.8 ± 0.4	2.9 ± 0.3	1.1	2.1 ± 0.29	3.3 ± 0.5	1.2
R136E	2.8 ± 0.4	2.9 ± 0.3	0.1	3.0 ± 0.12	3.5 ± 0.4	0.5

R136E mutation decreases backbone amide proton exchange

The contribution(s) of hydrogen bonding (H-bonding) toward the increased stability of mutant, R136E was examined by comparing the time-dependent hydrogen-deuterium exchange (H/D), monitored by NMR spectroscopy, of the R136E mutant and the wt-hFGF1. 2D ^{1}H-^{15}N Heteronuclear Single Quantum Coherence (^{1}H-^{15}N HSQC) spectra were collected, after 21 hours of H/D exchange in D_2O. Overlay of the ^{1}H-^{15}N HSQC of spectra for wt-hFGF1 and mutant, R136E, acquired independently in H_2O and D_2O under similar buffer conditions (Fig. 2 A and B), showed a good overlap of the ^{1}H-^{15}N crosspeaks in both the spectra suggesting that no significant conformational changes are caused due to the D_2O solvent. Some proteins are known to undergo subtle conformational changes or aggregation when they are exchanged into D_2O solvent [17]. The degree of H/D exchange was determined as a percentage for each residue in the wt-hFGF1 and mutant, R136E, ^{1}H-^{15}N HSQC spectra. Percent exchange was calculated from the ratio of crosspeak intensity between the deuterium ^{1}H-^{15}N HSQC spectra and H_2O ^{1}H-^{15}N HSQC spectra. Crosspeaks were then classified as completely exchanged (1-10%), significantly exchanged (10-50%), partially exchanged (50-90%), or resistant to exchange (90-100%) (Table 2).

Analysis of the data collected after 21 hours exchange in 100% D_2O revealed that, compared to wt-hFGF1, R136E has 14 additional residues which were not prominently exchanged with deuterium (Table 2). These results suggest additional H-bonds are induced in the protein due to the R136E mutation. In addition, these results are consistent with those of the denaturation experiments. Of the residues that are resistant to exchange in R136E, eight are in the HBR (V123, G124, L125, K132, G134, H138 G140, Q141) (Table 2). In the wt-hFGF1 structure, only five of the nineteen residues, which are resistant to exchange, are HBR residues

(V123, G124, K132, R133, Q141) (Table 2). This suggests that the stability of the HBR in the mutant, R136E, is increased due to the charge reversal mutation. In wt-hFGF1, ten residues in the HBR (K126, K127, G129, C131, G134, R136, T137, H138, Y139, G140) were found to completely exchange after 21 hours exposure to deuterium, while only four residues (C131, G134, T137, Y139) were completely exchanged in the mutant, R136E (Table 2), within this time period. As a larger number of residues in the HBR of the wt-hFGF1 had an increased susceptibility to H/D exchange, than in the mutant, R136E, this data collaborates with conclusions drawn from the denaturation experiments, which demonstrate an enhanced stability of the R136E mutant.

In wt-hFGF1 a total of 61 residues were identified to completely participate in H/D exchange, meaning that no corresponding crosspeak was found after 21 hours exposure to 100% D_2O (Table 2). Interestingly, in mutant, R136E, only 39 residues were classified as completely exchanged. Of these residues, 31 of them were common to the mutant, R136E, and wt-hFGF1, while 30 of these residues were unique to wt-hFGF1 and only 8 unique to R136E (Table 2). Overall, R136E contains 22 fewer residues whose backbone amide proton was completely exchanged with deuterium. These results suggest that R136E has additional stabilizing interactions, which prevent the exchange of several backbone amide protons of residues throughout the protein structure.

Interestingly, (in addition to the HBR residues previously mentioned) there are 30 specific residues, mostly outside the HBR, whose susceptibility toward H/D exchange is increased in the wt-hFGF1 compared to the mutant, R136E. Residues K23, K24, K26, H35, L37, L40, G43, D50, S52, L60, S61, V65, E67, I70, S72, E74, T83, D84, T92, A117, E118, A143, and D154 are all found to completely exchange in wt-hFGF1, having no visible crosspeak after

21 hours exposure to deuterium. However, the crosspeaks for these same residues in the mutant, R136E can be still observed after 21 hours exposure to deuterium, and therefore classified as significantly exchanged (L40, S52, E74, T83, D84, T92, E118), partially exchanged (K23, H35, D50, V65, A143, D154), or resistant to exchange (K24, K26, L37, G43, L60, S61, E67, I70, S72, A117) based on their crosspeak intensity (Table 2). Additionally, N32, D42, T48, S64, F122, F36, and D53 are residues outside of the HBR that were found to significantly or partially participate in H/D exchange in wt-hFGF1, while these same residues in the mutant, R136E, are not prominently exchanged with deuterium. Overall, these results indicate that the R136E mutation reduces the overall susceptibility of a total of 44 residues (4 in the HBR, 40 outside of the HBR) in hFGF1 to participate in H/D exchange, consequently stabilizing the R136E structure. These results correlate well with the interpretation of the denaturation experiments that R136E is more stable than wt-hFGF1.

Figure 2. Panel-**A** Overlay of the labeled ^{1}H-^{15}N HSQC of wt-hFGF1 in 90:10 H$_2$O:D$_2$O buffer (blue) and 100% D$_2$O buffer (red). (Panel-**B**) Overlay of the labeled ^{1}H-^{15}N HSQC of mutant, R136E, in 90:10 H$_2$O:D$_2$O buffer (blue) and 100% D$_2$O buffer (red).

Table 2. Degree of H/D exchange for each residue in wt-hFGF1 and mutant, R136E. Residues in red are in the HBR, and residues that are underlined are more highly susceptible to H/D exchange in the wt-hFGF1 structure than in the mutant, R136E.

Protein	Complete exchange (0-10%)	Significant Exchange (10-50%)	Partial Exchange (50-90%)	Resistant to Exchange (90-100%)
wt-hFGF1	K23, K24, K26, L28, C30, S31, H35, L37, L40, G43, V45, D50, S52, Q54, L60, S61, A62, V65, E67, I70, S72, T73, E74, T75, G76, Q77, M81, T83, D84, Y88, T92, N94, E96, C97, E101, E104, H107, Y111, S113, K115, H116, A117, E118, K119, N120, K126, K127, G129, C131, G134, R136, T137, H138, Y139, G140, A143, F146, L149, S152, D154, I156	N32, D42, T48, L58, S64, D82, R102, F122, N128, L145	F36, R38, T44, G47, D53, H55, G66, G85, G89, F99, L100, W121, L125, S130, V151, S153,	I39, Q57, Q59, V68, Y69, Y78, L79, A80, L87, L98, N109, T110, K114, V123, G124, K132, R133, Q141, L147,
R136E	L28, C30, S31, T44, V45, Q54, A62, G66, T73, T75, G76, Q77, Y78, L79, M81, Y88, N94, E96, C97, F99, E101, E104, H107, Y111, S113, K115, H116, K119, N120, W121, C131, R133, T137, Y139, L145, F146, L149, S152, I156	L40, G47, S52, L58, E74, A80, T83, D84, T92, L98, R102, E118, K126, E136	K23, H35, R38, D50, H55, Q59, V65, Y69, D82, G85, L87, T110, K127, N128, G129, S130, A143, L147, S153, D154	K24, K26, N32, F36, L37, I39, D42, G43, T48, D53, Q57, L60, S61, S64, E67, V68, I70, S72, G89, L100, N109, K114, A117, F122, V123, G124, L125, K132, G134, H138, G140, Q141, V151,

Stabilizing electrostatic interactions in the HBR of mutant hFGF1

MD simulations were run to shed light on the conclusions drawn from equilibrium unfolding and H/D exchange experiments, that mutation of R136 to glutamate increases the conformational stability of the protein. 4.8 μs MD simulations for both wt-hFGF1 and mutant R136E were completed using a truncated form of the hFGF1. The crystal structure (PDB code 1RG8) used for the simulations is of hFGF1 in the absence of heparin. A movie of each simulation is provided in the supplementary material (supplemental movie S12 and S13, Appendix 3). For each trajectory, the Cα root-mean-square deviation (RMSD) was measured as a function of time for the entire protein as well as for the HBR (Fig. 3A). The RMSD measured for wt-hFGF1 protein as a whole, as well as for the internal HBR increases at the 2.4 μs time mark from ~1 Å to ~3 Å and from ~0.5 Å to ~4 Å respectively. On the other hand, the RMSD for mutant, R136E measured for the entire protein remained consistent between ~1-2 Å while the

RMSD for the internal HBR is maintained at ~0.5 Å. Additionally, the root-mean-square

fluctuation (RMSF) for the Cα atoms indicates that the flexibility of the HBR in the wt-hFGF1

(residues 126-141) is significantly increased compared to mutant, R136E (Fig. 3B). These results

are consistent with the denaturation as well as the H/D exchange experiments as they suggest

that the R136E mutation induces interactions amongst residues in the HBR that reduce the

flexibility of this region, thereby increasing structural stability.
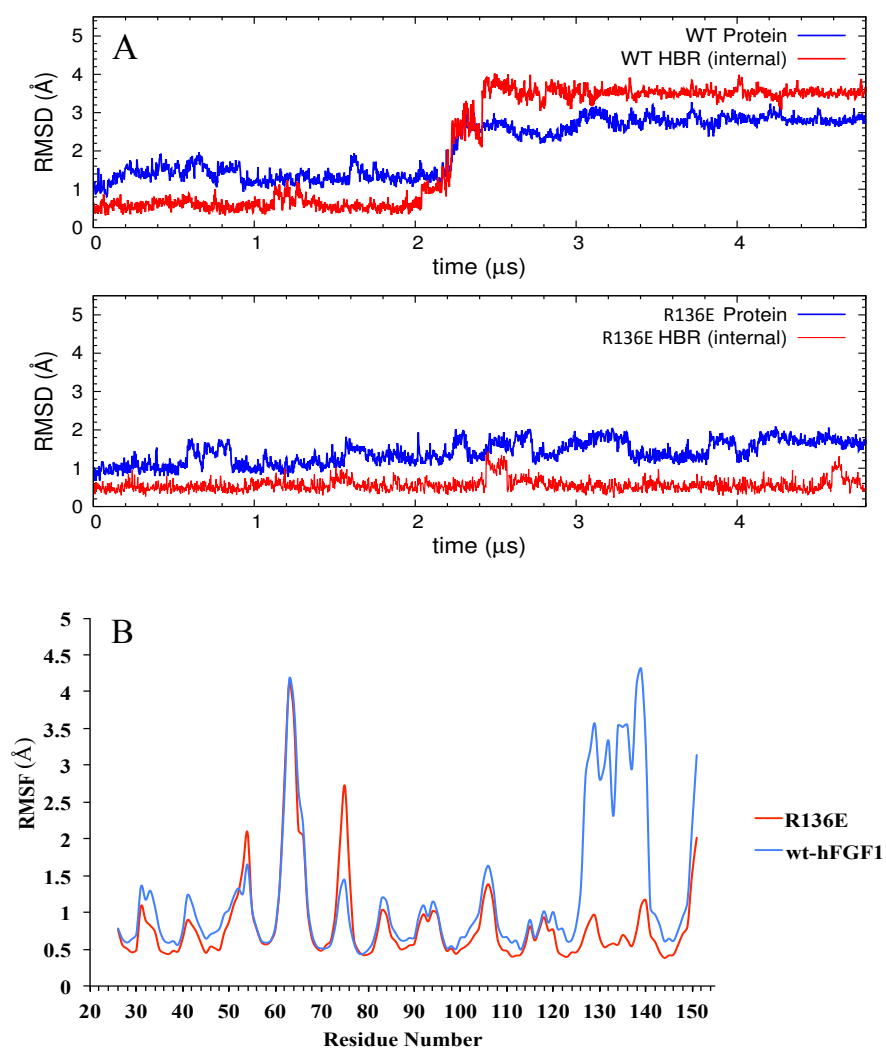
Figure 3. Panel-**A** RMSD of the backbone Cα atoms as a function of time for both the entire protein (Blue) and internal HBR (red) of wt-hFGF1 (top) and mutant, R136E (bottom). Panel-**B** overlay of RMSF values for mutant, R136E, (red) with wt-hFGF1 (blue).

To identify unique, stabilizing intramolecular interactions within the R136E mutant, detailed salt bridge and H-bond analyses were performed. Salt bridges were analyzed by measuring the distance between negatively charged side-chain carboxylate groups of aspartate/glutamate residues and the positively charged, side-chain ε-amino and guanidino groups of lysine and arginine residues, respectively, and then plotting the changes in these distances against time. Substitution of R136 with glutamate resulted in the induction of a new salt-bridge between residues E136 and R133 in the HBR, and furthermore, consistent salt bridges were also observed between E136 and K132 as well as between E136 and K126 (Fig. 4A and 4B). In addition, consistent salt-bridge interaction within the mutant, R136E simulation was observed between the side chain carboxyl group of residue D84 and the side chain guanidine group of R133 (Fig. 4C). Interestingly, the same salt bridge in wt-hFGF1 was disrupted at ~2.4 µs, but the carboxyl group of D84 reoriented to forge a new salt-bridge with the ε-amino group of neighboring lysine residue, K132 (Fig. 4D).

Several salt bridges were present out of the HBR in both the R136E mutant and the wt-hFGF1 including, E95-K114, E95-K115, E96-K115, E63-K26, E67-K114, D46-R38, and D53-R38 (Table-3). A unique salt-bridge was formed between D46 and K127 in wt-hFGF1 at the ~ 2.4 µs time mark, and is therefore considered to contribute to the conformational change observed in wt-hFGF1 (Fig. 4E).
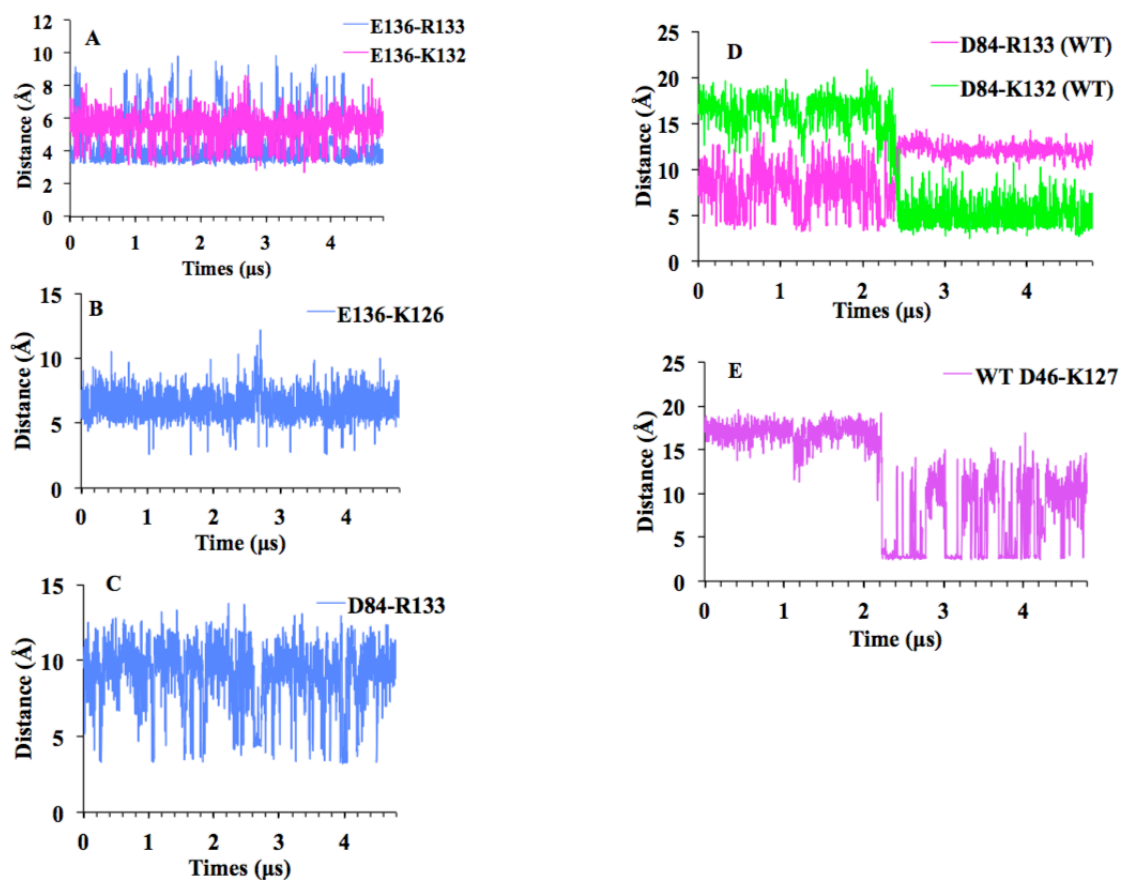
Figure 4. Time series of donor-acceptor distance for key salt-bridge interactions in mutant, R136E (Panel-**A**, Panel-**B**, and Panel-**C**), and wt-hFGF1 (Panel-**D** and Panel-**E**) structures.

Table 3. Stable salt bridge interactions in both wt-hFGF1 and mutant, R136E.

Stable Salt Bridges

wt-hFGF1	D46-K127	E95-K114	E95-K115	E96-K115	E63-K26	E67-K114	D46-R38	D53-R38	D84-R133/K132			
R136E		E95-K114	E95-K115	E96-K115	E63-K26	E67-K114	D46-R38	D53-R38	D84-R133	E136-R133	E136-K126	E136-K132

H-bond interactions that contribute to conformational change of wt-hFGF1

H-bond analysis of wt-hFGF1 revealed several interactions that seem to contribute to the conformational change of the protein structure. To define H-bonding based on the donor-H-

acceptor angle and donor- acceptor distance, a 30° cutoff angle and 3 Å cutoff distance is applied. Traces for three H-bond(s) involving residues in the HBR displayed transitions, beginning before the 2.4 μs time point, between the native (folded) and unfolded conformations of wt-hFGF1 (Fig. 5A). Particularly interesting is the interdomain H-bond between K127 and N32, which was disrupted at approximately 2 μs and the donor-acceptor distance was increased to 15 Å at 2.2 μs. The donor-acceptor distance of the main chain H-bond between K126 and S130, which was consistently stable up to 2 μs, was increased to 7 Å at 2.2 μs (indicating bond disruption), and leveled off at approximately 10 Å at 2.4 μs (Fig. 5A). Additionally, the donor-acceptor distance of the H138-Q141 H-bond was consistent around ~2 Å and then increases to 7 Å at 2.3 μs and increases again to 10 Å at 2.4 μs, (Fig. 5A). Similarly, the donor-acceptor distance of the Q141-R136 H-bond was disrupted once at approximately 2.3 μs when it increased to 8 Å and then a second time, at 2.4 μs, this time increasing well beyond 10 Å (Fig. 5B).

As these H-bond transitions begin before the prominent transition at 2.4 μs, observed in the RMSD trace for the overall protein structure and internal HBR, we believe that the dissociation of these three H-bonds contribute to the unfolding of the segment of wt-hFGF1, which contains residues K126-Q141. Interestingly, five of the seven residues involved in these four H-bonds (N32, K127, K126, R136, and H138), which were disrupted throughout the wt-hFGF1 MD simulation were also more susceptible to H/D exchange than they are in the mutant, R136E, as previously mentioned.

Clear transitions were also observed in the traces of other H-bonds in wt-hFGF1 including, Y139-N120, Y139-E104, S64-E67, and T44-D42; however, the donor-acceptor distances for all these bonds continued to increase beyond 2.4 μs before a final dissociation distance was stabilized (Fig. 5B and 5C). Again, there is correlation between the H/D exchange

data and MD simulation analysis for residues S64, E67, and D42, as these three residues, whose H-bonds were disrupted in the wt-hFGF1 MD simulation, were all more susceptible to H/D exchange in wt-hFGF1 than in mutant, R136E as previously mentioned. Interestingly, one H-bond in wt-hFGF1 between Y88 and E96 stabilized after the conformational change at 2.4 μs (Fig. 6B). Two H-bonds in wt-hFGF1 (S52-D50 and Y111-E101) remained consistently stable during the entire time span (4.8 μs) of the MD simulations (Figs. 6A and 6B). These H-bonds (S52-D50 and Y111-E101) were also consistently stable in the mutant, R136E, structure (Fig 7B and Fig. 8B). Another H-bond between the side chain carbonyl and side chain amine group of Q77 and Q91, located in beta-strands 6 and 7, was consistently found in the R136E mutant. Interestingly, this hydrogen bond was found missing in wt-hFGF1 (Fig. 7A). Additional inter-domain and local H-bonds that were consistently stable in the R136E mutant are shown in Fig. 7 (A and B) and Fig. 8 (A and B). However, one local H-bond between T75 and S72 was disrupted after 1.6 μs in the mutant, R136E MD simulation (Fig. 8B).
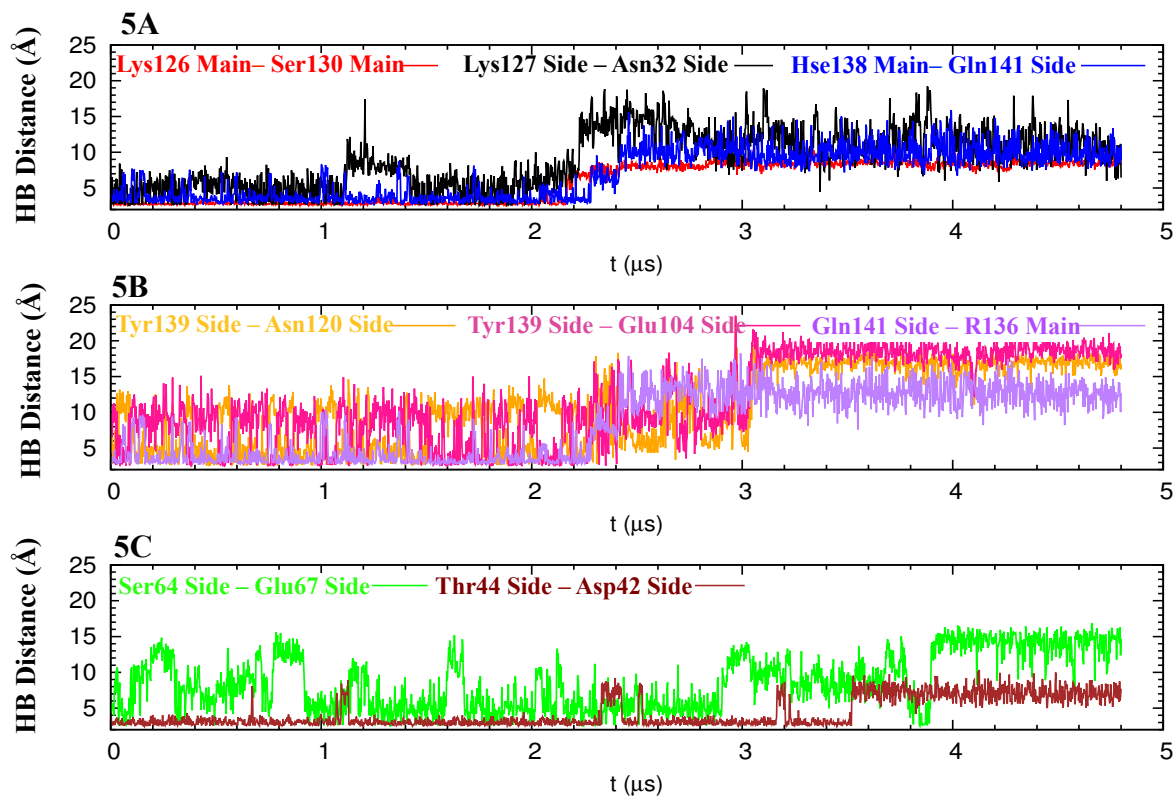
Figure 5. Time series of donor-acceptor distance for h-bonds that contribute to the conformational change observed in wt-hFGF1.
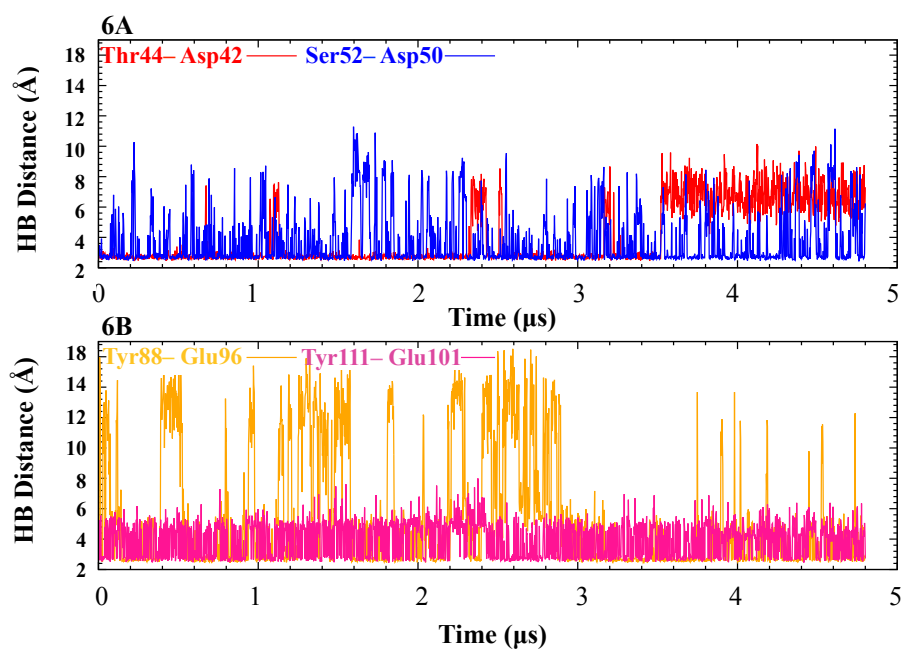
Figure 6. Time series of donor-acceptor distance for h-bonds that remain stable in wt-hFGF1 structure.
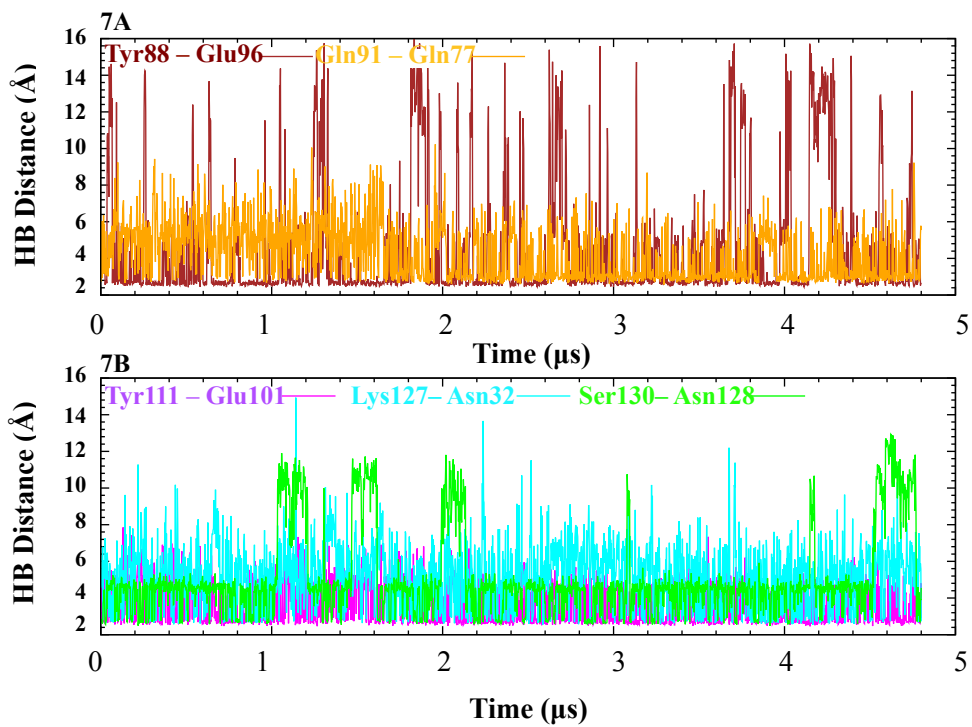
Figure 7. Time series of donor-acceptor distance for h-bonds that remain stable in mutant, R136E, structure.
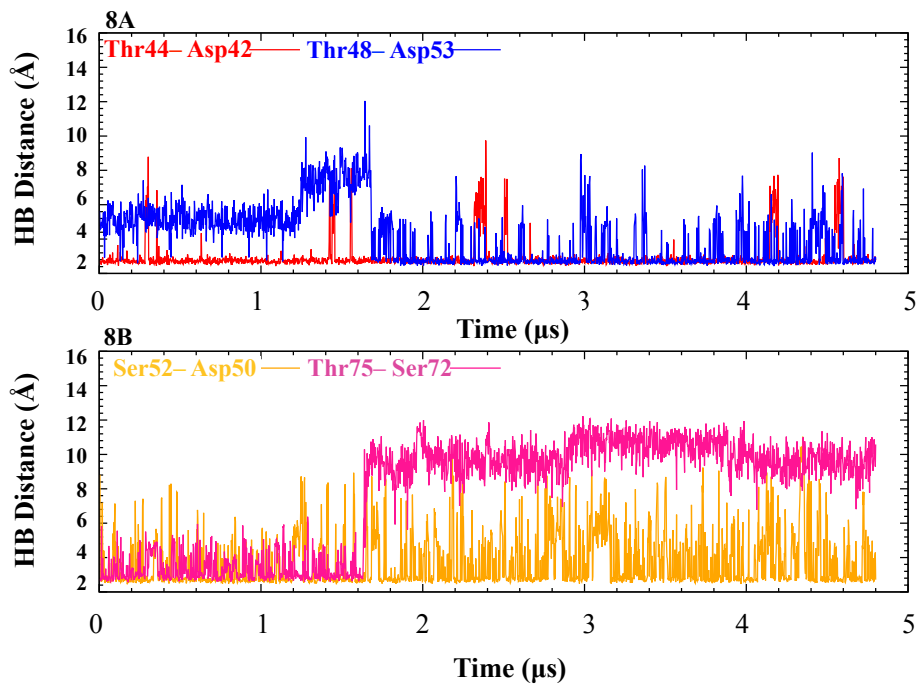

Figure 8. Time series of donor-acceptor distance for stable and non-stable h-bonds in mutant, R136E, structure.

Mutation R136E alters inter-domain and local interactions among residue pairs near and remote

to HBR

Dynamical network analysis was performed to obtain and compare cross-correlation

matrices of wild type and mutant proteins to identify pairs of residues that display different

behavior between mutant, R136E, and wt-hFGF1 structures [18]. The absolute difference

between the inter-residual cross-correlations between the mutant, R136E, and wt-hFGF1,

quantifying the absolute cross-correlation change in the cross-correlation of each residue pair due

to the R136E mutation as obtained from 4.8 μs of MD simulations is depicted in Fig. 9. This data

highlights multiple inter-domain interactions including several residues within the HS-binding

region that behaved differently between wt-hFGF1 and mutant, R136E systems (Fig. 9). Most

notable were the differences in the inter-domain interactions between R133 and D84, and

between K126 and N32, for wt-hFGF1 and mutant R136E. Each of these interactions was

formed between a canonical HS-binding residue and a residue located in a neighboring loop

region outside of the HBR. These differences are direct indicators that the charge reversal

mutation R136E in the HBR is altering interactions with a neighboring domain. This conclusion

agrees well, particularly for residue N32, with conclusions derived from H-bond analysis and

H/D exchange data. Differences between wt-hFGF1 and mutant systems for the D84-R133

interaction correspond with observations made from the salt bridge analysis previously

described. A consistent interaction between D84 and R133 was observed in the mutant system,

while in the wt-hFGF1 system, the D84-R133 interaction is disrupted and reformed as D84-K132

(Fig. 4C and 4D).

Additionally, differences were observed between the cross-correlations of residues C30

and I144/L145 as well as between T110 and I144. Variance in the behavior of these inter-domain

interactions indicates that mutation of R136E is affecting interactions entirely outside of the

HBR. Of further interest were the cross-correlation differences between residue pairs that are

spatially very distant from the HBR. One such pair of residues is Q59 and E67, which are

positioned on opposite sides of antiparallel beta strands 4 and 5, respectively (Fig. 9). Also

highlighted, are residues F36 and T48, positioned on opposite sides of antiparallel beta strands 2

and 3, respectively. Lastly, differences were observed between the cross-correlation of the inter-

domain interaction involving residues K26 and L58, which are positioned on antiparallel beta

strands 1 and 4 respectively. The differences in the cross-correlations among pairs Q59-E67, F36

and T48 as well as K26 and L58 suggest that mutation R136E alters local interactions among

hFGF1 residues that are spatially very distant from the HBR.
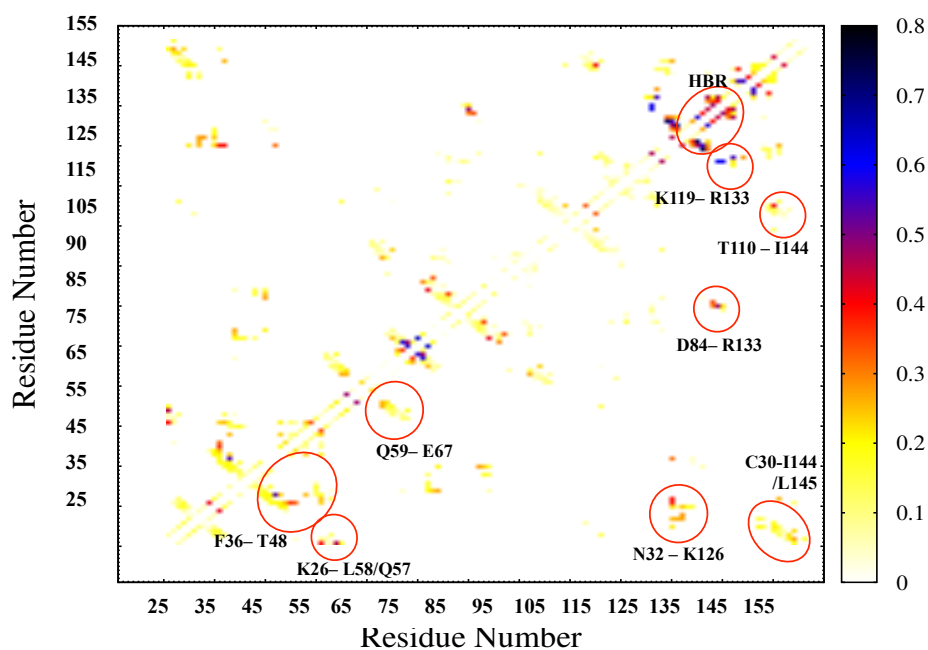
Figure 9. Absolute inter-residual cross-correlation difference of wt-hFGF1 and mutant, R136E structures ($|C_{ij} - C'_{ij}|$; see Dynamical Network Analysis in Materials and Methods). Key residue pairs whose behavior is different between wt-hFGF1 and mutant structures are circled in red and labeled.

Electrostatic potential maps highlighting the loop detachment within HBR of wt-hFGF1

Electrostatic potential maps were constructed using our initial hFGF1 model based on the crystal structure (PDB 1RG8). The electrostatic map of wt-hFGF1, without and with the R136E mutation included, shows that the negative charge disrupts the continuous region of positive charge in the HBR of hFGF1 (Fig. 10 A and B). Evidenced in the electrostatic potential map generated after MD simulations, the HBR is maintained as a concentrated region of positive charge for the mutant, R136E. Interestingly, the electrostatic potential map of wt-hFGF1 following MD simulation shows the HBR is no longer visible as a pocket of concentrated positive charge. Instead, the flexible loop within the HBR consisting of residues G134, P135, R136, and T137 protrude from the region in a way that suggests loop detachment. The electrostatic potential maps further support the conclusions drawn from equilibrium unfolding and NMR experiments that charge reversal at position 136 (R136E) stabilizes the HBR of hFGF1.
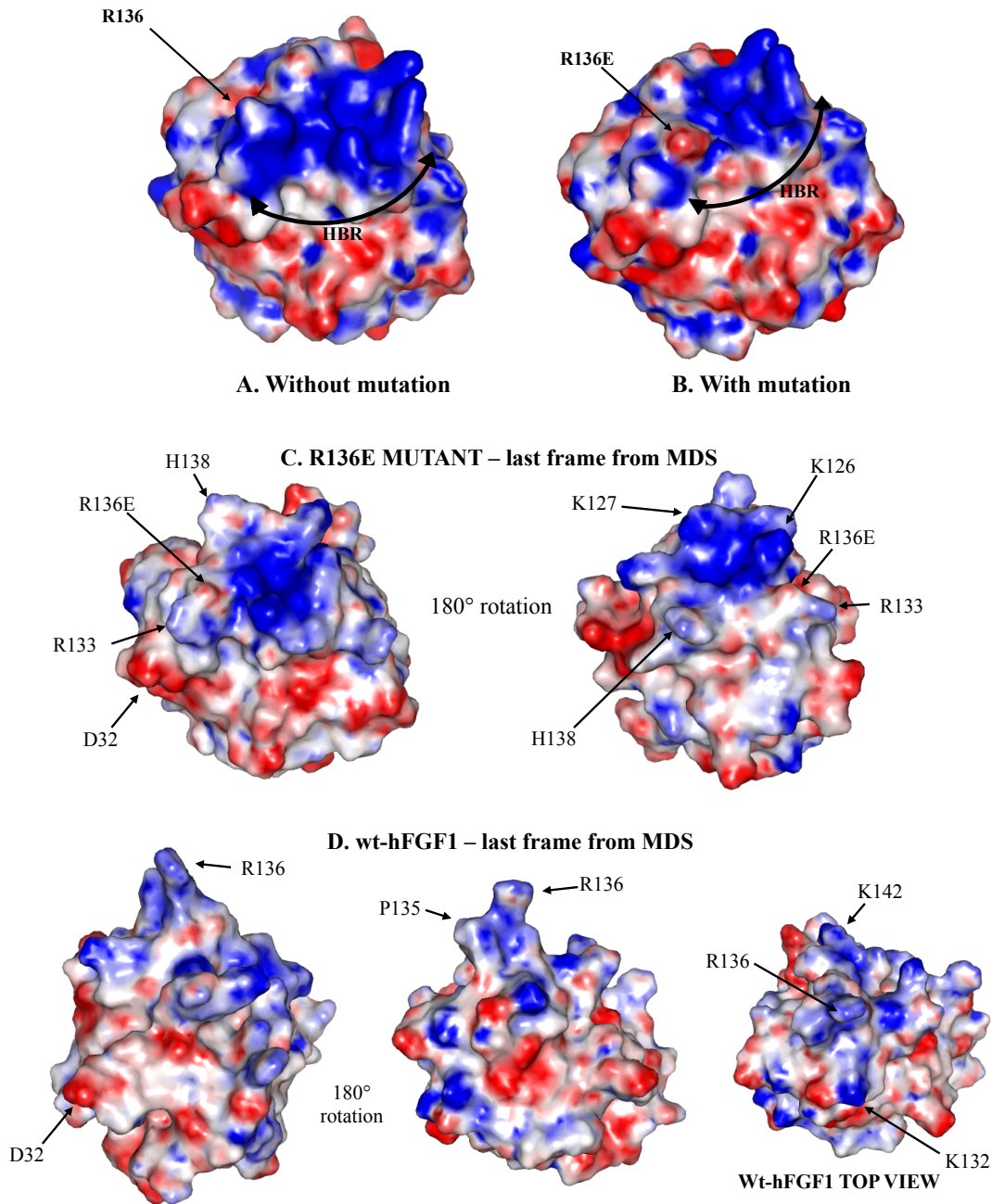
Figure 10. Panel-**A** Representation of the electrostatic potential in the three-dimensional structure of wt-hFGF1 before MD simulations were performed, showing the HBR as a region of concentrated positive charge colored in blue. Panel-**B** Representation of the electrostatic potential of the three-dimensional structure of hFGF1 showing that mutation of R136 to glutamate within the region of positive charge in the HBR (PDB 1RG8). Panel-**C** three-dimensional electrostatic potential map of the mutant structure after 4.8 μs of simulation, showing the recognizable HBR as a pocket of positive charge. Panel-**D** three-dimensional electrostatic potential map of the wt-hFGF1 structure after 4.8 μs of simulation showing no recognizable HBR.

Conclusion

A previous study of the designed hFGF1 mutation, R136E, has revealed an increase in the thermal and proteolytic stability of hFGF1 accompanied by a simultaneous decrease in the protein's affinity for HS [16]. Additionally, the cell proliferation activity of the R136E mutant was found to be about seven times higher than the wt-hFGF1 [16]. Herein, we believe that the enhanced activity of the mutant protein is a result of its increased structural stability. In this study, we have confirmed that the single charge-reversal substitution of R136 to glutamate in the HBR of hFGF1 increases the thermodynamic stability of the protein. We have also investigated the structural differences between mutant, R136E, and wt-hFGF1 at a molecular level using both 2D NMR and microsecond-level all-atom MD simulation.

To identify differences in the H-bonding pattern between the wt-hFGF1 and the R136E mutant, the degree of H/D exchange was monitored by HSQC spectroscopy. After 21 hours of exchange in D_2O, the amide protons of 62 residues in the wt-hFGF1 are completely exchanged while only 48 residues are completely exchanged in the R136E mutant. Interestingly, the amide protons of 33 residues in the R136E mutant do not exchange with D_2O as against 12 residues in wt-hFGF1. The increased number of key residues unique to R136E, which are resistant to H/D exchange leads us to believe that these residues significantly contribute to the increased structural stability of the R136E mutant.

Furthermore, analysis of MD simulations for both wt-hFGF1 and the R136E mutant, identify critical salt-bridge interactions in the HBR of mutant R136E structure involving residue E136 with R133, K126, and K132. Interestingly, these salt-bridges are not present in wt-hFGF1. We believe that, due to their location in the HBR, these interactions are largely responsible for the reduction in HS-binding affinity of the R136E mutant as compared to wt-hFGF1. Lastly,

dynamical network analysis revealed that the single charge reversal mutation, R136E, alters local and inter-domain interactions throughout the protein structure. Differences in the cross-correlation of inter-domain interactions in mutant, R136E, and wt-hFGF1 structures involving residues within the HBR are observed for residues R133-D84 as well as K126-N32. Correlation differences between mutant and wt-hFGF1 are also observed for inter-domain interactions completely outside of the HBR (C30-I144/L145, and T110-I144) and among residues, which are spatially distant from the HBR in the FGF1 beta barrel (Q59-E67, F36-T48, K26-L58). We conclude that these correlation differences contribute to the increased structural stability of the R136E mutant.

Materials and Methods

Materials: Quikchange II XL mutagenesis kits were supplied by Agilent, and Qiagen, USA supplied the DNA plasmid isolation kit. Novagen Inc., USA were the suppliers of DH5α and BL-21(DE3) competent cells. Cell culture medium was obtained from EMD Millipore, USA. Heparin Sepharose resin, used for protein purification(s), was obtained from GE Healthcare, USA. All buffer elements were obtained from VWR Scientific Inc, USA. Sigma and MP Biomedicals LLC were the suppliers of low molecular weight (~3kDa) heparin sodium salt. American Type Culture Collection (ATCC) was the supplier of NIH 3T3 cells, and additional cell culture reagents such as DMEM media, fetal bovine serum (FBS) and penicillin streptomycin were procured from Thermo Fisher Scientific USA.

Construction and purification of hFGF1 mutants: hFGF1 was cloned in pET-20b bacterial expression vector for site directed mutagenesis. Truncated FGF1, in which the first 14 amino terminal residues were removed, was used as template for all site-directed mutagenesis. Online

Agilent design software was used to create the forward and backward primers. Primers were then obtained from IDT DNA INC., USA. Following manufacturer instructions, QuikChange II XL kit(s) were used to perform site directed mutagenesis (SDM). Transformation of DH5α competent cells was performed following the standard heat shock method Wt-hFGF1 and the R136E mutant were both overexpressed in BL-21(DE3) *Escherichia coli* cells and cultured in lysogeny broth (LB) at 37°C and shaking at 250 rpm. Overexpressed cells were lysed using ultrasonication and the crude cell lysate was then centrifuged at 19,000 rpm to separate the protein(s) from the cell debris. Protein purifications of wt-hFGF1 and mutant hFGF1 were accomplished on a heparin Sepharose column by incrementally increasing the salt gradient in 10 mM sodium phosphate buffer containing 25mM $(NH_4)_2SO_4$ at pH 7.2 according to methods described previously [2, 11, 24]. The purity of FGF1 elute was confirmed by SDS-PAGE.

Equilibrium unfolding of hFGF1 mutants: Equilibrium unfolding of wt-hFGF1 and mutant hFGF1 was accomplished on a Jasco-1500 spectropolarimeter equipped with a fluorescence detector. Each spectrum was an average of 3 scans using a 1 cm quartz cell. Equilibrium thermal unfolding experiments were conducted using a protein concentration of 0.5 mg/mL in 10 mM phosphate buffer containing 100 mM NaCl and 25 mM $(NH_4)_2SO_4$ at pH 7.2. For experiments in D_2O buffer, protein solution was contained in 100 mM NaCl and 25 mM $(NH_4)_2SO_4$ at pH 6.5. For experiments performed in the presence of heparin, was present in a 1:10 protein to heparin ratio. Far-UV CD spectra were collected in 5 degree increments starting at 20°C and ending at 80°C. The fraction unfolded was calculated and plotted as a function of temperature. T_m, was determined as the temperature at which 50% of the protein population was denatured.

Urea induced equilibrium unfolding experiments were conducted at protein concentrations of approximately 3 μM in 10 mM phosphate buffer containing 10 mM NaCl and 25 mM $(NH_4)_2SO_4$ at pH 7.2. Urea was titrated, in identical volumes, into protein solutions up to concentrations of 6 M. Protein unfolding was individually monitored by 228 nm ellipticity and by the 308 nm / 350 nm emission intensity ratio. Fraction of unfolded protein population was determined from both sets of data and was plotted against concentration of the chemical denaturant. C_m, was determined as the concentration at which 50% of the protein population was denatured.

Nuclear Magnetic Spectroscopy: All NMR experiments were acquired on a Bruker 700 MHz NMR using 2K x 256 data points. Each experiment was performed with isotopically labeled protein at 25°C with a minimum protein concentrations of 300 μM in 10 mM phosphate buffer containing 100 mM NaCl and 25 mM $(NH_4)_2SO_4$ (pH 7.2). To the protein solution, 10% D_2O was added. $^1H – ^{15}N$ heteronuclear single quantum coherence (HSQC) spectra were collected after 21 hours of run time and data was analyzed using Sparky 3.114 software [33]. For amide proton exchange experiments, the protein samples were concentrated to ~0.5 mM by ultrafiltration (Millipore). Hydrogen-deuterium exchange was initiated by a series of buffer exchanges using ultrafiltration (Millipore) until the sample was completely equilibrated in D_2O solution containing 10 mM phosphate buffer as well as 100 mM NaCl and 25 mM $(NH_4)_2SO_4$ (pH 6.5). $^1H – ^{15}N$ HSQC spectra were collected after 21 hours of run time and data was analyzed using Sparky 3.114 software [33]. To calculate percentage exchange for each residue, crosspeak intensity was determined by the sum-over-box integration method in Sparky. The following equation was used to determine the final percentage exchange:

[Crosspeak intensity $_{(D2O\ 1H\ -\ 15N\ HSQC)}$ / Crosspeak intensity $_{(H2O\ 1H\ -\ 15N\ HSQC)}$] x100. Residues for which the crosspeak intensity in the deuterium ^{1}H – ^{15}N HSQC spectrum was 0-10%, 10-50%, 50-90%, or 90-100% of the crosspeak intensity in the H$_2$O ^{1}H – ^{15}N HSQC spectrum were classified as completely exchanged, significantly exchanged, partially exchanged, or resistant to exchange respectively.

Electrostatic potential maps: Electrostatic potential maps were created from the hFGF1 crystal structure (also used for MD simulations (PDB 1RG8)) within Pymol viewing software. Electrostatic potential maps following MD simulations were created from the last frame of the MD trajectory for both wt-hFGF1 and mutant, R136E.

Molecular dynamics simulation: The crystal structure of hFGF1 in the absence of heparin (Protein Data Bank code 1RG8) was used for the 4.8 μs simulations. To appropriately match the truncated form of hFGF1 used for equilibrium unfolding and NMR experiments, the first 11 amino acids from the N-terminus were removed using Pymol software. The protonation state of H138 in the heparin-binding region was verified using Propka 3.0 software [25]. The structures were first energy-minimized for 2000 steps using the conjugate gradient algorithm and then solvated in a water box of 16x16x16 Å^3 with TIP3P water [26, 27]. The solvent box was neutralized with a set concentration of 0.1 M NaCl. The structure was then refined through a series of steps to get the system ready for production runs. To prepare the system for equilibration, the protein backbone, side chains, and solvent molecules and ions were relaxed while keeping the hydrogen atoms fixed. Equilibration was performed in the NPT ensemble using NAMD 2.9 and the CHARMM36 force field [25, 28]. First, the side chains were relaxed

for 10 ps, while the backbone was fixed in the absence of solvent molecules. Then, holding all

protein atoms rigid, water molecules were relaxed throughout the system for 1,500 minimization

steps and followed by 50 ps of dynamics. Next, the final relaxation of solvent molecules around

the protein was performed with harmonic constraints using a 1 kcal/(mol Å^2) force constant.

Lastly, the temperature was increased in incremental steps (10 K per 2 ps) until a final

temperature of 300 K was reached. This operation was followed by 5 ns of dynamics. The 300 K

temperature was sustained by Langevin dynamics with a damping coefficient of 1 ps^{-1}, and

pressure (1 atm with a period of 100 fs and decay time of 50 fs) was sustained by the Langevin

piston method [29]. Using particle mesh Ewald (PME) method along with periodic boundary

conditions, long-distance electrostatic interactions were determined. Van der Waals as well as

electrostatic interactions beyond 12 Å were cut-off with a switching function [30]. The

production simulation time was 4.8 μs for both wild type and mutant hFGF1 that were conducted

using Anton 2 supercomputer [31]. All MD simulation analyses were performed using VMD 1.9

[32].

Dynamical network analysis:

Interresidual cross-correlation matrix for each system was constructed using the Dynamical

Network Analysis tool implemented in VMD [18]. The cross-correlation of a residue pair i and j

is defined as:

$$C_{ij} = \frac{\langle \Delta r_i(t) . \Delta r_j(t) \rangle}{\sqrt{\langle \Delta r_i(t)^2 \rangle \langle \Delta r_j(t)^2 \rangle}}$$

where $\Delta r_i(t) = r_i(t) - \langle r_i(t) \rangle$, $r_i(t)$ is the position of Cα atom of residue i at time t, and $\langle \cdot \rangle$ is

an average over all t. C_{ij} quantifies the linear correlation of the motion of Cα atoms of residues i

and j. Values 1.0 and -1.0 indicate strongest positive and negative correlations possible and 0.0 indicates the complete lack of any linear correlations. If C_{ij} and C'_{ij} are measured under two different simulation conditions (e.g., wild type vs mutant protein), $|C_{ij} - C'_{ij}|$ would quantify the absolute change due to the change in the condition (e.g., mutation).

Acknowledgements

Works Cited

1.   Katoh, M., Therapeutics Targeting FGF   Signaling Network in Human Diseases. Trends in Pharmacological Science, 2016. 37(12): p. 1081-1096.

2.   Zakrzewska, M., et al., Increased Protein Stability of FGF1 Can Compensate for Its Reduced Affinity for Heparin. Journal of Biological Chemistry, 2009. 284(37): p. 25388-25403.

3.   Miller, D., Compensation by Fibroblast Growth Factor 1 (FGF1) Does Not Account for the Mild Phenotypic Defects Observed in FGF2 Null Mice American Society for microbiology, 2000. 20: p. 2260-2268.

4.   Beenken, A., Plasticity in Interactions of Fibroblast Growth Factor 1 (FGF1) N Terminus with FGF Receptors Underlies Promiscuity of FGF1. J. Biol. Chem, 2012. 287(5): p. 30676-3078.

5.   Gardner, V., et al., Therapeutic Angiogenesis for Wound Healing. 2017, Cardiovascular Biotherapeutics Inc.: United States.

6.   Beenken, A.M., Moosa., The FGF family: biology, pathophysiology and therapy. National Review Drug Discovery 2009. 8: p. 235-253.

7.   Liu, W., Effective treatment of steatosis and steatohepatitis by fibroblast growth factor 1 in mouse models of nonalcoholic fatty liver disease. PNAS, 2016. 113(8): p. 2288-2293.

8.   Formiga, F.R., et. al., Controlled delivery of fibroblast growth factor-1 and neuregulin-1 from biodegradable microparticles promotes cardiac repair in a rat myocardial infarction model through activation of endogenous regeneration. Journal of Controlled Release, 2014. 173: p. 132-139.

9.   Brych, S., Structure and stability effects of mutations designed to increase the primary sequence symmetry within the core region of a β-trefoil. Protein Science 2001. 10: p. 2587–2599.

10.   Culajay, J.F., et al., Thermodynamic characterization of mutants of human fibroblast growth factor 1 with an increased physiological half-life. Biochemistry, 2000. 39(24): p. 7153-8.

11.   Zakrzewska, M., Design of fully active FGF-1 variants with increased stability. Protein Engineering, Design & Selection, 2004. 17(8): p. 603-611.

12.   Blaber, S.I., et al., Reversible Thermal Denaturation of Human FGF-1 Induced by Low Concentrations of Guanidine Hydrochloride. Biophysical Journal, 1999. 77(1): p. 470-477.

13.   Alsenaidy, M.A., An empirical phase diagram approach to investigate conformational stability of "second-generation" functional mutants of acidic fibroblast growth factor-1. Protein Science, 2012. 21: p. 418-432.

14.   Erzurum, V.Z., et al., R136K fibroblast growth factor-1 mutant induces heparin-independent migration of endothelial cells through fibrin glue. Journal of Vascular Surgery, 2003. 37(5): p. 1075-1081.

15.   Xia, X., et al., Properties of 2nd-Generation Fibroblast Growth Factor-1 Mutants for Therapeutic Application. PLOS-One, 2012. 7(11): p. e48210.

16.   Thallapuranam, S.K., Engineered Compositions of FGF and Methods of Use Thereof, A.I.P. Law, Editor. 2016: United States.

17.   Canales, A., et al., Solution NMR structure of a human FGF-1 monomer, activated by a hexasaccharide heparin-analogue. Febs Journal, 2006. 273(20): p. 4716-4727.

18.   Sethi, A., et al., Dynamical networks in tRNA: protein complexes. Proc.Natl. Acad. Sci., 2009. 106(16): p. 6620-6625.

19.   Harmer, N., Insights into the role of heparan sulfate in fibroblast growth factor signalling. Biochemical Society Transactions, 2006. 34(3): p. 442-445.

20.   Pellegrini, L., Role of heparan sulfate in fibroblast growth factor signalling: a structural view. Current Opinion in Structural Biology 2001. 11: p. 629–634.

21.   Pellegrini, L., et al., Crystal structure of fibroblast growth factor receptor ectodomain bound to ligand and heparin. Nature, 2000. 407(6807): p. 1029-1034.

22.   Stauber, D.J., A.D. DiGabriele, and W.A. Hendrickson, Structural interactions of fibroblast growth factor receptor with its ligands. PNAS, 2000. 97(1): p. 49-54.

23.   DiGabriele, A., Structure of a heparin-linked biologically active dimer of fibroblast growth factor. Nature, 1998. 393: p. 812-817.

24.   Zakrzewska, M., et al., Highly stable mutants of human fibroblast growth factor-1 exhibit prolonged biological action. J Mol Biol, 2005. 352(4): p. 860-75.

25.   Olsson, et al., Propka3: consistent treatment of internal and surface residues in empirical pKa predictions. J. Chem. Theory Comput., 2011. 7: p. 525-537.

26.   Jorgensen, W.L., et al., Comparison of simple potential functions for simulating liquid water. J Chem Phys 1983. 79: p. 926–935.

27.   Reid, J.K., On the method of conjugate gradients for the solution of large sparse systems of linear equations. In Reid J.K., Large Sparse Sets of Linear Equations (Academic Press, London), 1971: p. 231-254.

28.   Best, et al., Optimization of the additive CHARMM all-atom protein force field targeting improved sampling of the backbone ϕ, ψ and side-chain $\chi 1$ and $\chi 2$ dihedral angles. J. Chem. Theory Comput., 2012. 8: p. 3257-3273.

29.   Martyna, G.J., D.J. Tobias, and M.L. Klein, Constant pressure molecular dynamics algorithms. J. Chem. Phys., 1994. 101: p. 4177-4189.

30.   Darden, et al., Particle mesh Ewald: An N·log(N) method for Ewald sums in large systems. J. Chem. Phys., 1993. 98: p. 10089-10092.

31.   Shaw, D.E., et al., Anton 2: Raising the Bar for Performance and Programmability in a Special-Purpose Molecular Dynamics Supercomputer. 2014: p. 41-53.

32.   Humphrey, W., A. Dalke, and K. Schulten, VMD: Visual Molecular Dynamics. J. Mol. Graph., 1996. 14: p. 27-28, 33-38.

33.   Goddard, T.K., DG., SPARKY 3. University of California, San Francisco.

Conclusion

The studies conducted within this project have yielded detailed and interesting results that provide insight on the role of particular amino acids within the heparin-binding region (proline-135 and arginine-136) as well as outside of the heparin-binding region (aspartate-82 and aspartate-84) of hFGF1. These studies allude to the capacity of rationally designed site-directed mutagenesis to influence the inherent stability of hFGF1 and to the role of heparin within hFGF1 signaling. Additionally these studies highlight the unique molecular interactions that engender the heparin-independent stability and increased biological activity of the hFGF1 mutant, R136E.

The replacement of proline-135, with positive charge (P135K) was found to structurally destabilize hFGF1 by increasing the conformational flexibility of the protein backbone and the solvent-exposure of the hydrophobic surfaces typically buried within the protein core. This result is likely due to increased charge repulsion generated by the addition of a positive charge within a cluster of positively charged residues that constitute the heparin-binding region in the native conformation of wt-hFGF1. Not surprisingly, the P135K mutant demonstrated similar affinity to heparin as the wt-hFGF1, and the increase in thermostability of P135K in the presence of heparin was comparable to wt-hFGF1. Lastly, introduction of a positive charge at position 135 did not significantly alter the cell proliferation ability of the protein in the presence or absence of heparin compared to wt-hFGF1.

Substitution of P135 with glutamine (P135Q) did not significantly alter the structural stability of hFGF1, nor did it critically impact the cell proliferation activity of hFGF1. This mutant was measured to have a slightly higher binding affinity for the ligand, heparin, perhaps due to the increased conformational flexibility of the protein backbone as measured by LTD, which probably facilitates the most optimum interaction with heparin. However, the thermal

stability of the P135Q mutant was modestly less than wt-hFGF1 in both the absence and presence of heparin.

Introduction of a negative charge at position 135 (P135E) was a particularly interesting mutation, providing insight on the role of heparin within hFGF1 signaling. Introduction of a negative charge at position 135 did not alter the structural integrity of the protein. However, the heparin-binding affinity of the P135E mutant was three times higher than that of wt-hFGF1. Interestingly, the cell proliferation activity of the P135E mutant in the presence of heparin was statistically lower than heparin-bound wt-hFGF1. Altogether, these results suggest that the heparin-binding affinity of hFGF1 is not positively correlated to its cell proliferation activity.

Double mutants, P135K/R136E and P135E/R136E both exhibited reduced binding affinity toward heparin. Double mutant, P135K/R136E, was just as thermally stable as wt-hFGF1 in the absence of heparin, while the inherent stability of double mutant, P135E/R136E, was increased compared to wt-hFGF1. In the presence of heparin, the thermal stability of neither double mutant was increased, which is conceivably due to the reduced heparin-binding affinity as determined from ITC experiments. Interestingly the cell proliferation activity of these double mutants was statistically higher that wt-hFGF1 at maximum protein concentrations, which indicates that hFGF1 is not dependent on heparin for cell signaling.

From these mutagenesis studies, we conclude that the role of proline at position 135 is to help maintain structural integrity of the heparin-binding region of hFGF1. P135 seems to be a key modulator of the meticulous positioning and structural spacing of critical heparin-binding residues (R133 and R136) for optimum interaction and binding with the ligand heparin, which, due to the inherent instability of the wildtype protein, is essential for prolonging the bioavailability of wt-hFGF1.

The mutations performed on positions 82 and 84 are near to but outside of the heparin-binding region of hFGF1. None of the D82 or D84 mutations significantly altered the backbone conformational fold of the protein. D82R seems to alter the tertiary structure of the protein such that the hydrophobic surfaces are significantly more solvent- exposed and the flexibility of the protein backbone is significantly increased. The D82R/D84R double mutant, seems to influence the solvent exposure of the protein's hydrophobic surfaces as well as flexibility of the protein backbone in a similar manner, but to a lesser extent than the D82R mutant. Interestingly, the D82R mutation has a heparin-binding affinity that is increased ten-fold compared to wt-hFGF1. However, the thermal stability as well as the cell proliferation activity of the D82R mutant is modestly reduced to wt-hFGF1 in both the absence and presence of heparin. From these it can be concluded that the heparin-binding affinity of hFGF1 is not well correlated to its cell proliferation activity, and furthermore, that binding to heparin is not a mandatory prerequisite for hFGF1 mediated cell signaling.

The charge reversal mutation at position 84 (D84R) does not alter the structural integrity of the protein, and it does not significantly alter the thermal stability of the protein in either the absence or presence of heparin. However, the heparin-binding affinity of the D84R mutant is modestly increased compared to wt-hFGF1, as expected due to an extension of the heparin-binding pocket. Furthermore, despite an increase in the heparin-binding affinity, the D84R mutant was not any more active towards cell proliferation in the presence of exogenous heparin than wt-hFGF1. Again, this suggests that heparin-binding affinity is not well correlated to the cell proliferation activity of hFGF1.

Substitution of aspartate at position 82 with asparagine (D82N) did not significantly influence the structural stability or the thermal stability of hFGF1. It did modestly increase the

heparin-binding affinity of the protein as compared to wt-hFGF1. However, the cell proliferation activity of the D82N mutant in the presence of exogenous heparin was reduced (at the highest protein concentration used) compared to wt-hFGF1, and overall, the bioactivity of D82N was no different from wt-hFGF1. These results support the conclusion once again that heparin-binding affinity is not well correlated to the cell proliferation activity of hFGF1.

Lastly, as previously mentioned, the double charge reversal mutant, D82R/D84R, does modestly alter the structural stability of hFGF1, due to the presence of the D82R mutation. Interestingly, the heparin-binding affinity of the D82R/D84R double mutant is reduced by almost half compared to wt-hFGF1, and the increase in thermostability of this double mutant upon binding to heparin is also modestly reduced. However, in the presence of heparin, this double mutant is just as active toward cell proliferation as wt-hFGF1.

Overall, the equilibrium unfolding experiments performed on mutants P135E, P135K, P135Q within the heparin-binding region and mutants D82R, D84R, D82N, and D82R/D84R outside of the heparin-binding region consistently confirm the role of heparin as a structure-stabilizing agent of hFGF1. Analysis of the P135E, P135E/R136E, P135K/R136E, as well as all single and double mutants performed on positions 82 and 84 all suggest that heparin-binding affinity and cell proliferation activity of hFGF1 are not completely positively correlated. This lack of a clear positive correlation across five unique mutations within and outside of the heparin-binding pocket strongly suggests that hFGF1 is not dependent on binding to heparin for recognition and activation of a cell surface FGFR. This conclusion from our studies corresponds well with the conclusion(s) made by previous studies in this field, which have shown that inherently stabilized hFGF1 mutants with reduced affinity towards heparin can elicit a mitogenic response that is more robust than wt-hFGF1 in a heparin independent manner [1-3].

The final study of this project, specifically regarding the single mutant R136E, strongly suggests through equilibrium unfolding experiments using both heat and chemical denaturants, that the charge reversal mutation at position 136 significantly increased the stability of hFGF1 compared to wt-hFGF1. The intramolecular interactions that generate this increased stability were further probed through two-dimensional NMR and all-atom, microsecond length MDS experiments. Interestingly, using HSQC spectroscopy, it was discovered that the R136E mutant structure was more resistant to H/D exchange than wt-hFGF1. The backbone amide proton of 61 residues in wt-hFGF1 were completely exchanged with D_2O after 21 hours exposure to deuterium buffer while only 39 residues in the mutant, R136E, were completely exchanged. In addition, the mutant, R136E, structure had 33 residues that were resistant to exchange with D_2O (classified as "No exchange") while wt-hFGF1 had only 19 residues that were resistant to H/D exchange. The overall conclusion from these experiments is that the residues that are more resistant to H/D exchange in the mutant, R136E, structure are believed to be key residues that confer increased stability to hFGF1.

From analysis of the MD simulations, it was found that introduction of a negative charge at position 136 generates electrostatic interactions with critical heparin-binding residues R133, K126, and K132. As these salt-bridges are not present in the wt-hFGF1 simulation, we conclude that they are critical interactions that stabilize the HBR by minimizing the charge-charge repulsion, thereby significantly reducing the heparin-binding affinity of the mutant, R136E, protein. Furthermore, from the dynamical network analysis, several local as well as interdomain interactions were identified throughout the protein structure whose cross-correlation(s) are different between the mutant and wt-hFGF1 structures. Particularly, we conclude that differences in the cross-correlation of the interdomain interactions between residues R133-D84, C30-

I144/L145, K126-N32, Q59-E67, F36-T48, and K26-L58 all contribute to the stability of the

R136E mutant.

Works Cited

1. Xia, X., et al., Properties of 2nd-Generation Fibroblast Growth Factor-1 Mutants for Therapeutic Application. PLOS-One, 2012. 7(11): p. e48210.

2. Zakrzewska, M., et al., Highly stable mutants of human fibroblast growth factor-1 exhibit prolonged biological action. J Mol Biol, 2005. 352(4): p. 860-75.

3. Zakrzewska, M., et al., Increased Protein Stability of FGF1 Can Compensate for Its Reduced Affinity for Heparin. Journal of Biological Chemistry, 2009. 284(37): p. 25388-25403.

Future Perspectives

The results of this thesis provide clues for the design of hFGF1, which lacks heparin binding. There are many caveats for hFGF1 therapeutics that involve heparin. Heparin production is expensive, heparin is well known for its anti-coagulant properties, and additionally, heparin generates the release of excessive interstitial fluid which dilutes hFGF1 delivery to a wound [1]. Thus, advancement of wound healing and tissue regeneration therapeutics involving hFGF1 may be largely contingent on the creation of biologically active hFGF1 with diminished or no heparin binding. So far, understanding of the molecular mechanisms underlying hFGF1 signaling has been primarily based on the available crystal structures of the hFGF1/heparin/receptor complex [2-4]. Therefore, it will be interesting to determine the hFGF1 (which lacks heparin binding)– receptor complex in the absence of heparin.

Furthermore, not only does hFGF1 play significant roles in mitogenic activities, but recently, multiple studies have revealed unforeseen roles of hFGF1 in metabolic pathways related to insulin dependent glucose metabolism as well as adipose tissue remodeling [5, 6]. Analysis of the underlying molecular mechanisms has revealed that various threshold levels of hFGF1-receptor dimerization stability modulate the magnitude and selectivity of downstream signaling, which ultimately regulates the elicited response as a metabolic or mitogenic response [7]. For wt-hFGF1, receptor binding and dimerization is influenced by the protein's binding affinity for heparin. Therefore, understanding these hFGF1 signaling pathways with hFGF1 mutants that exhibit decreased heparin binding/lack heparin binding will provide strong clues regarding the partition of the hFGF1-induced cell proliferation and cellular metabolic pathways.

The knowledge gained from the studies performed here on the hFGF1-heparin interaction can further be extrapolated to other heparin-binding FGF isoforms. In addition, the influence of

hFGF1-heparin interactions on hFGF1-induced cell differentiation of stem cells can also lead to

new hFGF1 based therapeutics.

Works Cited

1.   Xia, X., et al., Properties of 2nd-Generation Fibroblast Growth Factor-1 Mutants for Therapeutic Application. PLOS-One, 2012. 7(11): p. e48210.

2.   Pellegrini, L., et al., Crystal structure of fibroblast growth factor receptor ectodomain bound to ligand and heparin. Nature, 2000. 407(6807): p. 1029-1034.

3.   Plotnikov, A.N., et al., Crystal Structures of Two FGF-FGFR Complexes Reveal the Determinants of Ligand-Receptor Specificity. Cell, 2000. 101: p. 413–424.

4.   DiGabriele, A., Structure of a heparin-linked biologically active dimer of fibroblast growth factor. Nature, 1998. 393: p. 812-817.

5.   Jonker, J.W., et al., A PPAR g -FGF1 axis is required for adaptive adipose remodelling and metabolic homeostasis. Nature, 2012. 485: p. 391–394.

6.   Suh, J.M., et al., Endocrinization of FGF1 produces a neomorphic and potent insulin sensitizer. Nature, 2014. 513: p. 436–439.

7.   Huang, Z., et al., Uncoupling the Mitogenic and Metabolic Functions of FGF1 by Tuning FGF1-FGF Receptor Dimer Stability. Cell Reports, 2017. 20: p. 1717–1728.
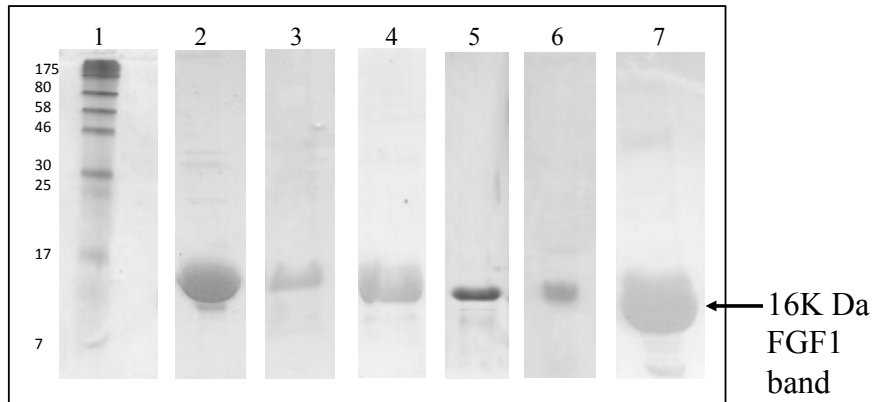
Figure S1: SDS PAGE of the purified wt-hFGF1 and designed mutants. Lane-1 is a commercial broad range NEB #7703 protein marker. Lanes 2, 4, 5, 6, and 7 represent the 1500 mM NaCl fractions of wt-hFGF1 and the designed mutants, P135Q, P135E, P135K, and P135K/R136E, respectively. Lane-3 represents the 500 mM NaCl fraction of the double mutant, P135E/R136E.
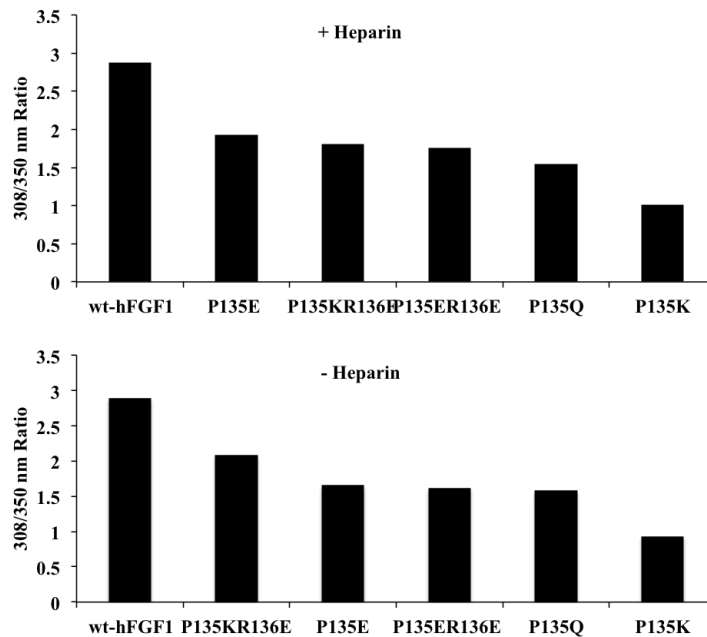

Figure S2: Ratio of 308nm/350 nm fluorescence emission intensity indicating the largest difference in tyrosine – tryptophan fluorescence for wt-hFGF1 and the smallest difference in tyrosine – tryptophan for designed mutant, P135K.
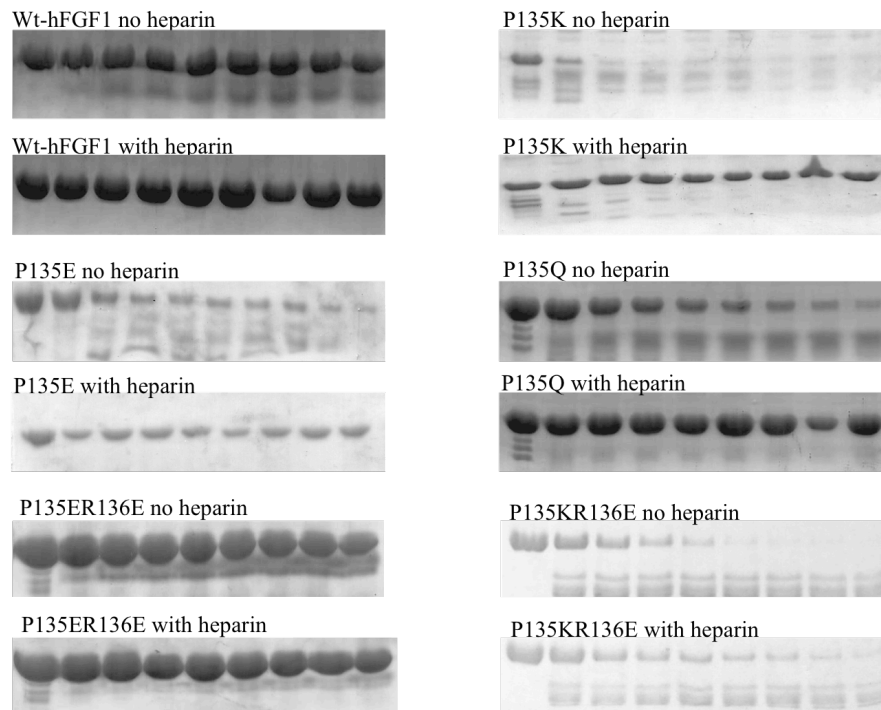
Figure S3: SDS PAGE representing the products of limited trypsin digestion of the wt-hFGF1and the designed mutants in the presence and absence of heparin.
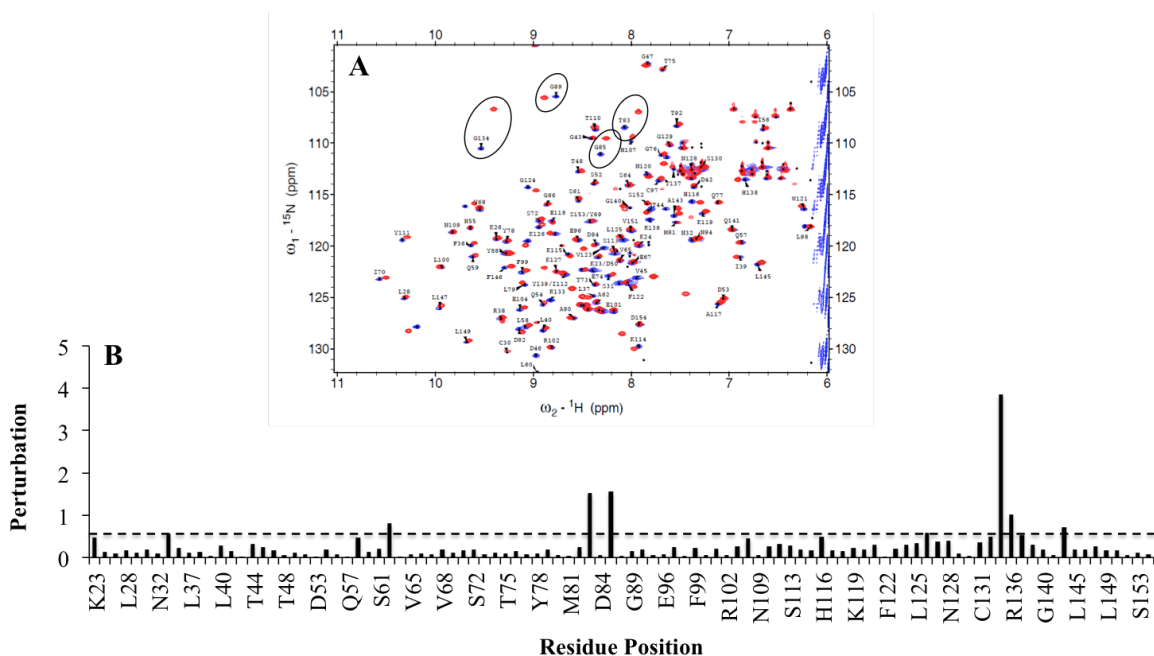
Figure S4: Panel – **A**, Superimposition of the ^{1}H-^{15}N HSQC spectra of wt-hFGF1 (red) over that of P135E/R136E mutant (blue). Panel – **B**, ^{1}H-^{15}N chemical shift perturbation due to the P135E/R136E mutation. The dashed line signifies an arbitrary threshold above which ^{1}H – ^{15}N chemical shift perturbations were considered to be significant. The ^{1}H-^{15}N chemical shift perturbation of individual residues were calculated using the formula, $(\sqrt{[(2\Delta\delta_{NH})^2 + (\Delta\delta_N)^2]})$**.**
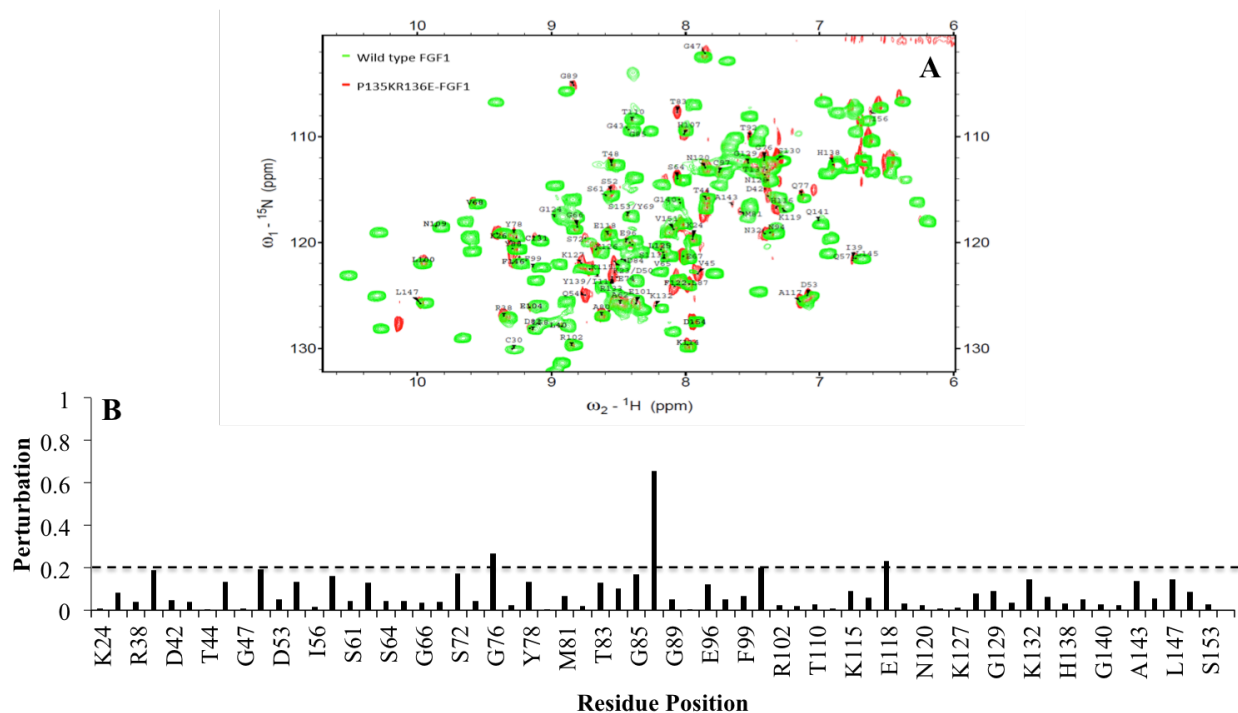
Figure S5: Panel – **A**, Superimposition of the ^{1}H-^{15}N HSQC of wt-hFGF1 (green) over that of P135K/R136E (red). Panel – **B**, ^{1}H-^{15}N chemical shift perturbation due to the P135K/R136E mutations. The dashed line signifies an arbitrary threshold above which ^{1}H – ^{15}N chemical shift perturbations were considered to be significant. The ^{1}H-^{15}N chemical shift perturbation of individual residues were calculated using the formula, ($\sqrt{[(2\Delta\delta_{NH})^2 + (\Delta\delta_N)^2]}$).
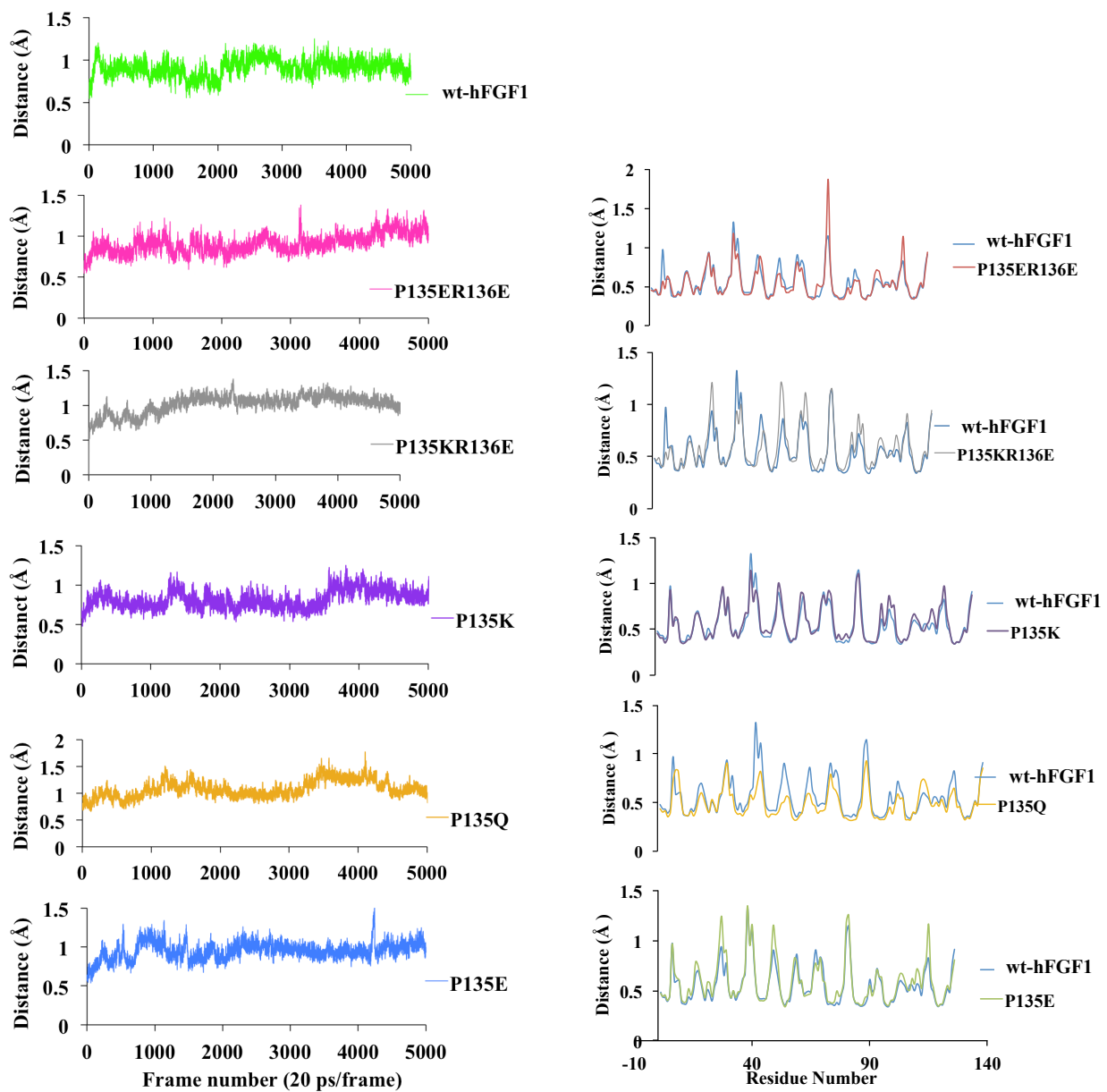
Figure S6: Panel-**A,** RMSD of the Cα backbone atoms as a function of time for each simulation. Panel-**B,** Overlay of RMSF values of each designed hFGF1 mutant in comparison to wt-hFGF1.
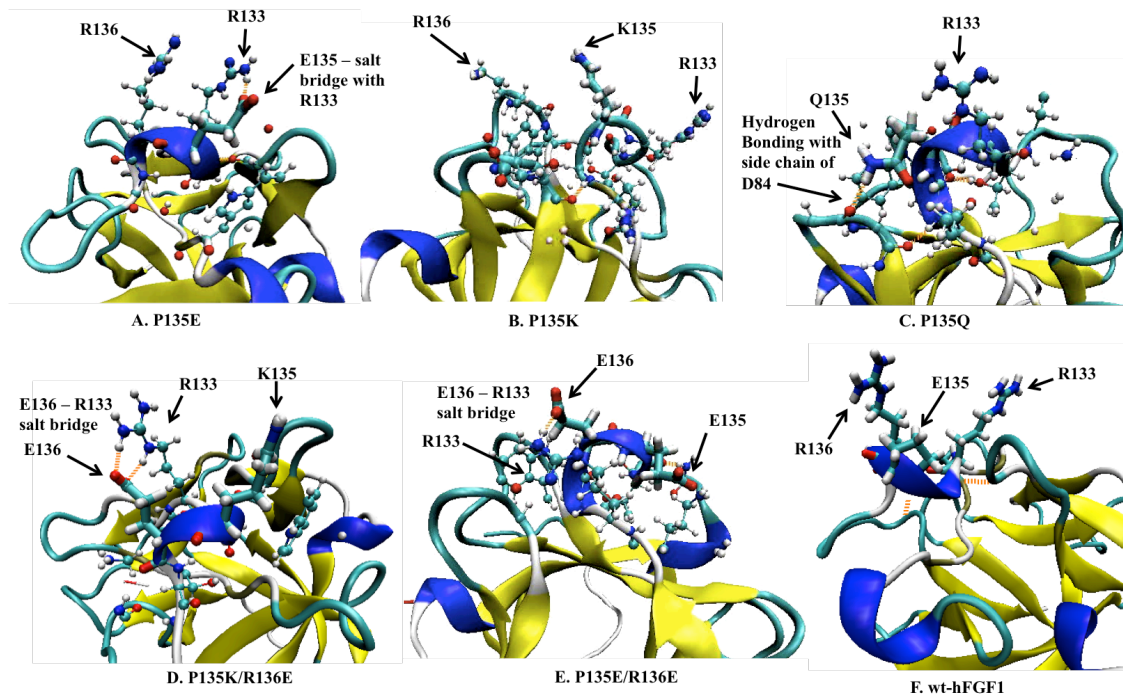
Figure S7: Still images of hFGF1 and the designed mutants [P135E (A), P135K (B), P135Q (C), P135K/R136E (D), P135ER136E (E), and wt-hFGF1 (F)] obtained from molecular dynamics simulation(s). The residue(s) of interest are shown as stick representation. Hydrogen bonding is shown as dashed orange lines. Additional amino acids, located within a spatial distance of 5 A° from the amino acid of interest are shown as CPK representation. Please see attached videos for visual of the full 100ns simulation.

Table S1: Salt bridge formations in MD simulations of wt-hFGF1 and designed hFGF1 mutations.

Protein	Salt Bridge Formations									
wt-hFGF1	D46-R38	D53-R38		E67-K114	E95-K115	E105-K132	E118-K119			
P135E	D46-R38	D53-R38	D84-R133	E67-K114	E95-K115	E105-K132		E135-R133		
P135K	D46-R38	D53-R38		E67-K114	E95-K115	E105-K132				
P135Q	D46-R38	D53-R38		E67-K114	E95-K115	E105-K132				
P135ER136E	D46-R38	D53-R38	D84-R133	E67-K114	E95-K115	E105-K132	E118-K119	E135-R133	E136-K132	E122-R133
P135KR136E	D46-R38	D53-R38		E67-K114	E95-K115	E105-K132	E118-K119			

Table 2: Thermodynamic values for the heparin interaction with hFGF1 mutants and wt-hFGF1

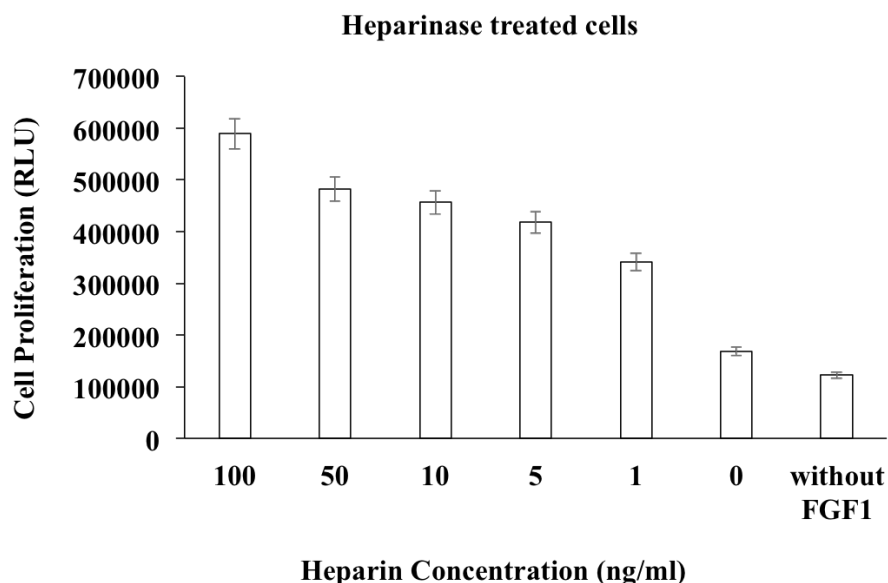| Protein	ΔH (k.cal/mol)	$-T\Delta S$ (k.cal/mol)
wt-hFGF1	-2.14 ± 0.4	-1.1
P135K	-0.85 ± 0.2	-0.06
P135E	-1.11 ± 0.2	-0.2
P135Q	-1.08 ± 0.6	-0.2
P135E/R136E	-0.85 ± 0.5	-0.08
P135K/R136E	-1.04 ± 0.73	-0.27

Heparinase treated cells

Figure S8: Proliferation of heparinase treated NIH3T3 cells in the presence of wt-hFGF1 (10ng/mL).

Supplementary Movie (SM) Captions:

SM 1: 100 ns molecular dynamics simulation of wt-hFGF1 showing residues R133, P135, and R136 in stick form. Hydrogen bonds are depicted by dashed orange lines.

SM 2: 100 ns molecular dynamics simulation of designed hFGF1 mutant P135E showing residue E135 in stick form and residues R133 and R136 in ball-stick form. Hydrogen bonds are depicted by dashed orange lines. Hydrogen bonding is visible between the side chains of residues E135 and R133.

SM 3: 100 ns molecular dynamics simulation of designed hFGF1 mutant P135K showing residue K135 in stick form and residues R133 and R136 in ball-stick form. Hydrogen bonds are depicted by dashed orange lines. No hydrogen bonds are visible between residues R133, K135, and R136.

SM 4: 100 ns molecular dynamics simulation of designed hFGF1 mutant P135Q showing residues Q135 in stick form. Hydrogen bonds are depicted by dashed orange lines. Hydrogen bonding is observed between the side chain carbonyl group and backbone amide group of Q135, as well as between the side chain amide group of Q135 and the carbonyl group on the backbone of residue D84.

SM 5: 100 ns molecular dynamics simulation of designed hFGF1 mutant P135ER136E showing residues E135 and E136 in stick form. Hydrogen bonds are depicted by dashed orange lines. Hydrogen bonding is visible between the side chain carboxyl group of E136 and the guanidinium head group of the R133 side chain.

SM 6: 100 ns molecular dynamics simulation of designed hFGF1 mutant P135KR136E showing residues K135 and E136 in stick form and residue R133 in ball-stick form. Hydrogen bonds are depicted by dashed orange lines. Hydrogen bonding is visible between the side chain amine group of K135 and the side chain carboxyl group of D84.

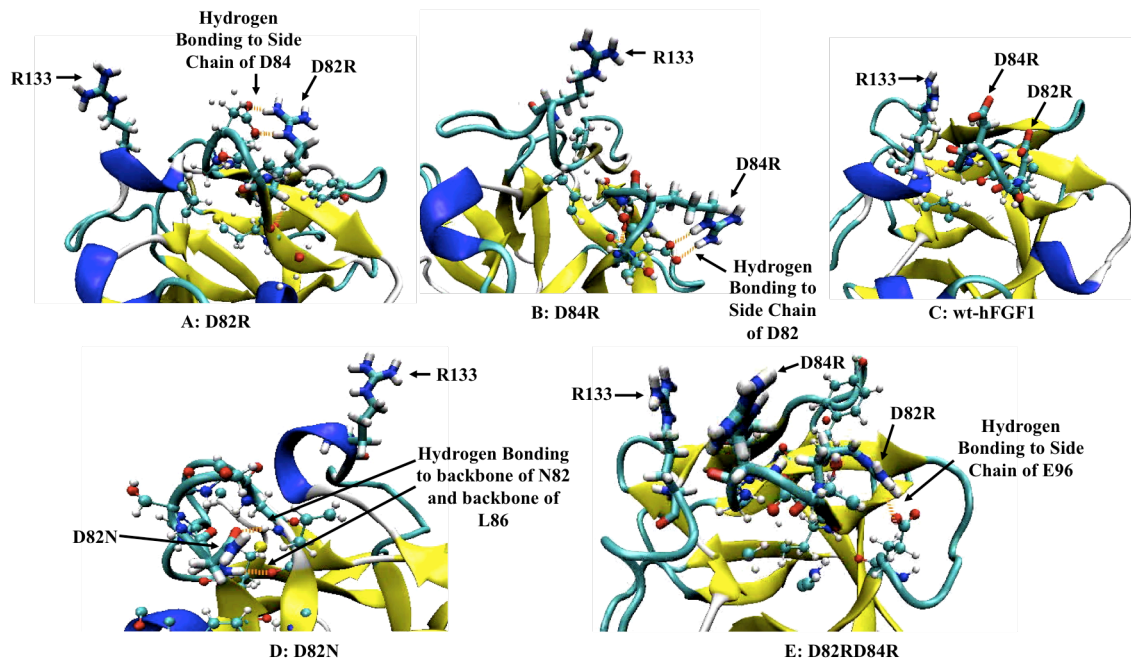**Appendix 2: Supplementary Material**

Figure S1: Still captions from molecular dynamic simulations of D82R (A), D84R (B), wt-hFGF1 (C), D82N (D), and D82R/D84R (E) showing the residue(s) of interest in stick representation, hydrogen bonding in dashed orange lines, and additional amino acids within 5 A° of the residue of interest in CPK representation. Please see attached videos.
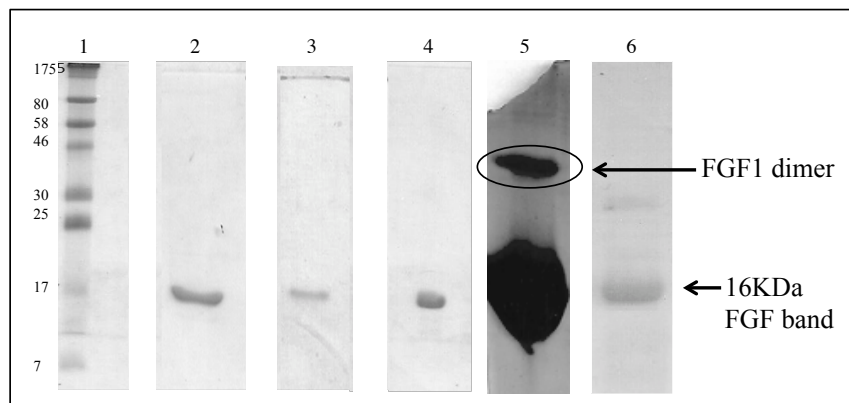

Figure S2: SDS PAGE analysis of purified WT and mutant forms of FGF1. Lane 1 is a commercial broad range protein marker (NEB #7703) and lanes 2, 3, 4, 5, and 6 are the 1500mM NaCl fractions of WTFGF, D82R, D84R, D82N, and D82RD84R respectively. All five proteins appear to be homogeneous migrated at same size just below the corresponding 17kDa band in the protein marker of lane 1. The circled band indicates the presence of a hFGF1 dimer.
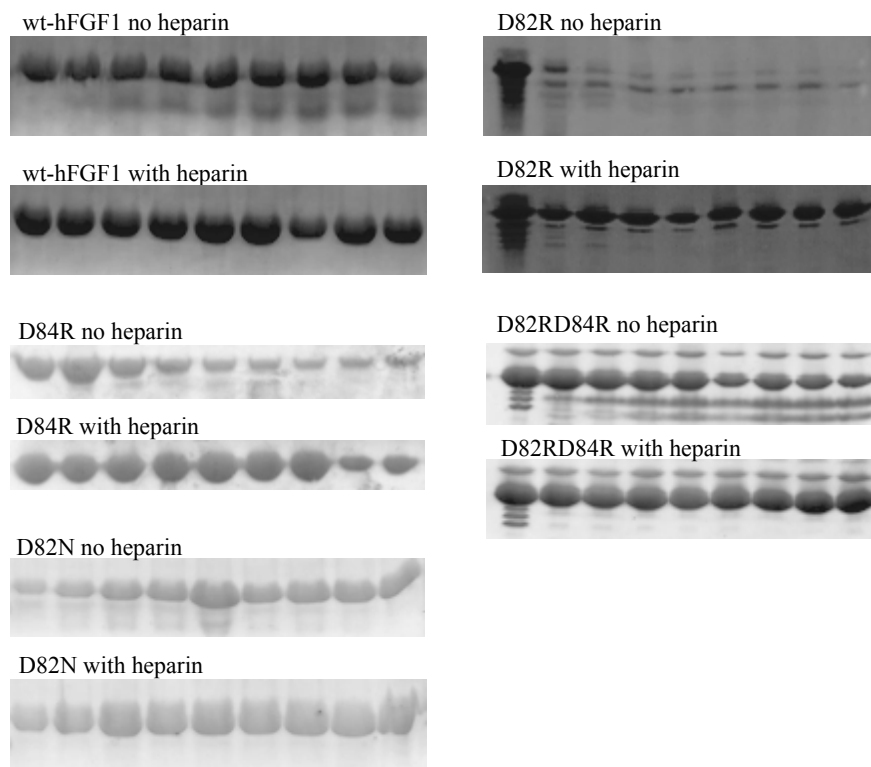
Figure S3: SDS PAGE analysis of the limited trypsin digestion of wild type and charge reversal mutants of hFGF1 in the presence and absence of heparin. Each lane indicates the amount of undigested protein at the respective 5 minute time intervals from time 0 minutes (far left lane) to 40 minutes (far right lane).
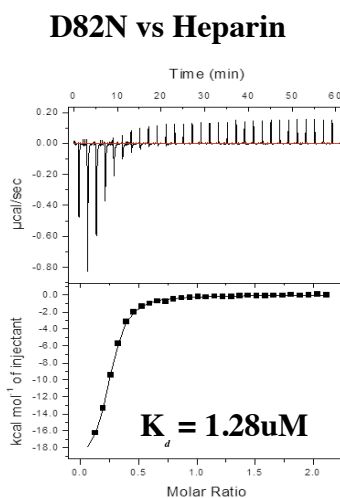

Figure S4: Isothermogram representing the titration of hFGF1 mutant, D82N, with heparin. The upper panel represents the raw heat changes that accompany the binding of the protein to heparin. The lower panels represent the best fit of the binding curve(s) to a one-site binding model. All ITC data have been corrected for heats of dilution.
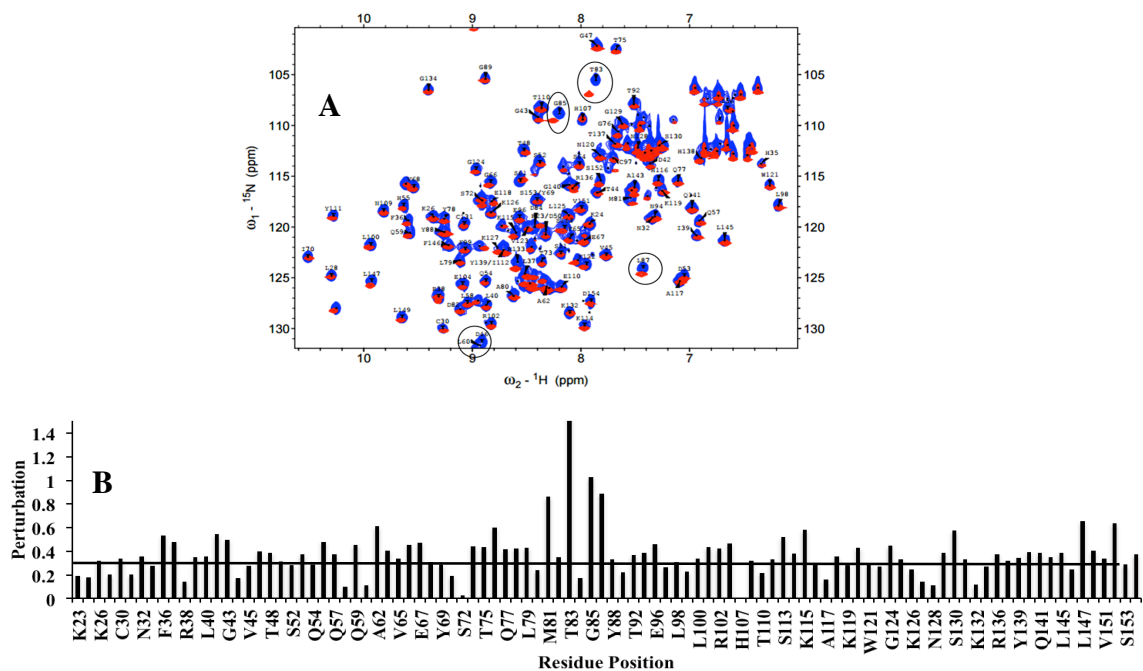
Figure S5: Panel –**A**, Overlay of the ^{1}H-^{15}N HSQC of wild type (red) and the D84R (blue) mutant of hFGF1. Panel-**B**, ^{1}H-^{15}N chemical shift perturbation observed due to the D82R mutation. The horizontal line represents the arbitrary threshold above which the ^{1}H-^{15}N chemical shift perturbation(s) was considered as significant. The ^{1}H-^{15}N chemical shift perturbation of individual residues were calculated using the formula, $(\sqrt{[(2\Delta\delta_{NH})^2 + (\Delta\delta_N)^2]})$

Figure S6: Panel –**A**, Overlay of the ^{1}H-^{15}N HSQC of wild type (yellow) and the D82N (red) mutant of hFGF1. Panel-**B**, ^{1}H-^{15}N chemical shift perturbation observed due to the D82R mutation. The horizontal line represents the arbitrary threshold above which the ^{1}H-^{15}N chemical shift perturbation(s) was considered as significant. The ^{1}H-^{15}N chemical shift perturbation of individual residues were calculated using the formula, ($\sqrt{[(2\Delta\delta_{NH})^2 + (\Delta\delta_N)^2]}$).

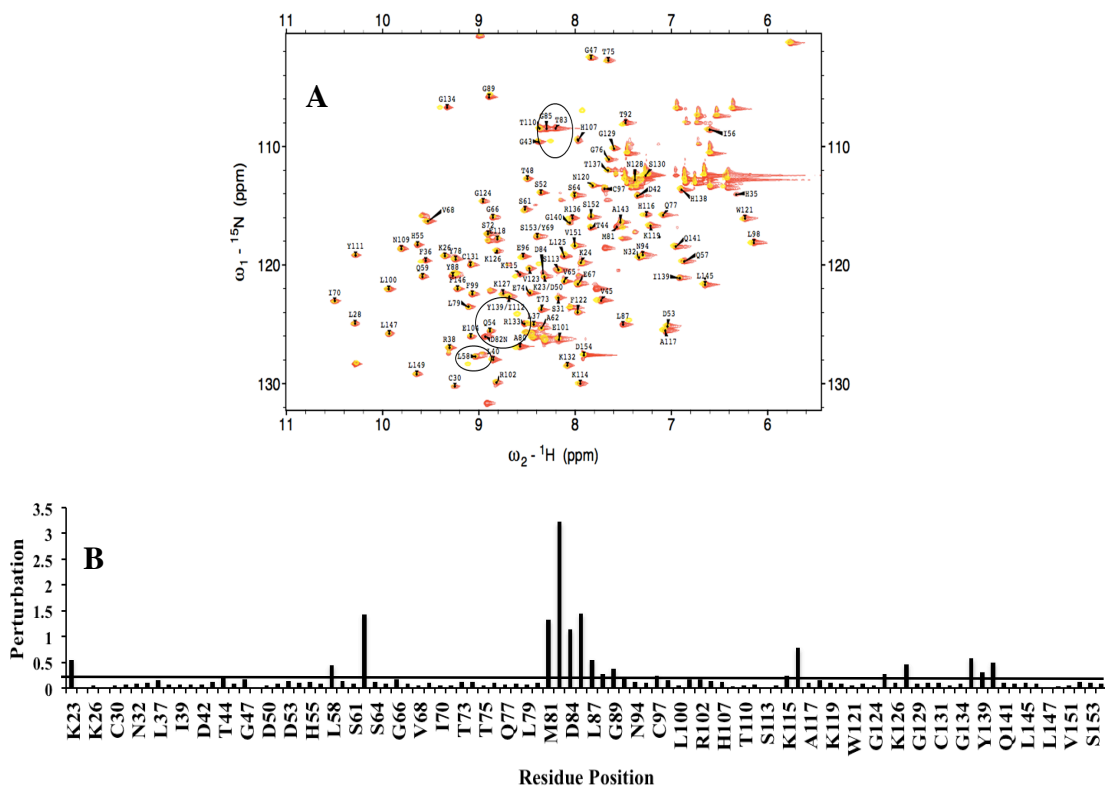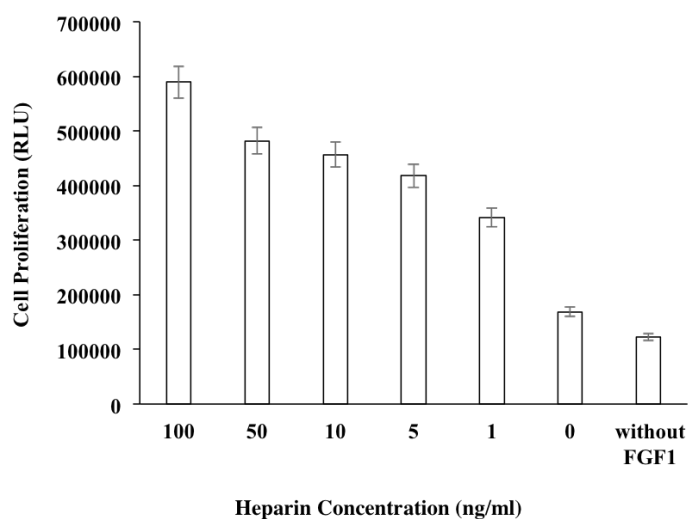**Figure S7:** Effect of heparin on the cell proliferation activity of wild type FGF-1 (10 ng/mL) on heparinase-treated NIH 3T3 cells.

Table S1: Standard deviation among triplicate cell proliferation assays for wt-hFGF1 and each hFGF1 mutant.

[Protein] (ng/mL)	No heparin					With heparin				
	0	0.4	2	10	50	0	0.4	2	10	50
wt-hFGF1	±2527.1	±3119.7	±3531.3	±1006.0	±4403.8	±1422.0	±2379.5	±571.8	±796.7	±3609.6
D82R	±246.3	±460.2	±1581.9	±2508.0	±580.2	±1541.5	±1330.4	±1345.7	±2753.7	±158.8
D84R	±3165.8	±1844.5	±3352.9	±1387.0	±3920.5	±3320.7	±1907.3	±3623.8	±1183.8	±1044.2
D82N	±625.5	±612.5	±3790.2	±1862.4	±1266.9	±1970.7	±460.9	±999.1	±2002.8	±1450.1
D82R/ D84R	±1665.2	±1292.7	±595.4	±691.7	±5165.6	±1258.1	±1392.8	±332.6	±555.3	±36616.0

Supplementary Movie (SM) Captions:

SM 7: 100 ns molecular dynamics simulation of wt-hFGF1 showing residues D82, D84, and R133 in stick form. Hydrogen bonds are depicted by dashed orange lines.

SM 8: 100 ns molecular dynamics simulation of designed hFGF1 mutant D82R showing residues R82, D84, and R133 in stick form. Hydrogen bonds are depicted by dashed orange lines. Hydrogen bonds are visible between the side chains of residues R82 and D84.

SM 9: 100 ns molecular dynamics simulation of designed hFGF1 mutant D84R showing residues D82, R84, and R133 in stick form. Hydrogen bonds are depicted by dashed orange lines. Hydrogen bonds are visible between the side chains of residues D82 and R84.

SM 10: 100 ns molecular dynamics simulation of designed hFGF1 mutant D82RD84R showing residues R82, R84, and R133 in stick form. Hydrogen bonds are depicted by dashed orange lines. No hydrogen bonds are observed between residues R82, R84, and R133.

SM 11: 100 ns molecular dynamics simulation of designed hFGF1 mutant D82N showing residues N82 and R133 in stick form. Hydrogen bonds are depicted by dashed orange lines. Hydrogen bonds are visible between the side chains of residues N82 and L86.

Appendix 3: Supplementary Material

Supplementary Movie (SM) Captions:

SM 12: 4.8 μs molecular dynamics simulation of wt-hFGF1 showing residue R136 in stick form. Surrounding residues in the heparin-binding region are shown in ball and stick form. Hydrogen bonds are depicted by dashed orange lines.

SM 13: 4.8 μs molecular dynamics simulation of designed hFGF1 mutant R136E showing residues E136 in stick form. Hydrogen bonds are depicted by dashed orange lines. Hydrogen bonds are visible between the side chains of residues E136 and R133.

Appendix 4: Biosafety committee approval

Kumar lab biosafety protocol number: 13004

UNIVERSITY OF ARKANSAS.

September 17, 2015

MEMORANDUM

TO: Dr. Suresh Kumar Thallapuranam

FROM: Dr. Ines Pinto
                 Institutional BioSafety Committee

RE: IBC Protocol Approval

IBC Protocol #:   13004

Protocol Title: "Survey of stabilizing mutations of Human Fibroblast Growth
                 Factor-1"

Approved Project Period: Start Date: August 09, 2015
                          Expiration Date: August 08, 2018

The Institutional Biosafety Committee (IBC) has approved the Renewal of Protocol
13004, "Survey of stabilizing mutations of Human Fibroblast Growth Factor-1". You
may continue your study.

If further modifications are made to the protocol during the study, please submit a
written request to the IBC for review and approval before initiating any changes.

The IBC appreciates your assistance and cooperation in complying with University and
Federal guidelines for research involving hazardous biological materials.